

DEVELOPMENT OF NMDA RECEPTORS IN AN INHIBITORY CIRCUIT

POSTNATAL DEVELOPMENT OF NMDA RECEPTORS IN AN IMMATURE INHIBITORY
CIRCUIT

By SHAWNIYA ALAGESWARAN, B.Sc.

A Thesis Submitted to the School of Graduate Studies in Partial Fulfilment of the
Requirements for the Degree Master of Science

McMaster University © Copyright by Shawniya Alageswaran, August 2022

McMaster University MASTER OF SCIENCE (2022) Hamilton, Ontario (Neuroscience)

TITLE: Postnatal Development of NMDA Receptors in an Immature Inhibitory Circuit

AUTHOR: Shawniya Alageswaran, B.Sc. (McMaster University)

SUPERVISOR: Dr. Deda C. Gillespie

NUMBER OF PAGES: xiii, 80

LAY ABSTRACT

To precisely locate a sound in space, the brain compares intensity and timing differences in sound between both ears. Interconnected structures in the brainstem perform this task, and the connections between these structures must be precise to accurately attend to sound. The process of developing this precision is called refinement, and it occurs early in the development of the brain after birth. To understand refinement and how to fix it when it goes awry, we need to understand the mechanisms available to the brain during this period. In this study, I looked at the development of NMDA receptors, which are implicated in refinement. I found that the number and composition of NMDA receptors in these structures change throughout refinement, suggesting that there are different types of NMDA receptors involved during refinement.

ABSTRACT

For optimal function, neural circuits require precise connectivity. Neural circuits achieve this precision through developmental refinement that typically takes place in early postnatal life. N-methyl-D-aspartate receptors (NMDARs) are known mediators of developmental refinement in many glutamatergic circuits and are hypothesized to mediate refinement in glutamate-releasing immature inhibitory circuits of the superior olivary complex (SOC). Physiological studies in the SOC have shown that NMDAR activity is high at birth, occurs primarily through NMDARs that contain the GluN2B subunit, and decreases rapidly over the first two postnatal weeks. These studies did not distinguish whether the decrease in GluN2B-mediated NMDAR activity could be due to a subunit substitution or an overall reduction in NMDAR expression. Using fluorescent *in situ* hybridization and immunohistochemistry, I assessed the expression of NMDAR subunits during early postnatal development in the rat SOC's primary and periolivary nuclei: the lateral superior olive, the medial superior olive, the medial nucleus of the trapezoid body, the ventral nucleus of the trapezoid body, the lateral nucleus of the trapezoid body, and the superior periolivary nucleus. I found that all NMDAR subunit transcripts decreased between postnatal days 0 and 28 in all nuclei. All subunits in the GluN2 subunit family – GluN2A, GluN2B, GluN2C, and GluN2D – showed varying expression patterns, which are consistent with a subunit substitution. These results suggest the involvement of different NMDAR subtypes during circuit refinement in glutamate-releasing immature inhibitory circuits and a decline in NMDARs when the circuit reaches its mature state. The developmental profile of NMDARs might suggest the events taking place during refinement.

ACKNOWLEDGEMENTS

I would like to thank my supervisor, Dr. Deda Gillespie, for welcoming me into her lab. Thank you to my fellow lab members for their camaraderie, and a special thank you to Siyi Ma for her invaluable guidance and motivation throughout my time in the lab. I would also like to thank my supervisory committee, Dr. Katrina Choe and Dr. Margaret Fahnestock, for their helpful feedback throughout my degree. Finally, I would like to express my gratitude to my family and friends for their never-ending love and support.

TABLE OF CONTENTS

Introduction	1
Inhibitory Circuit Refinement in the Superior Olivary Complex	2
MNTB.....	3
LSO.....	3
MSO.....	3
VNTB.....	4
LNTB.....	4
SPN.....	4
Glutamate’s Role in the Refinement of the MNTB to LSO pathway.....	4
NMDARs.....	5
NMDAR Structure.....	5
GluN1 family.....	5
GluN2 family.....	6
GluN3 family.....	6
NMDAR function and its relevance to inhibitory circuits.....	7
Changes in NMDAR subunit composition in circuit refinement.....	8
NMDARs in the immature MNTB-to-LSO pathway.....	8
Objective.....	9
Methods	10
Animals.....	10
RNAscope Fluorescent <i>In-Situ</i> Hybridization.....	10
Tissue Preparation.....	10
RNAscope Fluorescent Multiplex Assay.....	11
DAPI Counterstain and NeuroTrace Flanking Sections.....	12
NeuroTrace Counterstain.....	13
Imaging.....	13
Image Analysis.....	13
GluN1/2 Target Probes.....	13
Control Probes.....	14
Statistical Analysis.....	15
Immunohistochemistry.....	15
Tissue Preparation.....	15
GluN1 Staining.....	16
Imaging.....	17
Image Analysis.....	17
Statistical Analysis.....	17
Results	18
Control probe analysis.....	18
Development of NMDAR subunits in immature auditory brainstem nuclei.....	35
MNTB.....	35

LSO.....	40
MSO.....	45
VNTB.....	50
LNTB.....	54
SPN.....	58
GluN1 Protein in the MNTB, LSO, and MSO.....	63
Discussion	66
Changes in NMDAR mRNA expression in primary and periolivary SOC nuclei.....	66
Changes in control probe expression.....	66
GluN1 protein expression.....	67
Differentiating subunit substitution from a decrease in NMDAR expression.....	67
Temporal order of subunit changes between nuclei.....	68
Limitations.....	68
Troubleshooting.....	70
Conclusion	71
References	72

LIST OF FIGURES AND TABLES

Table 1	Primary and secondary antibody information.....	17
Table 2	Age-related changes in median positive control mRNA expression in the MNTB of Litter 1 rats.....	20
Table 3	Age-related changes in median positive control mRNA expression in the LSO of Litter 1 rats.....	21
Table 4	Age-related changes in median positive control mRNA expression in the MSO of Litter 1 rats.....	21
Table 5	Age-related changes in median positive control mRNA expression in the VNTB of Litter 1 rats.....	21
Table 6	Age-related changes in median positive control mRNA expression in the LNTB of Litter 1 rats.....	21
Table 7	Age-related changes in median positive control mRNA expression in the SPN of Litter 1 rats.....	22
Table 8	Age-related changes in median negative control mRNA expression in the MNTB of Litter 1 rats.....	24
Table 9	Age-related changes in median negative control mRNA expression in the LSO of Litter 1 rats.....	25
Table 10	Age-related changes in median negative control mRNA expression in the MSO of Litter 1 rats.....	25
Table 11	Age-related changes in median negative control mRNA expression in the VNTB of Litter 1 rats.....	25
Table 12	Age-related changes in median negative control mRNA expression in the LNTB of Litter 1 rats.....	25
Table 13	Age-related changes in median negative control mRNA expression in the SPN of Litter 1 rats.....	26
Table 14	Age-related changes in median positive control mRNA expression in the MNTB of Litter 2 rats.....	28
Table 15	Age-related changes in median positive control mRNA expression in the LSO of Litter 2 rats.....	29
Table 16	Age-related changes in median positive control mRNA expression in the MSO of Litter 2 rats.....	29
Table 17	Age-related changes in median positive control mRNA expression in the VNTB of Litter 2 rats.....	29
Table 18	Age-related changes in median positive control mRNA expression in the LNTB of Litter 2 rats.....	30
Table 19	Age-related changes in median positive control mRNA expression in the SPN of Litter 2 rats.....	30
Table 20	Age-related changes in median negative control mRNA expression in the MNTB of Litter 2 rats.....	33

Table 21 Age-related changes in median negative control mRNA expression in the LSO of Litter 2 rats.....	33
Table 22 Age-related changes in median negative control mRNA expression in the MSO of Litter 2 rats.....	33
Table 23 Age-related changes in median negative control mRNA expression in the VNTB of Litter 2 rats.....	34
Table 24 Age-related changes in median negative control mRNA expression in the LNTB of Litter 2 rats.....	34
Table 25 Age-related changes in median negative control mRNA expression in the SPN of Litter 2 rats.....	34
Table 26 Age-related changes in median NMDAR subunit mRNA expression in the MNTB of Litter 1 rats.....	38
Table 27 Age-related changes in median NMDAR subunit mRNA expression in the MNTB of Litter 2 rats.....	40
Table 28 Age-related changes in median NMDAR subunit mRNA expression in the LSO of Litter 1 rats.....	43
Table 29 Age-related changes in median NMDAR subunit mRNA expression in the LSO of Litter 2 rats.....	45
Table 30 Age-related changes in median NMDAR subunit mRNA expression in the MSO of Litter 1 rats.....	48
Table 31 Age-related changes in median NMDAR subunit mRNA expression in the MSO of Litter 2 rats.....	50
Table 32 Age-related changes in median NMDAR subunit mRNA expression in the VNTB of Litter 1 rats.....	53
Table 33 Age-related changes in median NMDAR subunit mRNA expression in the VNTB of Litter 2 rats.....	54
Table 34 Age-related changes in median NMDAR subunit mRNA expression in the LNTB of Litter 1 rats.....	57
Table 35 Age-related changes in median NMDAR subunit mRNA expression in the LNTB of Litter 2 rats.....	58
Table 36 Age-related changes in median NMDAR subunit mRNA expression in the SPN of Litter 1 rats.....	61
Table 37 Age-related changes in median NMDAR subunit mRNA expression in the SPN of Litter 2 rats.....	62

Figure 1	Schematic diagram of a coronal section through the mature rat superior olivary complex (SOC) with indicated inputs to and within SOC nuclei.....	2
Figure 2	RNAscope Image Analysis workflow in QuPath for a P12 rat SOC with probes for GluN1, GluN2A, and GluN2B mRNA.....	14
Figure 3	Mean mRNA/cell for positive control probes, Polr2A, PPIB, and UBC, in Litter 1 rat SOC nuclei from P0 to P28.....	18
Figure 4	Mean mRNA/cell for negative control probes, dapB, in Litter 1 rat SOC nuclei from P0 to P28.....	22
Figure 5	Mean mRNA/cell for positive control probes, Polr2A, PPIB, and UBC, in Litter 2 rat SOC nuclei from P0 to P28.....	26
Figure 6	Mean mRNA/cell for negative control probes, dapB, in Litter 2 rat SOC nuclei from P0 to P28.....	31
Figure 7	Mean NMDAR subunit mRNA expression/cell in the MNTB of Litter 1 rats.....	37
Figure 8	Mean NMDAR subunit mRNA expression/cell in the MNTB of Litter 2 rats.....	39
Figure 9	Mean NMDAR subunit mRNA expression/cell in the LSO of Litter 1 rats.....	42
Figure 10	Mean NMDAR subunit mRNA expression/cell in the LSO of Litter 2 rats.....	44
Figure 11	Mean NMDAR subunit mRNA expression/cell in the MSO of Litter 1 rats.....	47
Figure 12	Mean NMDAR subunit mRNA expression/cell in the MSO of Litter 2 rats.....	49
Figure 13	Mean NMDAR subunit mRNA expression/cell in the VNTB of Litter 1 rats.....	52
Figure 14	Mean NMDAR subunit mRNA expression/cell in the VNTB of Litter 2 rats.....	53
Figure 15	Mean NMDAR subunit mRNA expression/cell in the LNTB of Litter 1 rats.....	56
Figure 16	Mean NMDAR subunit mRNA expression/cell in the LNTB of Litter 2 rats.....	57
Figure 17	Mean NMDAR subunit mRNA expression/cell in the SPN of Litter 1 rats.....	60
Figure 18	Mean NMDAR subunit mRNA expression/cell in the SPN of Litter 2 rats.....	61
Figure 19	Median GluN1 expression in the MNTB, LSO, and MSO of 1 litter of rats.....	63
Figure 20	Representative images of GluN1 protein expression in primary nuclei, MNTB, LSO, and MSO, of the rat SOC from P0 to P28.....	64

LIST OF ABBREVIATIONS AND SYMBOLS

a.u.	Arbitrary Units
ABD	Agonist-binding domain
AMPA	α -amino-3-hydroxy-5-methyl-4-isoxazolepropionic acid receptor
AVCN	Anteroventral Cochlear Nucleus
BSA	Bovine Serum Albumin
CNS	Central Nervous System
CTD	C-terminal domain
DapB	4-hydroxy-tetrahydrodipicolinate reductase
DAPI	4',6-diamidino-2-phenylindole
EPSP	Excitatory Postsynaptic Potential
EtOH	Ethanol
GluN1 (1)	Glutamate ionotropic receptor NMDA type subunit 1
GluN2A (A)	Glutamate ionotropic receptor NMDA type subunit 2A
GluN2B (B)	Glutamate ionotropic receptor NMDA type subunit 2B
GluN2C (C)	Glutamate ionotropic receptor NMDA type subunit 2C
GluN2D (D)	Glutamate ionotropic receptor NMDA type subunit 2D
GluN3A	Glutamate ionotropic receptor NMDA type subunit 3A
GluN3B	Glutamate ionotropic receptor NMDA type subunit 3B
Kcnb1	Potassium voltage-gated channel subfamily B member 1
Kcnh1	potassium voltage-gated channel subfamily H member 1
IC	Inferior Colliculus
ICC	Inferior Central Colliculus
ILD	Interaural Level Difference
ITD	Interaural Time Difference
LNTB	Lateral Nucleus of the Trapezoid Body
LSO	Lateral Superior Olive
LTD	Long-term depression
LTD	Long-term depression
LTP	Long-term potentiation
MNTB	Medial Nucleus of the Trapezoid Body
Mobp	Myelin-associated oligodendrocyte basic protein
Mog	Myelin-oligodendrocyte glycoprotein
mRNA	Messenger Ribonucleic Acid
MSO	Medial Superior Olive
NA	Numerical Aperture
NDS	Normal Donkey Serum
NeuN	Neuronal Nuclei
NMDAR	N-methyl-D-aspartate Receptor
NTD	N-terminal domain

OCT	Optimal Cutting Temperature
P	Postnatal Day
p	Probability
PBS	Phosphate-Buffered Saline
PFA	Paraformaldehyde
POLR2A (+)	Polymerase (RNA) II (DNA directed) polypeptide A
PPIB (o)	Peptidylprolyl isomerase B
RNA	Ribonucleic Acid
RT	Room Temperature
SEM	Standard Error of Mean
SOC	Superior Olivary Complex
SPN	Superior Olivary Nucleus
TPEN	<i>N,N,N',N'</i> -tetrakis(2-pyridinylmethyl)-1,2-ethanediamine
UBC (▽)	Ubiquitin C
VCN	Ventral Cochlear Nucleus
VGLUT3	Vesicular Glutamate Transporter 3
VNTB	Ventral Nucleus of the Trapezoid Body
χ^2 (df)	Chi-square (degrees of freedom)

DECLARATION OF ACADEMIC ACHIEVEMENT

This project was started by Enakshi Singh for her master's thesis in Dr. Deda Gillespie's Lab, where she measured GluN1, GluN2A, and GluN2B mRNA in the rat MNTB, LSO, and MSO. I continued this project and measured the expression of mRNA in the GluN1 and GluN2 family and GluN1 protein in the primary nuclei and three of the periolivary nuclei of the superior olivary complex. I collected and sectioned all the rat brains for *in-situ* hybridization and immunohistochemistry. Siyi Ma from the Gillespie Lab helped me optimize the fluorescent *in-situ* hybridization assay and set up image acquisition parameters on the confocal microscope. I performed subsequent *in-situ* hybridization assays. I independently performed the immunostaining and Nissl staining runs. I imaged the tissue sections and analyzed the mRNA and protein data.

Introduction

For optimal function, neural circuits require precise connectivity (Goodman and Shatz 1993). Neural circuits achieve this precision through developmental refinement that typically occurs in early postnatal life. In general, immature neuronal circuits start with excess synaptic connections, and these connections get refined via reorganization and adjustment of synaptic strength (Goodman and Shatz 1993). Our understanding of the rules and cellular mechanisms underlying inhibitory circuit refinement contains many gaps (for review, see Katz and Shatz 1996 and Gamlin et al. 2018). Considering that the optimal function of the nervous system rests on a balance of excitatory and inhibitory activity and the shaping of neuronal responses through inhibitory inputs, understanding inhibitory circuit refinement is crucial (Wehr and Zador 2003; Wilent and Contreras 2005).

The auditory brainstem contains tonotopically organized inhibitory circuitry, permitting experimental analysis of developing precise inhibitory connections (Kapfer et al. 2002). Specifically, inhibitory projections from the medial nucleus of the trapezoid body (MNTB) to the lateral superior olive (LSO), in the auditory brainstem, provide a model system for characterizing the events of inhibitory circuit refinement (Sanes and Friauf 2000). The LSO integrates excitatory inputs from the ipsilateral cochlear nucleus and inhibitory inputs from the ipsilateral MNTB, driven by the contralateral cochlear nucleus, to compute interaural level differences for azimuthal sound localization of high-frequency sounds (Kapfer et al., 2002). To cue that a higher frequency sound is arriving from the same source, both the excitation from excitatory inputs and inhibition from inhibitory inputs must arrive in a precise temporal and tonotopic register at the LSO. As in excitatory circuits, the developing MNTB-LSO pathway undergoes structural and functional refinement via synapse elimination and strengthening (Sanes and Siverls 1991; Rietzel and Friauf 1998; Kim and Kandler 2003). During this period of synaptic refinement, when GABA and glycine are depolarizing (Ehrlich et al. 1999; Kim and Kandler 2003), the release of glutamate from the MNTB activates postsynaptic N-methyl D-aspartate receptors (NMDARs) on the dendrites of LSO principal neurons, suggesting that this inhibitory circuit may use NMDAR-mediated mechanisms in its refinement (Gillespie et al. 2005).

NMDARs exist as heterotetramers consisting of two obligatory GluN1 subunits and two GluN2A-D and/or GluN3A-B subunits (Monyer et al. 1992). Different NMDAR subtypes confer specific kinetic, pharmacological, and signaling properties to a circuit and may have differential effects on plasticity (Monyer et al. 1992; Liu et al. 2004). Glutamate-releasing immature inhibitory pathways may use NMDAR-mediated mechanisms during refinement, but the role of these receptors in inhibitory circuit refinement remains unclear.

The subunit composition of NMDARs is plastic. As early postnatal development progresses, NMDARs in the LSO show decreased sensitivity to a GluN2B-specific

antagonist, a reduction in charge transfer, and the AMPAR:NMDAR-mediated current ratio in the LSO increases (Case and Gillespie 2011). It is not clear to what extent that these changes are due to a reduction in GluN2B-containing NMDARs or a reduction in NMDARs in general. The developmental profile of NMDAR subtypes in the MNTB-LSO pathway can inform us of the rules and mechanisms involved during inhibitory circuit refinement.

Inhibitory Circuit Refinement in the Superior Olivary Complex

The superior olivary complex (SOC) exemplifies the importance of balanced inhibitory and excitatory activity. It consists of nuclei in the vertebrate auditory brainstem that are linchpins in binaural processing for sound localization. For precise binaural processing to occur, these nuclei must be tuned through refinement. The position, shape, and location of the nuclei differ between species, and the following descriptions of these features describe the rat SOC, unless otherwise stated (Figure 1). The nuclei of the SOC can receive input from both the ipsilateral and contralateral cochlear nuclei, from descending projections of the inferior colliculus (IC), and other SOC nuclei (Illing et al. 2000). The lateral lemniscus and IC receive projections from nuclei of the SOC (Schwartz 1992). The MNTB, LSO, and medial superior olive (MSO) form the three primary nuclei of the SOC for binaural sound processing for azimuthal sound localization (Irving and Harrison 1967). Surrounding the primary nuclei of the SOC are several periolivary nuclei, including the ventral nucleus of the trapezoid body (VNTB), the lateral nucleus of the trapezoid body (LNTB), and the superior periolivary nucleus (SPN).

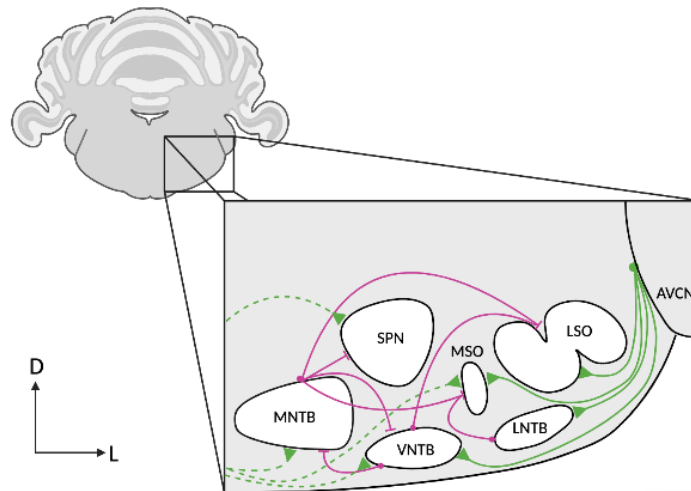


Figure 1. Schematic diagram of a coronal section through the mature rat superior olivary complex (SOC) with indicated inputs to and within SOC nuclei. Green lines indicate depolarizing inputs. Magenta lines indicate hyperpolarizing inputs. Dashed lines indicate input from the contralateral ventral cochlear nucleus. D: dorsal; L: lateral; AVCN: anteroventral cochlear nucleus; LSO: lateral superior olive; LNTB: lateral nucleus of the

trapezoid body; MSO: medial superior olive; SPN: superior periolivary nucleus; VNTB: ventral nucleus of the trapezoid body; MNTB: medial nucleus of the trapezoid body.

MNTB

The MNTB is the medial-most nucleus of the SOC, located in the trapezoid body. There are three neuron types in the MNTB: principal neurons, multipolar neurons, and elongate neurons (Schwartz 1992). The MNTB receives tonotopically organized depolarizing input from globular bushy cells of the contralateral anteroventral cochlear nucleus (AVCN) onto its principal neurons, forming characteristically large synapses called “Calyces of Held” (Morest 1968). The tonotopic organization of the MNTB along the mediolateral axis follows a high-to-low frequency mapping (Sommer et al. 1993). Mature MNTB principal cells provide hyperpolarizing, glycinergic input to the ipsilateral LSO and the ipsilateral MSO. The MNTB is commonly referred to as a sign-inverting nucleus because of this shift from depolarizing input to hyperpolarizing output. Other projection targets include various periolivary nuclei and the lateral lemniscus (Sommer et al. 1993).

LSO

The LSO is the lateral-most nucleus of the SOC. In rats, the LSO has a characteristic S-shape and contains seven types of neurons: bipolar neurons, multipolar neurons, small multipolar cells, banana-like cells, bushy cells, unipolar cells, and marginal cells (Rietzel and Friauf 1998). The bipolar neurons are thought to compute interaural level differences (ILD) for azimuthal sound localization of high-frequency sounds. As studied in the cat SOC, bipolar neurons receive tonotopically organized depolarizing input from spherical bushy cells of the ipsilateral AVCN and hyperpolarizing input from principal cells of the ipsilateral MNTB (Cant and Casseday 1986). In cats, chinchillas, and gerbils, the lateral limb of the LSO has been shown to correspond to low-frequency sounds, and the medial limb of the LSO has been shown to correspond to high-frequency sounds (Tsuchitani 1977; Caspary and Faingold 1989; Sanes et al. 1990). In cats, the medial, or high-frequency, limb mainly projects to the contralateral inferior central colliculus (ICC), and the lateral, or low-frequency, limb mainly projects to the ipsilateral IC (Glendenning et al. 1992).

MSO

The MSO is between the MNTB and LSO. MSO neurons have bipolar morphology, and their cell bodies align in a dorsoventral column, with their dendrites extending mediolaterally (Stotler 1953). MSO neurons compute interaural time differences (ITD) for azimuthal sound localization of low-frequency sounds. Along the dorsoventral axis, MSO neurons receive tonotopically organized depolarizing input from the spherical bushy cells of the ipsilateral and contralateral AVCN (Cant and Casseday 1986; Yin and Chan 1990). Higher frequencies map onto the ventral end, and lower frequencies map onto the dorsal end (Guinan et al. 1972; Müller 1990). The MSO also receives

hyperpolarizing, glycinergic input from the LNTB and MNTB (Kiss and Majorossy 1983; Cant and Hyson 1992; Kuwabara and Zook 1992). The MSO provides glutamatergic input to the ipsilateral and contralateral IC (Glendenning et al. 1992).

VNTB

The VNTB is ventromedial to the MSO and lateral to the MNTB. It contains topographically organized cell types, including medial olivocochlear system neurons and glycinergic neurons (Warr and Beck 1996). Projections from the ipsilateral inferior central colliculus innervate the ventral half of the VNTB (Vetter et al. 1993). It also receives input from the ipsilateral and contralateral VCN and the ipsilateral MNTB (Kuwabara and Zook 1992). Neurons in the medial olivocochlear system of the VNTB send projections to the ipsilateral and contralateral cochlear outer hair cells (Warr and Beck 1996). Additional projection sites include the molecular layer of the contralateral dorsal cochlear nucleus, the ipsilateral MNTB, the ipsilateral and contralateral LSO, and the ipsilateral IC (Warr and Beck 1996; Albrecht et al. 2014).

LNTB

The LNTB is ventral to the primary nuclei, in the trapezoid body. It contains round neurons, stellate cells, and fusiform cells (Weinrich et al. 2018). It receives depolarizing input from globular bushy cells of the ipsilateral cochlear nucleus and spherical bushy cells of the contralateral cochlear nucleus (Smith et al. 1993). The LNTB provides glycinergic input to the ipsilateral MSO, the ipsilateral cochlear nucleus, and the IC (Nordeen et al. 1983; Spangler et al. 1987).

SPN

The SPN is dorsal to the MNTB. It contains tonotopically organized GABAergic neurons that receive depolarizing input from the contralateral ventral cochlear nucleus and hyperpolarizing input from the ipsilateral MNTB (Banks and Smith 1992; Sommer et al. 1993). The mediolateral axis maps onto high-to-low frequency sounds (Willard and Ryugo). SPN neurons send topographically organized projections to the ipsilateral ICC through the lateral lemniscus, where the medial SPN neurons project to the ventromedial ICC and the lateral SPN neurons project to the dorsolateral ICC (Saldaña and Merchañ 1992).

Glutamate's Role in the Refinement of the MNTB to LSO pathway

Before hearing onset, corresponding to postnatal day 12 in rats, during the first postnatal week, the spontaneous activity generated from the immature cochlea drives functional refinement and establishes the tonotopic organization of inputs to the LSO (Tritsch et al. 2010; Clause et al. 2014). During this period, GABA and glycine release from the MNTB onto the LSO is depolarizing (Ehrlich et al. 1999). Notably, in addition to GABA and glycine release, the MNTB also releases glutamate onto the LSO (Gillespie et

al. 2005). By genetically deleting VGLUT3 (vesicular glutamate transporter 3), which is expressed at a number of non-glutamatergic synapses, researchers have shown that the release of glutamate is crucial for refinement (Noh et al. 2010; Case et al. 2014). Glutamate released in the immature MNTB to LSO pathway activates NMDA receptors (Gillespie et al. 2005). The presence of both depolarizing GABA and glycine and glutamate during a period of refinement suggests that the release of all three neurotransmitters and NMDAR activity may be required for refinement (Case et al. 2011; Case et al. 2014).

NMDARs

Explanations of how neural circuits develop seldom occur without the mention of NMDARs. These receptors are ionotropic glutamate receptors that are permeable to Ca^{2+} and Na^+ . They are typically found on the postsynaptic membrane, but they can be found presynaptically as well (Banerjee et al. 2016). NMDARs differ from other ionotropic glutamate receptors (i.e., alpha-amino-3-hydroxy-5-methyl-isoxazolepropionic acid receptors (AMPA) and kainate receptors) because of several defining properties, including 1) sensitivity to membrane potential, as they are blocked by Mg^{2+} at resting membrane potential, 2) slow kinetics due to the slow unbinding of glutamate, and 3) co-agonist (glycine or D-serine) binding for activation (Paoletti et al. 2013).

NMDAR Structure

NMDARs are heterotetramers (Mayer 2006). The C-terminal domain (CTD) is located intracellularly and is responsible for receptor trafficking and associating the receptor with signaling cascades. The extracellular region of the receptor contains the N-terminal domain (NTD) and the agonist-binding domain (ABD). The NTD is involved in assembling subunits and allosteric regulation of the receptor. There are three transmembrane segments (M1, 3, and 4) and a pore loop (M2). The pore of the NMDAR is blocked by Mg^{2+} at resting membrane potential and can be blocked by different pharmacological antagonists: MK-802, memantine, and ketamine.

The three NMDAR subunit families are based on sequence homology: GluN1, GluN2, and GluN3. Conventional NMDARs contain subunits from the GluN1 and GluN2 families. Each subunit in a subunit family is encoded by a separate gene. Different isoforms of a subunit are produced via alternative splicing. Each NMDAR contains two obligatory GluN1 subunits and 2 GluN2 and/or GluN3 subunits. The subunit and splice variant composition of an NMDAR determines the receptor's kinetic, pharmacological, and gating properties (Paoletti et al. 2013).

GluN1 family

The GluN1 subunit has eight possible isoforms: GluN1-1a-4a and GluN1-1b-4b (Hollmann 1999). The expression of each isoform is heterogeneous across the nervous

system, and a single NMDA receptor can have two different GluN1 isoforms. The GluN1 isoform of the NMDAR influences the receptor's ability to be inhibited by protons and Zn^{2+} , and to be potentiated by polyamines (Cull-Candy and Leszkiewicz 2004). The GluN1-a isoforms have variable C-terminal domain lengths, which result in variable receptor trafficking properties among isoforms (Paoletti et al. 2013). These isoforms also have slower decay constants than their GluN1-b counterparts. The GluN1-b isoforms have an N1 cassette, which alters the receptor's gating and pharmacological properties. The ABD of the GluN1 subunit binds glycine or D-serine.

GluN2 family

The GluN2 family contains 4 subunits: GluN2-A, -B, -C, and -D. The ABD of the GluN2 subunit binds glutamate. Depending on the type of GluN2 subunit it contains, an NMDAR can have variations in its kinetic, pharmacological, and gating properties: 1) speed of decay (i.e., decay constant), 2) the magnitude of current decay, 3) sensitivity to Zn^{2+} and Mg^{2+} , 4) permeability to Ca^{2+} , 5) agonist, co-agonist, and antagonist sensitivity, and 6) channel open probability. The characteristic properties conferred by each GluN2 subunit result in NMDAR subtypes having characteristic responses to presynaptic activity.

GluN2A-containing receptors have the fastest decay constant. GluN2D-containing receptors have the slowest decay constant. GluN2B- and GluN2C-containing receptors have similar decay constants (Cathala et al. 2000). In comparison to GluN2-C- or -D-containing NMDARs, GluN2-A- or -B-containing NMDARs have higher conductances, higher Ca^{2+} permeability, and higher Mg^{2+} sensitivity (Momiya et al. 1996). GluN2A-containing receptors have a higher open probability than GluN2-B-, -C-, or -D-containing receptors, with GluN2-C- or -D-containing receptors showing the lowest open probability.

The different GluN2 subunits vary in their sensitivity to co-agonists and antagonists. Zn^{2+} acts as a stronger antagonist of GluN2A-containing NMDARs (Paoletti et al. 1997). Ifenprodil and Ro 25-6981 selectively inhibit GluN2B-containing NMDARs (Williams 1993). Protons preferentially inhibit GluN2B- or GluN2D-containing receptors (Paoletti et al. 2013). Extracellular polyamines enhance GluN2B-containing receptors. Specific pharmacological antagonists to GluN2A-, C-, or D-containing NMDARs do not show high specificity and have not been studied as extensively (Cull-Candy and Leszkiewicz 2004; Paoletti and Neyton 2007).

GluN3 family

The GluN3 family of subunits contains two types: GluN3-A and -B. These subunits are typically in triheterotetrameric NMDARs with GluN2 subunits, where the NMDAR displays decreased Ca^{2+} permeability and decreased conductance (Perez-Otano et al. 2001). GluN3-containing NMDARs show a decreased degree of Mg^{2+} blockade and are

not sensitive to glutamate (Chatterton et al. 2002). The agonist binding domain of these subunits binds glycine or D-serine.

NMDAR function and its relevance to inhibitory circuits

Once activated through membrane depolarization, agonist binding, and co-agonist binding, NMDARs can affect synaptic transmission and synapse strength. NMDARs shape current decay in the depolarizing response of the postsynaptic neuron to pre-synaptic activity due to the receptor's slow kinetics resulting from slow glutamate unbinding. Therefore, NMDARs affect the influx of cations into the postsynaptic cell (Forsythe and Westbrook 1988). Accordingly, GABAergic interneurons with fast decay times, like fast-spiking interneurons, tend to have a low AMPAR:NMDAR-mediated current ratio (Angulo et al. 1999).

In addition to altering membrane kinetics, NMDARs trigger a host of intracellular signalling pathways upon activation, through Ca^{2+} -mediated pathways. One of these pathways is the nitric oxide synthase pathway. An increase in intracellular Ca^{2+} results in the production of nitric oxide (Garthwaite et al. 1988; Bredt and Snyder 1989; Christopherson et al. 1999). NMDARs and the machinery to produce nitric oxide are physically linked: the GluN2B subunit of GluN2B-containing NMDARs and neural nitric oxide synthase form a complex via postsynaptic density protein 95 to link the complex to the plasma membrane (Christopherson et al. 1999). Interestingly, proper refinement of the retinotectal projection depends on NMDAR activity and blocking NMDAR activity in the chick embryo tectum results in decreased nitric oxide synthase activity (Ernst et al. 1999). Blocking nitric oxide synthesis produced the same deficit. As a result, the ipsilateral retinotectal projection, which is eliminated during normal refinement, fails to be eliminated. This suggests that synapse elimination during the development of this pathway is mediated by NMDAR activity that results in downstream production of nitric oxide. Nitric oxide can activate presynaptic guanylate cyclase, which results in increased cGMP levels, ultimately increasing GABA release (Castillo et al. 2011). NMDAR activity is also necessary for GABAergic neuron development. For example, perturbing Ca^{2+} influx through NMDARs by genetically mutating the ion channel pore in immature GABAergic hippocampal neurons reduces mIPSC frequency (Gu et al. 2016).

An influx of extracellular Ca^{2+} through NMDARs can trigger short-term (e.g., milliseconds to minutes) and long-term changes (e.g., hours to days) in the synapse's strength (Bliss and Collingridge 1993), which can ultimately affect how a circuit processes information (see Malenka and Nicoll, 1993 for review). A long-term increase in synaptic strength is referred to as long-term potentiation (LTP), and a long-term decrease in synaptic strength is referred to as long-term depression (LTD). Conversely, a short-term increase in synaptic strength is referred to as short-term potentiation (STP), and a short-term decrease in synaptic strength is referred to as short-term depression (STD). Factors such as the magnitude and duration of presynaptic activity contribute to which form of plasticity gets induced (Malenka and Nicoll 1993).

NMDARs can be located at synapses and in extrasynaptic regions. Factors like the location of the receptor on the postsynaptic membrane with respect to the presynaptic terminal can also change the postsynaptic neuron's response to extrasynaptic glutamate release (i.e., spillover) (Kullmann and Asztely 1998). Extrasynaptic NMDARs modulate the intrinsic excitability of GABAergic neurons in the prefrontal cortex slices of adult mice (Yao et al. 2022). When NMDARs are blocked, intrinsic excitability of these neurons was reduced, and when NMDARs are activated, intrinsic excitability was enhanced. This modulatory capacity was specific to extrasynaptic GluN2C- and GluN2D-containing NMDARs. In the auditory brainstem, glutamate released from immature AVCN and the immature MNTB can activate the LSO from either pathway (Alamilla and Gillespie 2011). This spillover of glutamate from either immature pathway activates the same population of NMDARs, which happen to be GluN2B-containing NMDARs. The presence of different NMDAR subtypes during development could reflect how they contribute to the needs of the circuit at different stages of development. For example, GluN2B- or GluN2C-containing NMDARs allow for more charge transfer than GluN2A-containing subunits, which can influence synaptic integration and plasticity (Monyer et al. 1992; Liu et al. 2004).

Changes in NMDAR subunit composition in circuit refinement

NMDARs change subunit composition throughout development, in addition to other timescales. These changes in subunit composition can affect how a circuit integrates neuronal signals during refinement. The differing degrees of conductances, degrees of Mg^{2+} blockade, and permeabilities conferred by GluN2 subunits affect the contribution of an NMDAR to synaptic integration and plasticity.

Several general trends in the GluN2 and GluN3 subunit family have been observed in the CNS (Monyer et al. 1994). GluN2D is the primary subunit in the embryonic brain and declines in the adult brain. From the embryonic stage to the first postnatal week, GluN2B expression prevails. GluN2C expression occurs after the first postnatal week. During the first two postnatal weeks, GluN2A expression increases and becomes widely expressed in the adult CNS.

In activity-dependent refinement, many circuits strengthen inputs using LTP, a process that usually contains NMDAR activity (Cramer and Sur 1995). At hippocampal CA1 synapses, blocking GluN2A-containing NMDARs can bias a synapse towards LTD, and blocking GluN2B-containing NMDARs can bias a synapse towards LTP (Liu et al. 2004). GluN2B-containing NMDARs mediate a large proportion of charge transfer during LTD (Paoletti et al. 2013). Throughout the CNS, a subunit substitution from predominantly GluN2B-containing NMDARs to predominantly GluN2A-containing NMDARs is often a proxy for circuit maturation (Philpot et al. 2001).

NMDARs in the immature MNTB-to-LSO pathway

Many classic glutamatergic circuits and glutamate-releasing immature inhibitory circuits in the auditory brainstem are suspected to refine through the involvement of NMDARs. For example, in immature classic glutamatergic circuits in the thalamus, genetic deletion of NMDARs impairs pruning and strengthening (Zhang et al. 2013). Because subunit composition affects the kinetics and pharmacology of NMDARs, the subunit composition in a circuit can be identified experimentally using targeted pharmacology for specific subunits and by measuring changes in stimulus-response at different time points in development.

In the MNTB to LSO pathway, researchers have shown that when the NMDAR-mediated response is pharmacologically isolated, there is an increase in charge transfer from P0 to P8, followed by a sharp decline at P9 (Case and Gillespie 2011). The decrease in charge transfer suggests that there was a reduction in NMDAR activity. This was further supported by an observed increase in the AMPAR: NMDAR-mediated excitatory postsynaptic currents (EPSC) ratio at P9. During this same period, the LSO also shows a reduction in ifenprodil sensitivity, a GluN2B-specific antagonist, suggesting a potential subunit substitution. Similar properties have been shown in the mouse MNTB, where the contribution of NMDARs to evoked EPSCs decreases and the contribution of AMPARs to evoked EPSCs increases around a similar timeline (Joshi and Wang 2002). The researchers additionally measured EPSCs in the MNTB in the presence of ifenprodil, Zn^{2+} , or TPEN (to remove endogenous Zn^{2+}). They found that ifenprodil had an increasing effect over the first two postnatal weeks, suggesting an increase in GluN2B expression early in development. Zn^{2+} and TPEN had little to no effect on the measured EPSCs, suggesting a subunit substitution from GluN2B- to GluN2A-containing NMDARs is unlikely, as Zn^{2+} acts as an antagonist of GluN2A-containing NMDARs and the absence of Zn^{2+} and TPEN sensitivity suggests a lack of GluN2A-containing NMDARs. Despite observing an overall reduction in NMDAR activity, the extent to which this reduction is due to a reduction in GluN2B-containing NMDARs is unclear (Case et al. 2011).

Objective

To address this question anatomically, I measured the expression of GluN1 and GluN2 subunits in the described nuclei of the rat SOC from birth to circuit maturation. In comparison to cats, chinchillas, and gerbils, other organisms used in auditory brainstem research, rats can hear at higher frequencies, indicating that they are better specialized at using their LSO (Gould and Morgan 1941). Although rats have similar hearing at higher frequencies to mice, rats are better models for refinement in the MNTB-LSO pathway because the development of MNTB-LSO pathway in rats is five days, vs. four days in mice (Kandler and Friauf 1995; Kim and Kandler 2003). Further, glutamate release in the MNTB-LSO pathway during refinement is a well-established phenomenon in rat (Gillespie et al. 2005). Therefore, the rat LSO provides a stronger model to study the refinement of inhibitory inputs. The composition of NMDARs may indicate the rules and cellular mechanisms available to the immature inhibitory circuit during refinement.

Methods

Animals

All animal procedures were performed per the Canadian Council on Animal Care Guidelines and were approved by the Animal Research Ethics Board of McMaster University. I collected brains from three litters of Sprague-Dawley rats, born on-site. The first litter used for *in-situ* hybridization was born to an untimed pregnant female shipped from Charles River Laboratories, Inc. (Hartford, CT, USA). The second litter for *in-situ* hybridization and the litter for immunohistochemistry were born to two different females bred on-site. In total, two litters were used for *in-situ* hybridization and one litter was used for immunohistochemistry.

Collection Timepoints

The following collection timepoints were used in each litter: postnatal day (P) 0, P4, P8, P12, P16, P20, P24, and P28, with one pup used at each timepoint. Rats were randomly selected from each litter to remove bias toward either sex (complete sex characterization for each litter is not available - see Discussion).

RNAscope Fluorescent *In-Situ* Hybridization

Tissue Preparation

Tissue sections were prepared according to the following instructions provided by Advanced Cell Diagnostic for fixed frozen sample preparation for the RNAscope Fluorescent Multiplex assay (Wang et al. 2012). Each rat was anesthetized with an intraperitoneal injection of sodium pentobarbital (120 mg/kg of body weight). They were then perfused transcardially with room-temperature RNase-free 0.1M phosphate-buffered saline (PBS) (1 mL/g of body weight) and then with ice-cold 4% paraformaldehyde (PFA) in RNase-free PBS (1 mL/g of body weight) (16% PFA - Alfa Aesar). The brains were rapidly removed and were postfixed in 4% PFA in RNase-free PBS for 24 hours at 4°C. The brains were then cryoprotected in 10%, 20%, and then 30% RNase-free sucrose in RNase-free PBS. After cryoprotection, the brainstems were removed by making a coronal cut 2mm rostral to lambda. The brainstem was equilibrated to Optimal Cutting Temperature (OCT) Compound (Tissue-Tek) for 2-5 minutes and then embedded in an OCT-filled aluminum mould. The brains were then frozen in isopentane cooled to -80°C in a dry-ice-100% ethanol (EtOH) slurry. The frozen brains were kept at -80°C in an airtight container until sectioning.

Sectioning

After equilibrating the frozen brains to the cryostat chamber's temperature (-16°C) for 1 hour, 10-micron serial sections of the SOC were sectioned at the cryostat and mounted onto SuperFrost Plus slides (Fisher Scientific). Two sections were mounted per slide for the *in-situ* hybridization assay. Two unilateral SOCs were analyzed per target protein and one unilateral SOC was analyzed per control protein. To annotate SOC nuclei in DAPI-counterstained sections, flanking sections to be stained with NeuroTrace 640/660 were collected onto SuperFrost Plus Slides. To ensure the mounted sections contained SOC nuclei, I collected flanking sections onto subbed gelatin-coated slides and performed a fast Nissl stain. For the fast Nissl staining, I immersed the mounted sections in 0.5% (weight/volume) cresyl violet acetate in ddH₂O (Alfa Aesar) for 3-5 minutes at room temperature (RT) and then in 95% EtOH at RT for 1-2 minutes. I could then determine whether the enclosed sections contained the nuclei of the SOC in real-time by imaging the stained sections on a widefield microscope at 10x air magnification. After collecting the sections, the slides for fluorescent *in-situ* hybridization were air-dried at -20°C and then stored at -80°C until the RNAscope Assay was performed. The slides for the NeuroTrace 640/660 stain were stored at -20°C until they were stained.

RNAscope Fluorescent Multiplex Assay

For each litter, slides for ages P0-P12 were processed in one assay, and slides for ages P16-P28 were processed in another assay due to space constraints in the hybridization oven. The slides were washed in RT RNase-free PBS for 5 minutes to remove residual OCT Compound and then were baked at 60°C for 30 minutes to dry the sections. They were then postfixed in freshly prepared 4% PFA in RNase-free PBS (16% PFA - Alfa Aesar) for 15 minutes at 4°C. The slides were then dehydrated at RT in increasing concentrations of EtOH: 50% EtOH in dH₂O, 70% EtOH in dH₂O, and 100% EtOH. To pre-treat the tissue sections for mRNA detection, the slides were submerged in boiling (98-102°C) Target Retrieval solution for 5 minutes. Immediately after the target retrieval step, the slides were washed twice in RT distilled water to remove the Target Retrieval solution, followed by a rinse in RT 100% EtOH to dehydrate the sections. A hydrophobic barrier (ImmEDGE Pen, Vector Laboratories) was drawn on each slide to encircle both tissue sections. After the barrier was set, Protease III solution was applied to completely cover each tissue section. The sections were incubated with Protease III for 30 minutes at 40°C to expose RNA that would be blocked by RNA-protein crosslinks from fixation (Nuovo et al. 2009), followed by two washes in RT distilled water. The slides were then incubated in RNAscope mRNA probe solutions for 2 hours at 40°C to allow for the mRNA probes to bind to their targets. Each section was completely covered in the probe solution.

In each *in-situ* hybridization run, 4 slides were used for each age and each slide was treated with 1 of 4 mRNA probe solutions: 1) GluN1, GluN2A, and GluN2B, 2) GluN1, GluN2C, and GluN2D, 3) ubiquitin C (UBC), polymerase (RNA) II (DNA directed)

polypeptide A (Polr2A), and peptidylprolyl isomerase B (PPIB) (positive control probes), and 4) 4-hydroxy-tetrahydrodipicolinate reductase (dapB) (negative control probe).

After probe incubation, the slides were incubated at 40°C in the following signal amplification solutions: 1) AMP 1-FL for 30 minutes, 2) then AMP 2-FL for 15 minutes, 3) then AMP 3-FL for 30 minutes, and 4) then AMP 4-FL ALT C for 15 minutes. After each amplification step, the slides were washed twice for 2 minutes at RT in 1X Wash Buffer. The last amplification step, the AMP 4-FL ALT C solution, labelled the mRNA probes with the following fluorophores: GluN2A, GluN2C, and PPIB with Atto 647, GluN2B, GluN2D, and POLR2A with Atto 550, and GluN1 and UBC with Alexa 488. DapB mRNA probes were labelled with all three fluorophores.

Control Probes

The RNAscope assay provides one positive control target mRNA per fluorophore: Polr2A, PPIB, and UBC. Polr2A, polymerase (RNA) II (DNA directed) polypeptide A, enables core promoter sequence-specific DNA binding activity(PubChem). PPIB, peptidylprolyl isomerase B, enables RNA polymerase binding activity(PubChem). UBC, ubiquitin C, enables protease binding activity(PubChem). These specific positive control probes are recommended in the RNAscope assay to compare against target probes of similar expression levels, measured by mRNA copies per cell. For example, UBC is to be compared with target probes that have medium-high expression levels, PPIB is to be compared with target probes with medium expression levels, and Polr2A is to be compared with target probes with low expression levels. Because the expression levels of the target probes used in this assay were unknown, I did not compare the expression of specific positive control probes to the target probes. Instead, I used positive control probe expression to ensure that the tissue preparation protocol I used yielded sections with good RNA quality by assessing whether the measured expression levels in the positive control probes were at the expected levels set by the assay guidelines. I measured control probe expression at each timepoint to assess whether there were age-related changes in control probe expression. To ensure low background staining and that the tissue sections were correctly prepared, a probe for DapB, a bacterial gene, was used as the negative control(PubChem).

DAPI Counterstain and NeuroTrace Flanking Sections

P0-P12 slides from litter 1 were counterstained with DAPI. After the last 1X Wash Buffer wash, excess liquid was removed from the slides and 4 drops of DAPI were applied to each section. The sections were incubated in DAPI for 30 seconds at RT. Immediately after removing excess DAPI from the slides, ProLong Gold Antifade Mounting medium was applied to each slide. After the slides were coverslipped, the slides were sealed with clear nail polish. The slides were stored in a dark slide box at 4°C until they were imaged at least 24 hours later. The sections were imaged within two weeks of the assay.

The flanking sections were stained with NeuroTrace 640/660. Before applying the NeuroTrace stain, the sections were rehydrated in PBS for at least 40 minutes. Then, the sections were washed in 0.1% Triton X-100 in PBS for 10 minutes. After washing the sections for 5 minutes, twice, in PBS, 200 μ L of 0.4% (volume/volume) NeuroTrace 640/660 in PBS was applied to each slide. The slides were incubated in NeuroTrace for 20 minutes in a dark slide box at RT. The slides were washed 10 minutes, 3 times, in PBS, and then ProLong Gold Antifade Mounting medium was applied to each slide. After the slides were coverslipped, they were sealed with clear nail polish. The slides were stored in a dark slide box at 4°C until they were imaged at least 24 hours later. The sections were imaged within two weeks of the assay.

NeuroTrace Counterstain

P16-P28 slides from litter 1 and all slides from litter 2 were counterstained with NeuroTrace 435/455, instead of DAPI, using an unvalidated protocol provided by Advanced Cell Diagnostics that worked for other users of the assay. After the last 1X Wash Buffer wash, the slides were rinsed twice with dH₂O. Then, 200 μ L of 20% (volume/volume) NeuroTrace 435/455 in RNase-free PBS was applied to each section. After incubating the slides for 20 minutes in a dark slide box at RT, the slides were washed for 5 minutes, twice, in RNase-free PBS. ProLong Gold Antifade Mounting medium was applied onto each slide. After the slides were coverslipped, they were sealed with clear nail polish. The slides were stored in a dark slide box at 4°C until they were imaged at least 24 hours later. The sections were imaged within two weeks of the assay.

Imaging

All images were acquired on a confocal microscope (Zeiss LSM700). For target probe slides, two unilateral SOCs were imaged with tile-scanning using a 40x oil objective (NA = 1.4). For control probe slides, only a single unilateral SOC was imaged. Acquisition settings were kept constant for all images acquired within a litter, except for an adjustment of the laser power and gain for the NeuroTrace 435/455 counterstain used in the P16-P28 slides in the first litter.

Image Analysis

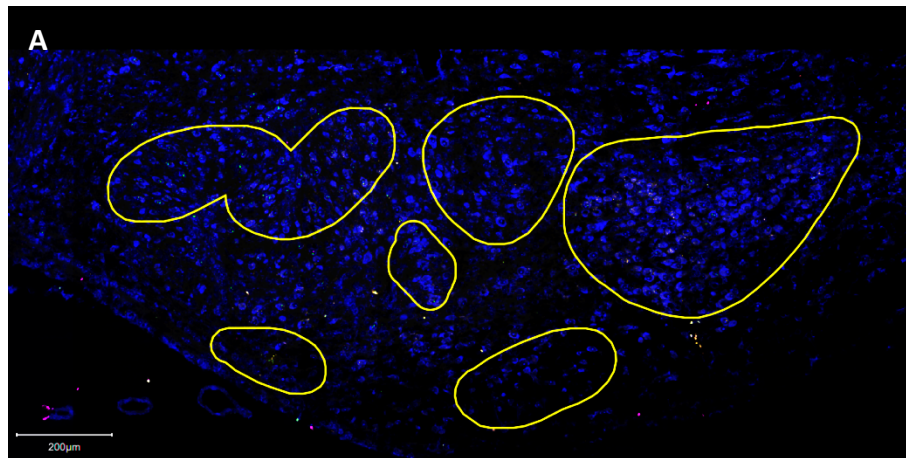
GluN1/2 Target Probes

Using ImageJ, each czi image file was converted into a tiff image sequence, consisting of raw, unaltered images of the 4 channels. The tiff images for the probe channels were randomly assigned a new title using a MATLAB code from the Watanabe Lab (2020), and the experimenter was kept blind to the real identity of the images for the entirety of the image analysis. The randomized tiff images for the probes were combined with the counterstain image in ImageJ to make a 4-channel tiff stack for image analysis. The

MNTB, VNTB, LNTB, SPN, LSO, and MSO of each image were manually annotated in QuPath using flanking NeuroTrace 640/660 images or the NeuroTrace 435/455 counterstain (Bankhead et al. 2017) (Figure 2A). Cells in each annotated nucleus were detected by running a CellPose script (Stringer et al. 2021) in QuPath with the 'cyto' path model and a pixel size of 0.5 (Figure 2B). All other parameters were defaults in the CellPose script. A count of the number of cells detected in each section is found under each figure of mean expression levels in the Results section. To detect the probes, the Subcellular Detection feature of QuPath was used with the following parameters: Smooth before detection = TRUE, Split by intensity = TRUE, Split by shape = TRUE, Expected spot size = 0.5 microns², Min spot size = 0.05 microns², Max spot size = 2 microns², and Include clusters = TRUE (Figure 2C). The threshold values for probe detection were adjusted for each channel to ensure that all probe signal was detected, and that noise was not included. The probe signal was distinguishable from the noise signal by eye due to the shape and size of the probe signal (see Figure 2C). The number of detected probes in each randomized tiff image, in each cell of each annotation, was extracted from QuPath for statistical analysis.

Control Probes

The probe detection workflow for the target probes was used for control images, with the exception that the probe channels in the control images were not randomized. Both litters met the positive and negative probe quality control guidelines stated by Advanced Cell Diagnostics.



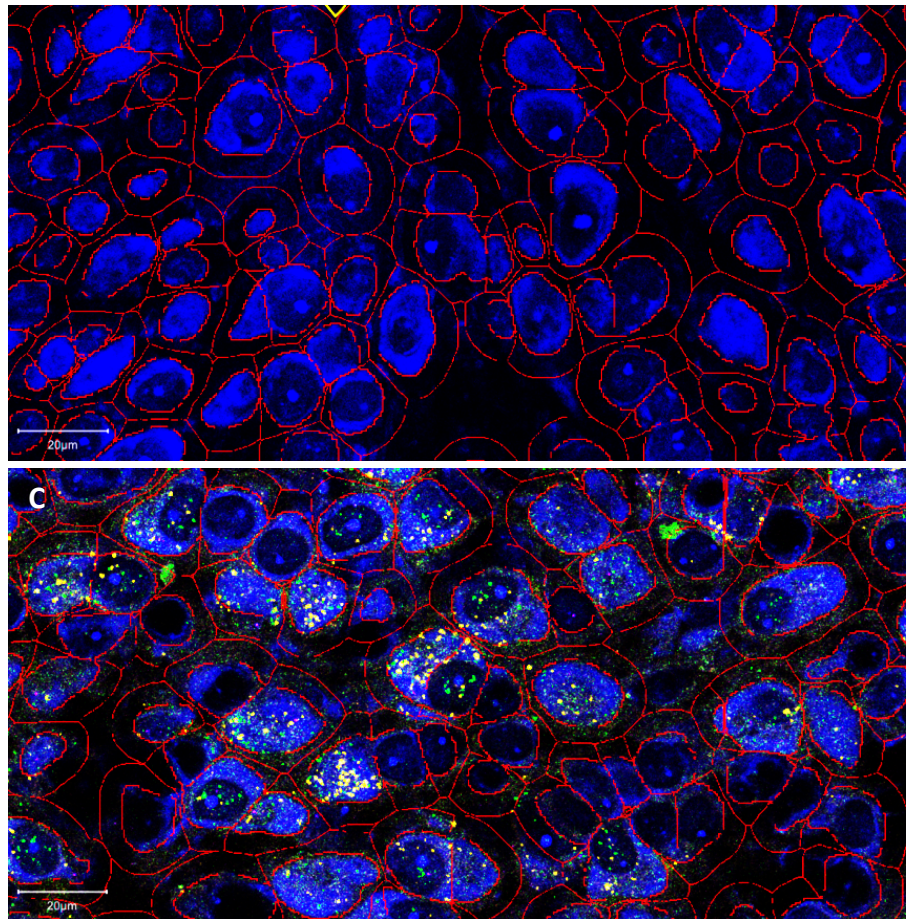


Figure 2. RNAscope Image Analysis workflow in QuPath for a P12 rat SOC with probes for GluN1, GluN2A, and GluN2B mRNA. After annotating primary and periolivary nuclei (A), a CellPose detection algorithm was used to detect neurons in each nucleus (B). Probes were detected in each channel using the 'Subcellular Detection' feature in QuPath (C). A: Scale bar = 200 μm . B and C: Scale bar = 20 μm .

Statistical Analysis

The probe detection data were analyzed in R using custom scripts. For each age, probe, and nucleus, the number of dots per cell was positively skewed. Therefore, I used non-parametric statistical tests to conduct my analyses. For each nucleus and probe combination, I used the Kruskal-Wallis test, a non-parametric version of a one-way ANOVA, to determine whether the number of dots per cell changed significantly with age. To determine whether there were significant differences between specific ages, I used the pairwise Wilcoxon test with a Bonferroni correction for multiple comparisons. I set statistical significance at $p < 0.05$ for both tests.

Immunohistochemistry

Tissue Preparation

Tissue was prepared as described by Zhang et al (2018)(Zhang et al. 2018) and Liu and Wong-Riley(Liu and Wong-Riley 2002) (2002). Each rat was anesthetized with an intraperitoneal injection of sodium pentobarbital (120 mg/kg of bodyweight). They were then perfused transcardially with PBS (RT) (1 mL/g of bodyweight) and then with ice-cold freshly prepared 4% PFA in PBS for 5 minutes. The brains were rapidly removed, and the brainstems were removed by making a coronal cut 2mm rostral to lambda. The brainstems were postfixed by immersion in freshly prepared 4% PFA in PBS at 4°C for 1 hour. After fixation, the brainstems were cryoprotected in 10%, 20%, and then 30% sucrose in PBS at 4°C. The brainstem was equilibrated to Optimal Cutting Temperature (OCT) Compound (Tissue-Tek) for 2-5 minutes and then embedded in an OCT-filled mould. The brainstems were frozen and sectioned using the same procedure for *in-situ* hybridization. After collecting the sections, the slides were stored at -20°C until the immunostaining was performed.

GluN1 Staining

Three sections per timepoint were stained for GluN1. The sections were counterstained with NeuroTrace 435/455 to visualize cell bodies and annotate SOC nuclei during image analysis. A control without the primary antibody was run for each timepoint. All sections were stained in the same run.

On-slide staining was performed as described by Zhang et al (2018)(Zhang et al. 2018) and Liu and Wong-Riley (2002)(Liu and Wong-Riley 2002). A hydrophobic barrier (Immedge Pen) was drawn on each slide to enclose the sections. Once the barrier was dry, the sections were rehydrated twice in RT PBS, and then they were washed three times in RT freshly prepared 0.5% bovine serum albumin (BSA) in PBS (buffer). The sections were blocked overnight at 4°C in a solution (blocking solution) containing 5% normal donkey serum (NDS) and 1% Triton-X-100 in buffer. The sections were washed five times in RT PBS and then incubated in the primary antibody (diluted in the blocking solution) for 48 hours at 4°C (Table 1). The sections were then washed five times in RT PBS and then incubated in the secondary antibody diluted in 5% NDS in buffer for 2 hours at RT in the dark (Table 1). The following steps were performed in the dark at RT. The sections were washed five times in buffer and then 5 times in PBS. After counterstaining the sections with 1:50 NeuroTrace 435/455 for 20 minutes, the sections were washed three times in PBS. Fluoromount Gold mounting medium was applied to the slides, and the slides were coverslipped and sealed with clear nail polish. The slides were stored in a dark slide box at 4°C until they were imaged at least 24 hours later. The sections were imaged within two weeks of the staining run.

Table 1. Primary and secondary antibody information

Antigen	Dilution	Host	Manufacturer, Cat. #	Antibody Characterization
GluN1 From Manufacturer's website: "Fusion protein containing amino acids 1- 564 of the NR1 subunit of rat NMDA receptor"	1:250	Mouse, mono- -clonal	PhosphoSolutions, #1508-NR1	From Manufacturer's website: "Western blot of 10 µg of rat hippocampal lysate [showed] specific immunolabeling of the ~120 kDa NR1 subunit of the NMDA receptor."

Fluorophore	Dilution	Host	Target	Manufacturer, Catalogue #
Alexa 647	1:500	Donkey	Mouse	Jackson ImmunoResearch, 715-605-151

Imaging

All images were acquired on a confocal microscope (Zeiss LSM700). 3 unilateral SOC were imaged with tile-scanning using a 20x air objective (NA = 1.4). For primary delete control slides, only a single unilateral SOC was imaged. Acquisition settings were kept constant for all images.

Image Analysis

Raw, unaltered images were analyzed in QuPath. For each image, the MNTB, MSO, and LSO of each SOC were annotated. Minimum and maximum pixel intensity,

mean pixel intensity, standard error of the mean, and median pixel intensity for each nucleus were computed.

Statistical Analysis

Pixel data were analyzed in R using custom scripts. For each age and nucleus, pixel intensity values were positively skewed. Therefore, I used non-parametric statistical tests to conduct my analyses. For each nucleus, I used the Kruskal-Wallis test to determine whether the mean pixel intensity changed significantly with age. To determine which ages were significantly different, I used the pairwise Wilcox test with a Bonferroni correction for multiple comparisons. I set statistical significance at $p < 0.05$.

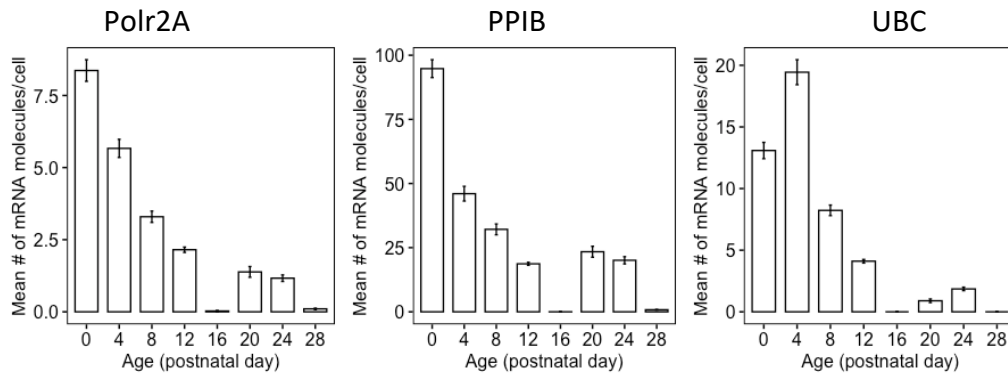
Results

Control probe analysis

Litter 1 positive control probe expression

In litter 1, there was a significant difference in median Polr2A expression across ages in the MNTB, LSO, MSO, and SPN (Figure 3, Table 2, 3, 4, and 7). With PPIB expression, there were significant differences across ages in all nuclei (Figure 3, Table 2-7). With UBC expression, there were significant differences across ages in the MNTB, LSO, MSO, VNTB, and SPN (Figure 3, Table 2, 3, 4, 5, and 7). There were statistically significant differences in expression between most ages (Table 2-7).

MNTB

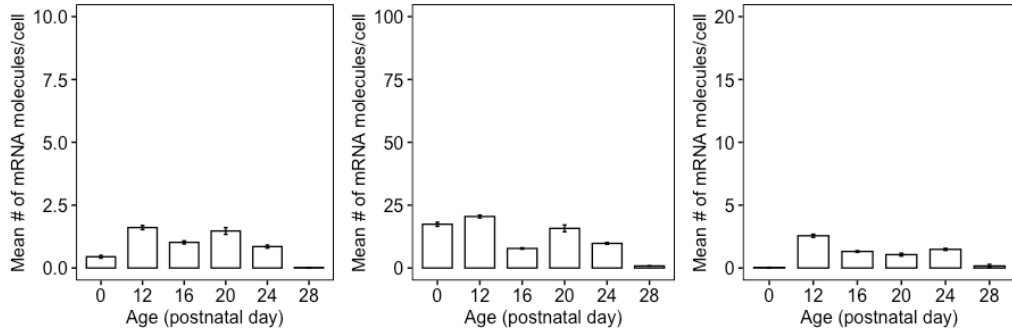


LSO

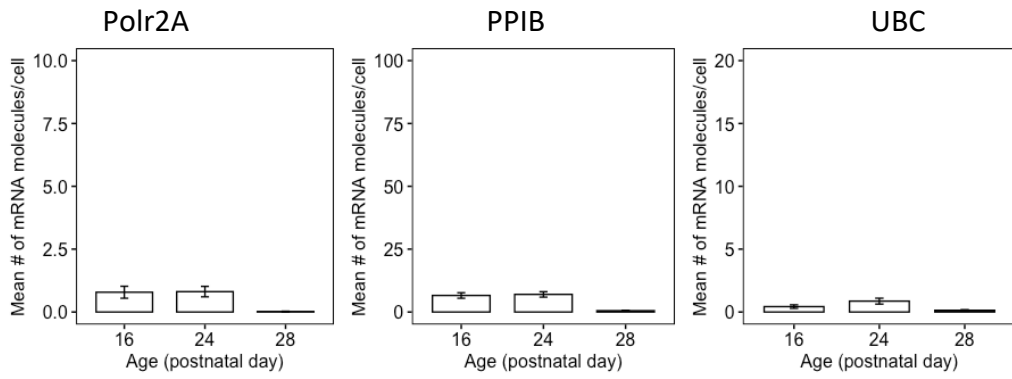
Polr2A

PPIB

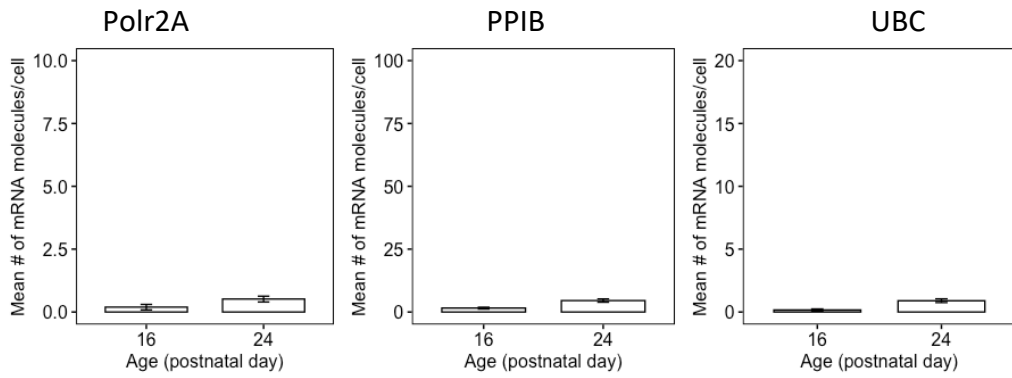
UBC



MSO

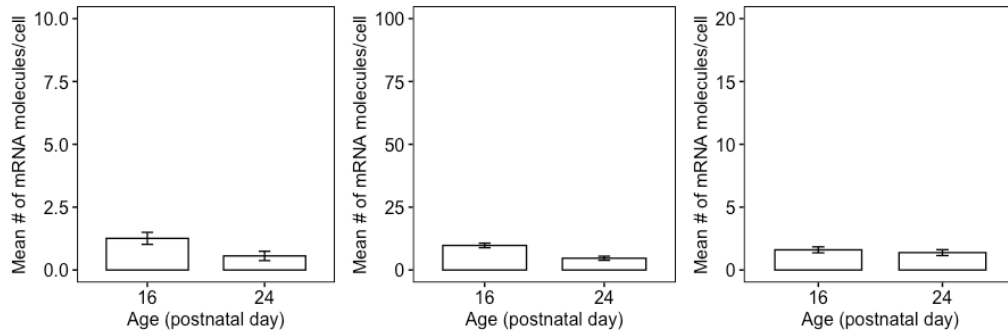


VNTB



LNTB

Polr2A PPIB UBC



SPN

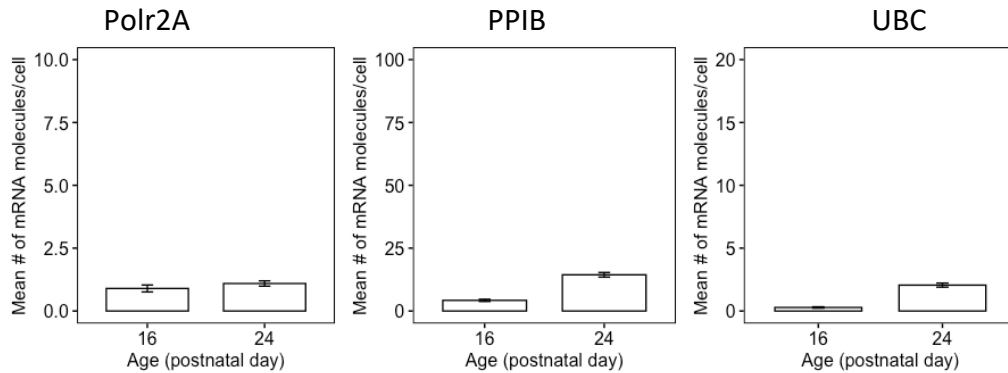


Figure 3: Mean mRNA/cell for positive control probes, Polr2A, PPIB, and UBC, in Litter 1 rat SOC nuclei from P0 to P28. There was a statistically significant difference in median Polr2A expression across ages in the MNTB, LSO, MSO, and SPN ($p < 0.05$ on Kruskal-Wallis Test). With PPIB expression, there were statistically significant differences across ages in all nuclei ($p < 0.05$ on Kruskal-Wallis Test). With UBC expression, there were significant differences across ages in the MNTB, VNTB, LSO, MSO, and SPN ($p < 0.05$ on Kruskal-Wallis Test). There were statistically significant differences in all three probes in expression between most ages ($p < 0.05$ on Paired Wilcoxon Rank Sum Test) (Tables 2-7). Error bars are mean \pm SEM. MNTB cell counts: P0 = 230, P4 = 230, P8 = 278, P12 = 649, P16 = 111, P20 = 47, P24 = 249, and P28 = 178. LSO cell counts: P0 = 392, P12 = 444, P16 = 713, P20 = 157, P24 = 690, and P28 = 436. MSO cell counts: P16 = 28, P24 = 37, and P28 = 107. VNTB cell counts: P16 = 31 and P24 = 68. LNTB cell counts: P16 = 59 and P24 = 34. SPN cell counts: P16 = 146, and P24 = 256.

Table 2. Age-related changes in median positive control mRNA expression in the MNTB of Litter 1 rats. The following symbols, + (Polr2A), o (PPIB), ∇ (UBC), indicate a significant relationship between two ages ($p < 0.05$ on Paired Wilcoxon Rank Sum Test) for the corresponding mRNA.

Age	P0	P4	P8	P12	P16	P20	P24
P4	+o∇						
P8	+o∇	+o∇					
P12	+o∇	+o∇	+o∇				
P16	+o∇	+o∇	+o∇	+o∇			
P20	+o∇	+o∇	+∇	∇	+o∇		
P24	+o∇	+o∇	+o∇	+∇	o∇	o	
P28	+o∇	+o∇	+o∇	+o∇	o	+o∇	+o∇

Table 3. Age-related changes in median positive control mRNA expression in the LSO of Litter 1 rats. The following symbols, + (Polr2A), o (PPIB), ∇ (UBC), indicate a significant relationship between two ages ($p < 0.05$ on Paired Wilcoxon Rank Sum Test) for the corresponding mRNA.

Age	P0	P12	P16	P20	P24
P12	+o∇				
P16	+o∇	+o∇			
P20	+∇	o∇	+o		
P24	+o∇	+o∇	o	+o	
P28	+o	+o∇	+o∇	+o∇	+o∇

Table 4. Age-related changes in median positive control mRNA expression in the MSO of Litter 1 rats. The following symbols, + (Polr2A), o (PPIB), ∇ (UBC), indicate a significant relationship between two ages ($p < 0.05$ on Paired Wilcoxon Rank Sum Test) for the corresponding mRNA.

Age	P16	P24
P24		
P28	+o∇	+o∇

Table 5. Age-related changes in median positive control mRNA expression in the VNTB of Litter 1 rats. The following symbols, + (Polr2A), o (PPIB), ∇ (UBC), indicate a significant

relationship between two ages ($p < 0.05$ on Paired Wilcoxon Rank Sum Test) for the corresponding mRNA.

Age	P16
P24	○▽

Table 6. Age-related changes in median positive control mRNA expression in the LNTB of Litter 1 rats. The following symbols, + (Polr2A), ○ (PPIB), ▽ (UBC), indicate a significant relationship between two ages ($p < 0.05$ on Paired Wilcoxon Rank Sum Test) for the corresponding mRNA.

Age	P16
P24	○

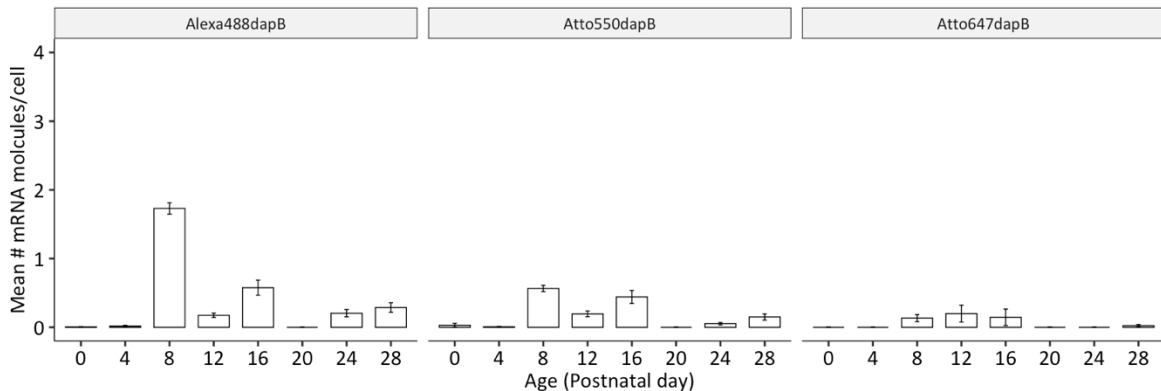
Table 7. Age-related changes in median positive control mRNA expression in the SPN of Litter 1 rats. The following symbols, + (Polr2A), ○ (PPIB), ▽ (UBC), indicate a significant relationship between two ages ($p < 0.05$ on Paired Wilcoxon Rank Sum Test) for the corresponding mRNA.

Age	P16
P24	+○▽

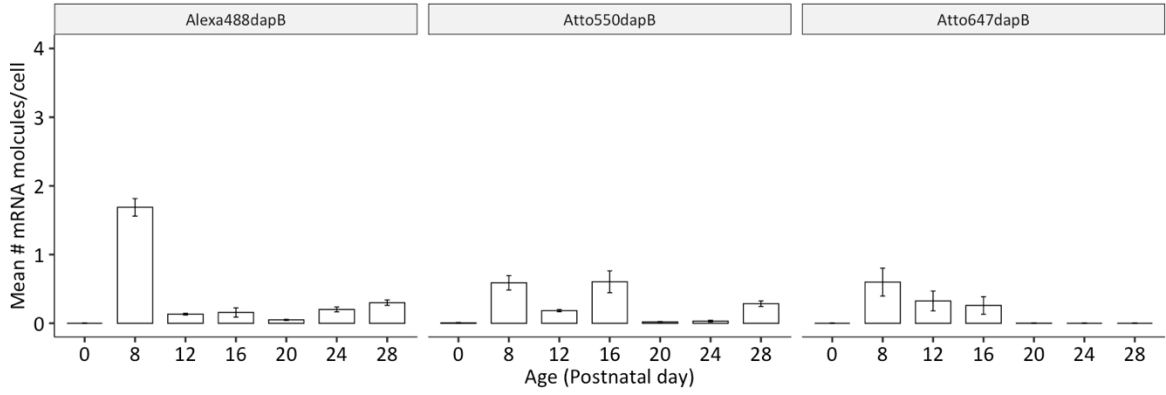
Litter 1 negative control probe expression

For negative control probe expression (dapB) in litter 1, there were also significant differences across ages in the MNTB and the LSO in all 3 fluorophore channels, in the VNTB in Alexa 488 and Atto 550, in the SPN in Atto 550 and Atto 647, and the LNTB in Atto 550 (Figure 4). There were statistically significant differences in median dapB expression between most ages (Tables 8-13).

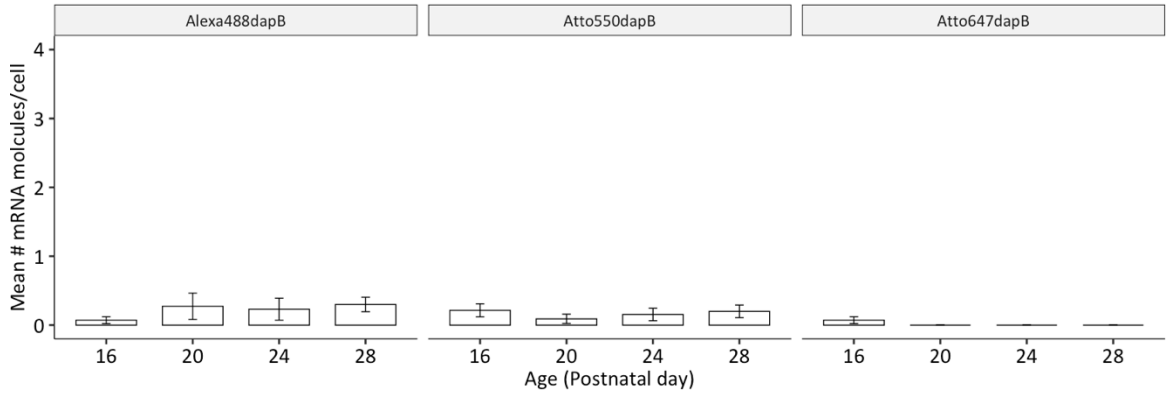
MNTB



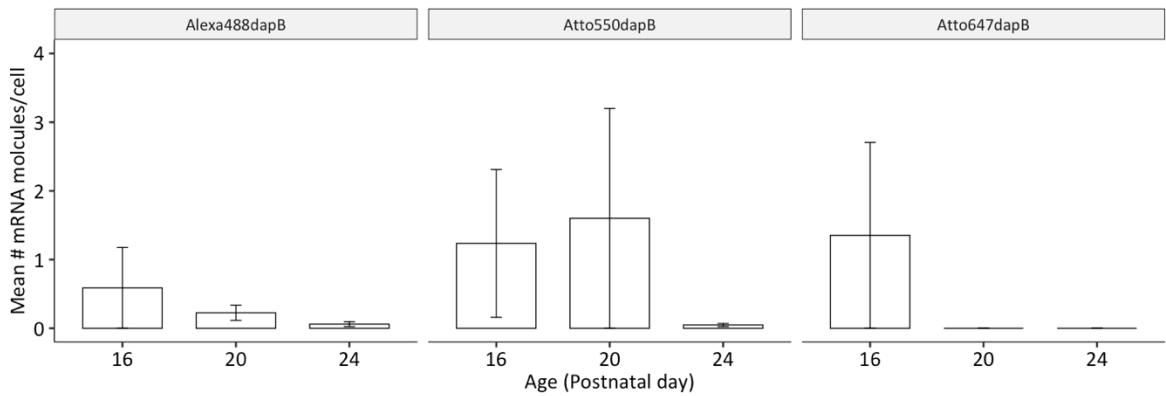
LSO



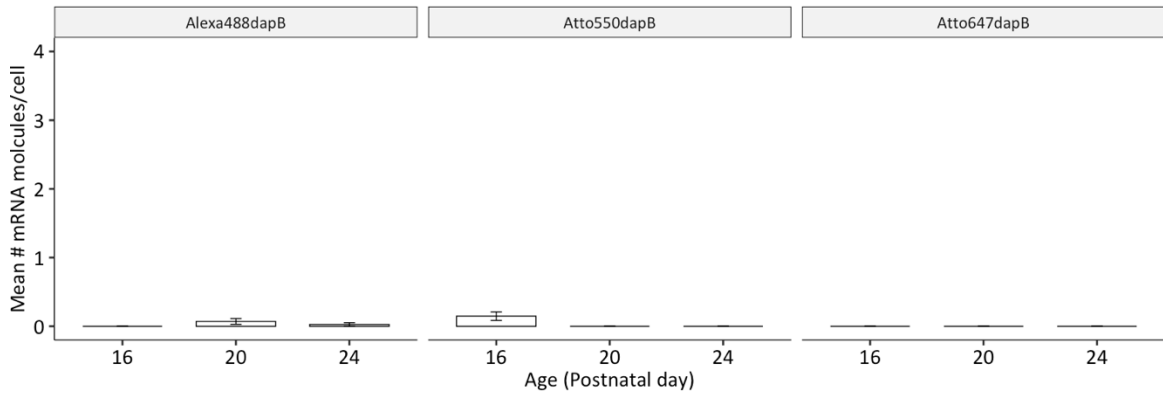
MSO



VNTB



LNTB



SPN

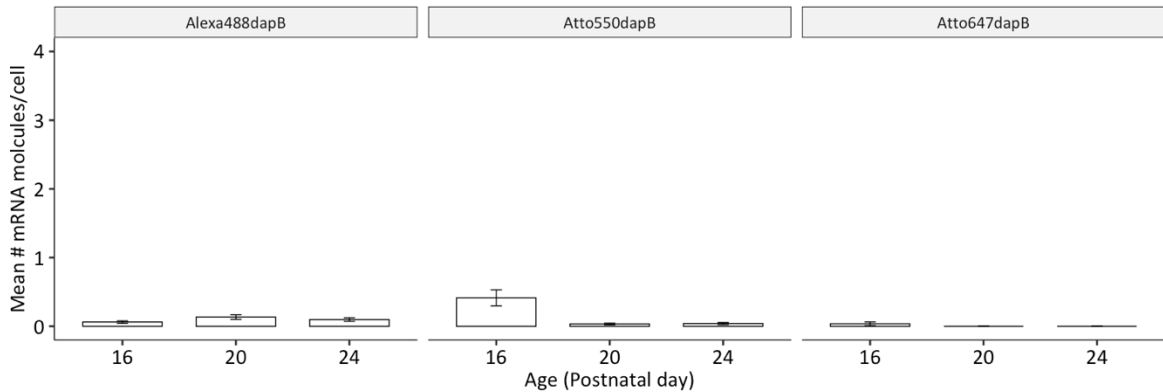


Figure 4: Mean mRNA/cell for negative control probes, dapB, in Litter 1 rat SOC nuclei from P0 to P28. There were significant differences across ages in the MNTB and the LSO in all 3 fluorophore channels, in the VNTB in Alexa 488 (left) and Atto 550 (middle), in the SPN in Atto 550 and Atto 647 (right), and the LNTB in Atto 550 ($p < 0.05$ on Kruskal-Wallis Test). There were statistically significant differences in median dapB expression between most ages ($p < 0.05$ on Paired Wilcoxon Rank Sum Test). Error bars are mean \pm SEM. MNTB cell counts: P0: 212, P4 = 290, P8 = 466, P12 = 534, P16 = 118, P20 = 100, P24 = 152, and P28 = 87. LSO cell counts: P0 = 532, P8 = 766, P12 = 1020, P16 = 522, P20 = 821, P24 = 572, and P28 = 204. MSO cell counts: P16 = 28, P20 = 33, P24 = 26, and P28 = 20. VNTB cell counts: P16 = 51, P20 = 40, and P24 = 84. LNTB cell counts: P16 = 34, P20 = 57, and P24 = 39. SPN cell counts: P16 = 196, P20 = 239, and P24 = 154.

Table 8. Age-related changes in median negative control mRNA expression in the MNTB of Litter 1 rats. The number of “+” indicates the number of channels that had a significant difference in median dapB expression between 2 given ages ($p < 0.05$ on Paired Wilcoxon Rank Sum Test).

Age	P0	P4	P8	P12	P16	P20	P24
P4							
P8	+++	+++					
P12	+++	+++	++				
P16	++	+++	+	++			
P20			++	++	++		
P24	+	+	+++		++	+	
P28	++	++	++			++	

Table 9. Age-related changes in median negative control mRNA expression in the LSO of Litter 1 rats. The number of “+” indicates the number of channels that had a significant difference in median dapB expression between 2 given ages ($p < 0.05$ on Paired Wilcoxon Rank Sum Test).

Age	P0	P8	P12	P16	P20	P24
P8	+++					
P12	+++	++				
P16	+++	+	++			
P20	+	+++	+++	++		
P24	+	+++	++	++	+	
P28	++	++	++	+	++	++

Table 10. Age-related changes in median negative control mRNA expression in the MSO of Litter 1 rats. The number of “+” indicates the number of channels that had a significant difference in median dapB expression between 2 given ages ($p < 0.05$ on Paired Wilcoxon Rank Sum Test).

Age	P16	P20	P24
P20			
P24			
P28			

Table 11. Age-related changes in median negative control mRNA expression in the VNTB of Litter 1 rats. The number of “+” indicates the number of channels that had a

significant difference in median dapB expression between 2 given ages ($p < 0.05$ on Paired Wilcoxon Rank Sum Test).

Age	P16	P20
P20		
P24	+	

Table 12. Age-related changes in median negative control mRNA expression in the LNTB of Litter 1 rats.

Age	P16	P20
P20	+	
P24	+	

Table 13. Age-related changes in median negative control mRNA expression in the SPN of Litter 1 rats. The number of “+” indicates the number of channels that had a significant difference in median dapB expression between 2 given ages ($p < 0.05$ on Paired Wilcoxon Rank Sum Test).

Age	P16	P20
P20	+	
P24	+	

Litter 2 positive control probe expression

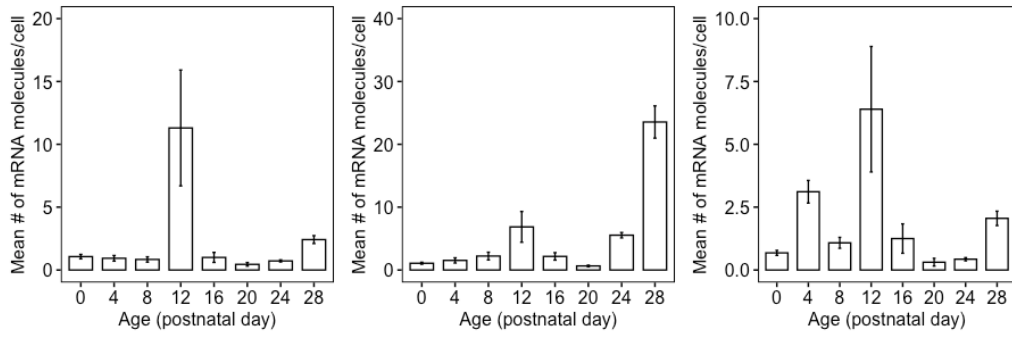
With the positive control probe expression in litter 2, there was a significant difference in median Polr2A, PPIB, and UBC expression across ages, in all nuclei (Figure 5). There were statistically significant differences in expression between most ages (Tables 14-19).

MNTB

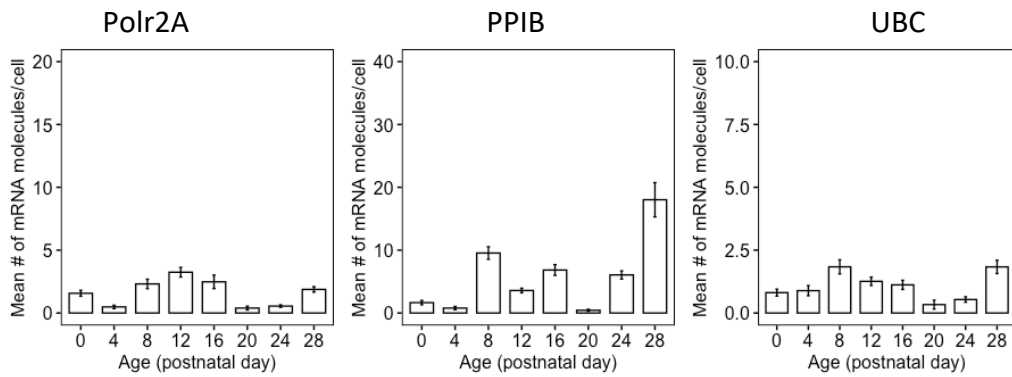
Polr2A

PPIB

UBC



LNTB



SPN

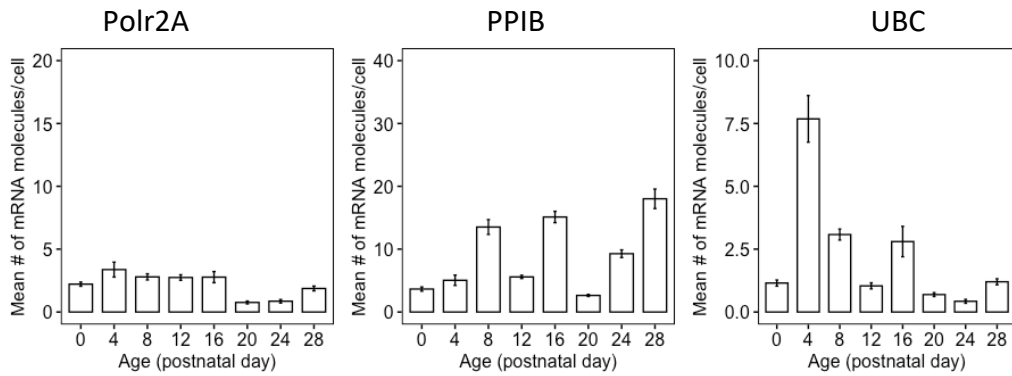


Figure 5: Mean mRNA/cell for positive control probes, Polr2A, PPIB, and UBC, in Litter 2 rat SOC nuclei from P0 to P28. There was a significant difference in median Polr2A, PPIB,

and UBC expression across ages, in all nuclei ($p < 0.05$ on Kruskal-Wallis Test). There were statistically significant differences in expression between most ages ($p < 0.05$ on Paired Wilcoxon Rank Sum Test). Error bars are mean \pm SEM. MNTB cell counts: P0: 166, P4 = 354, P8 = 542, P12 = 553, P16 = 517, P20 = 528, P24 = 360, and P28 = 539. LSO cell counts: P0 = 211, P4 = 438, P8 = 507, P12 = 795, P16 = 981, P20 = 935, P24 = 882, and P28 = 879. MSO cell counts: P0 = 29, P4 = 61, P8 = 55, P12 = 22, P16 = 79, P20 = 47, P24 = 78, and P28 = 60. VNTB cell counts: P0 = 91, P4 = 44, P8 = 37, P12 = 43, P16 = 48, P20 = 100, P24 = 119, and P28 = 93. LNTB cell counts: P0 = 37, P4 = 27, P8 = 61, P12 = 77, P16 = 67, P20 = 105, P24 = 69, and P28 = 90. SPN cell counts: P0 = 126, P4 = 249, P8 = 185, P12 = 254, P16 = 323, P20 = 244, P24 = 167, and P28 = 218.

Table 14. Age-related changes in median positive control mRNA expression in the MNTB of Litter 2 rats. The following symbols, + (Polr2A), o (PPIB), ∇ (UBC), indicate a significant relationship between two ages ($p < 0.05$ on Paired Wilcoxon Rank Sum Test) for the corresponding mRNA.

Age	P0	P4	P8	P12	P16	P20	P24
P4	o ∇						
P8	o ∇	o ∇					
P12	o ∇	∇	o ∇				
P16	o	+o ∇	+ ∇	+o ∇			
P20	+ ∇	+o ∇	+o ∇	+o	+o ∇		
P24	+o ∇	+ ∇	+o ∇	+ ∇	+o ∇	+o ∇	
P28	o	+o ∇	+o ∇	+o ∇	o ∇	+o ∇	+o ∇

Table 15. Age-related changes in median positive control mRNA expression in the LSO of Litter 2 rats. The following symbols, + (Polr2A), o (PPIB), ∇ (UBC), indicate a significant relationship between two ages ($p < 0.05$ on Paired Wilcoxon Rank Sum Test) for the corresponding mRNA.

Age	P0	P4	P8	P12	P16	P20	P24
P4	+o ∇						
P8	o ∇	+o					
P12	o	+o ∇	o ∇				
P16	o	+ ∇	+ ∇	+o ∇			
P20	+o ∇						
P24	+o ∇	o ∇	+o ∇	+ ∇	+o ∇	+o ∇	
P28	o ∇	+o ∇	o ∇	o ∇	+o	+o ∇	+o ∇

Table 16. Age-related changes in median positive control mRNA expression in the MSO of Litter 2 rats. The following symbols, + (Polr2A), o (PPIB), ∇ (UBC), indicate a significant relationship between two ages ($p < 0.05$ on Paired Wilcoxon Rank Sum Test) for the corresponding mRNA.

Age	P0	P4	P8	P12	P16	P20	P24
P4	∇						
P8	o∇	o					
P12	+o	+o∇	∇				
P16	o	o∇	∇	+			
P20	+o∇	+∇	+o∇	+o	+o∇		
P24	+∇	+o∇	+∇	+	o∇	o	
P28	o	o∇	∇	+		+o∇	o∇

Table 17. Age-related changes in median positive control mRNA expression in the VNTB of Litter 2 rats. The following symbols, + (Polr2A), o (PPIB), ∇ (UBC), indicate a significant relationship between two ages ($p < 0.05$ on Paired Wilcoxon Rank Sum Test) for the corresponding mRNA.

Age	P0	P4	P8	P12	P16	P20	P24
P4	∇						
P8		∇					
P12	+o	+	+				
P16		∇					
P20	+∇	∇	∇	+o∇	∇		
P24	o	o∇	o∇	+∇	o	+o∇	
P28	o∇	+o	+o	o	+o∇	+o∇	+o∇

Table 18. Age-related changes in median positive control mRNA expression in the LNTB of Litter 2 rats. The following symbols, + (Polr2A), o (PPIB), ∇ (UBC), indicate a significant relationship between two ages ($p < 0.05$ on Paired Wilcoxon Rank Sum Test) for the corresponding mRNA.

Age	P0	P4	P8	P12	P16	P20	P24
P4	+						
P8	o	+o					
P12	o	+o	o				
P16	o	+o					

P20	+o▽	▽	+o▽	+▽	+o▽		
P24	+o	o	+▽	+▽	+	+o▽	
P28	o	+o		▽	o	+o▽	+o▽

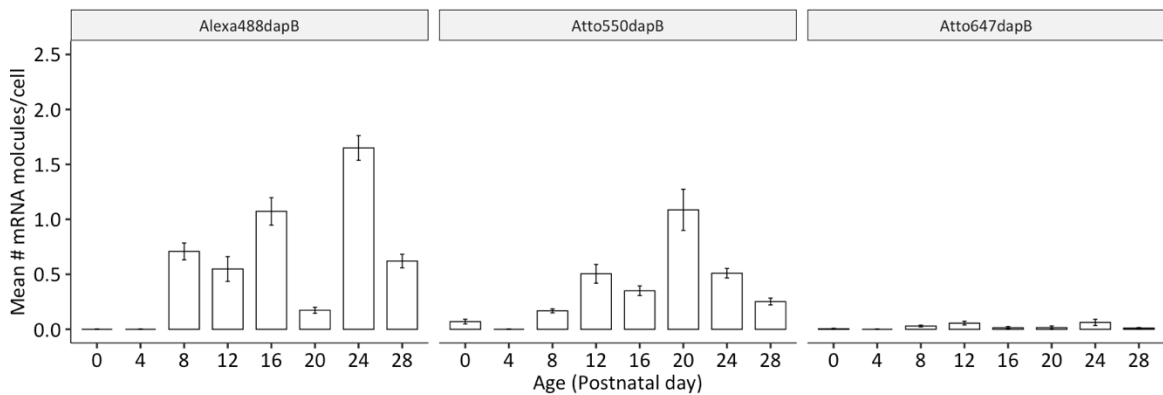
Table 19. Age-related changes in median positive control mRNA expression in the SPN of Litter 2 rats. The following symbols, + (Polr2A), o (PPIB), ▽ (UBC), indicate a significant relationship between two ages ($p < 0.05$ on Paired Wilcoxon Rank Sum Test) for the corresponding mRNA.

Age	P0	P4	P8	P12	P16	P20	P24
P4	▽						
P8	o▽	o▽					
P12	o	o▽	o▽				
P16	+o	+o▽	+▽	+o▽			
P20	+▽	+▽	+o▽	+o	+o▽		
P24	+o▽	+o▽	+▽	+o▽	+o▽	o	
P28	o	+o▽	+▽	+o		+o▽	+o▽

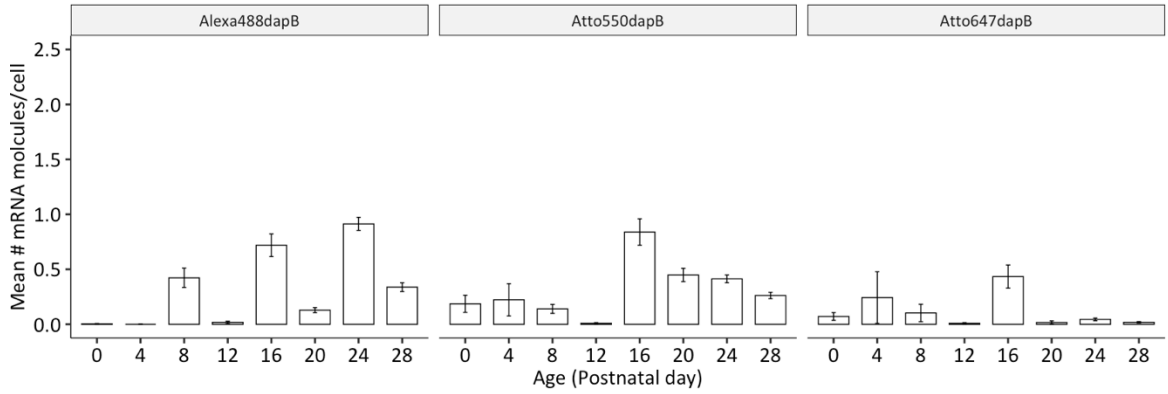
Litter 2 negative control probe expression

In litter 2, there were significant differences across ages in dapB expression in the MNTB and the LSO in all 3 fluorophore channels, and in the VNTB, LNTB, MSO, and SPN in Alexa 488 and Atto 550 (Figure 6). There were statistically significant differences in median dapB expression between most ages (Tables 20-25).

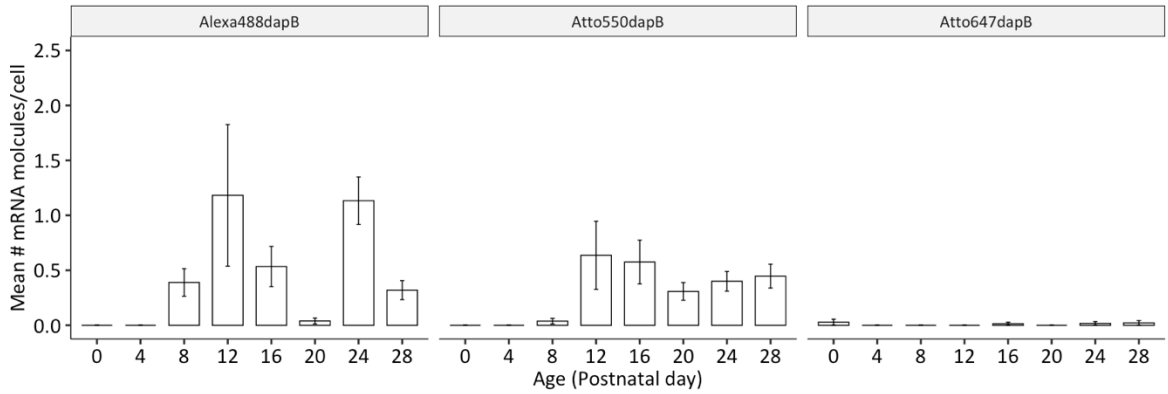
MNTB



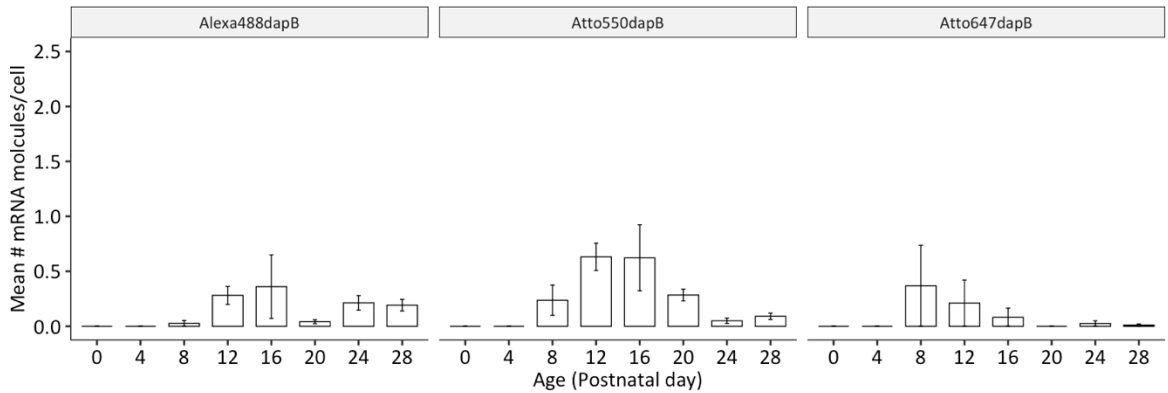
LSO



MSO



VNTB



LNTB

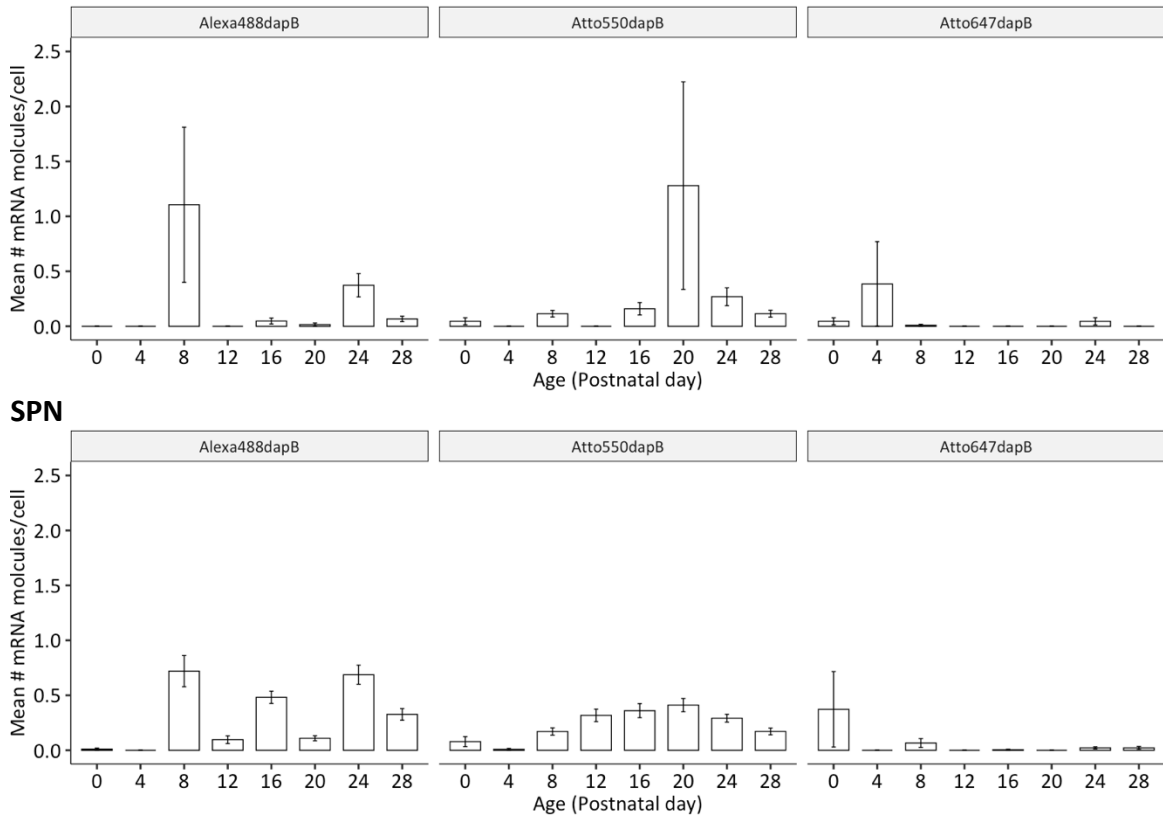


Figure 6: Negative Control (dapB) mRNA expression in Litter 2 rat SOC nuclei. There were statistically significant differences across ages in dapB expression in the MNTB and the LSO in all 3 fluorophore channels, and in the VNTB, LNTB, MSO, and SPN in Alexa 488 (left) and Atto 550 (middle) ($p < 0.05$ on Kruskal-Wallis Test). There were statistically significant differences in median dapB expression between most ages ($p < 0.05$ on Paired Wilcoxon Rank Sum Test). Error bars are mean \pm SEM. MNTB cell counts: P0: 230, P4 = 149, P8 = 586, P12 = 412, P16 = 291, P20 = 405, P24 = 514, and P28 = 461. LSO cell counts: P0 = 296, P4 = 387, P8 = 594, P12 = 234, P16 = 889, P20 = 694, P24 = 702, and P28 = 409. MSO cell counts: P0 = 36, P4 = 23, P8 = 54, P12 = 11, P16 = 73, P20 = 42, P24 = 60, and P28 = 47. VNTB cell counts: P0 = 49, P4 = 28, P8 = 38, P12 = 57, P16 = 61, P20 = 120, P24 = 80, and P28 = 99. LNTB cell counts: P0 = 44, P4 = 26, P8 = 114, P12 = 35, P16 = 63, P20 = 68, P24 = 67, and P28 = 105. SPN cell counts: P0 = 102, P4 = 121, P8 = 182, P12 = 104, P16 = 222, P20 = 202, P24 = 326, and P28 = 187.

Table 20. Age-related changes in median negative control mRNA expression in the MNTB of Litter 2 rats. The number of “+” indicates the number of channels that had a significant difference in median dapB expression between 2 given ages ($p < 0.05$ on Paired Wilcoxon Rank Sum Test).

Age	P0	P4	P8	P12	P16	P20	P24
-----	----	----	----	-----	-----	-----	-----

P4							
P8	+	+					
P12	+	+	+				
P16	+	+	+	+			
P20			+	+	+		
P24	+	+	+		+	+	
P28	+	+	+				+

Table 21. Age-related changes in median negative control mRNA expression in the LSO of Litter 2 rats. The number of “+” indicates the number of channels that had a significant difference in median dapB expression between 2 given ages ($p < 0.05$ on Paired Wilcoxon Rank Sum Test).

Age	P0	P4	P8	P12	P16	P20	P24
P4							
P8	+	++					
P12			++				
P16	++	+++	+	++			
P20	+++	++	++	++	+++		
P24	++	++	++	++	+	+	
P28	++	++	+	++		+	+

Table 22. Age-related changes in median negative control mRNA expression in the MSO of Litter 2 rats. The number of “+” indicates the number of channels that had a significant difference in median dapB expression between 2 given ages ($p < 0.05$ on Paired Wilcoxon Rank Sum Test).

Age	P0	P4	P8	P12	P16	P20	P24
P4							
P8							
P12	++	+	+				
P16	++		+				
P20	++		+	+	+		
P24	++	+	+			+	
P28	++		+				

Table 23. Age-related changes in median negative control mRNA expression in the VNTB of Litter 2 rats. The number of “+” indicates the number of channels that had a significant difference in median dapB expression between 2 given ages ($p < 0.05$ on Paired Wilcoxon Rank Sum Test).

Age	P0	P4	P8	P12	P16	P20	P24
P4							
P8							
P12	++	+					
P16	+						
P20	+			+			
P24				+	+	+	
P28				+			

Table 24. Age-related changes in median negative control mRNA expression in the LNTB of Litter 2 rats. The number of “+” indicates the number of channels that had a significant difference in median dapB expression between 2 given ages ($p < 0.05$ on Paired Wilcoxon Rank Sum Test).

Age	P0	P4	P8	P12	P16	P20	P24
P4							
P8							
P12							
P16							
P20							
P24	+					+	
P28							+

Table 25. Age-related changes in median negative control mRNA expression in the SPN of Litter 2 rats. The number of “+” indicates the number of channels that had a significant difference in median dapB expression between 2 given ages ($p < 0.05$ on Paired Wilcoxon Rank Sum Test).

Age	P0	P4	P8	P12	P16	P20	P24
P4							
P8	+	++					
P12	+	+	+				
P16	++	++		+			
P20	+	++	+		+		
P24	++	++		+		+	
P28	+	++	+	+		+	+

Development of NMDAR subunits in immature auditory brainstem nuclei

The differences in subunit mRNA expression from P0 to P28 for GluN1, GluN2-A, -B, -C, and -D in each nucleus are summarized in table and graph form for each litter. The GluN1 immunohistochemistry data are summarized in graph form.

MNTB

GluN1 mRNA

In litter 1, the mean GluN1 mRNA/cell was highest at P0 and decreased towards P28 (Figure 7). There was a statistically significant difference in median GluN1 mRNA/cell in the MNTB at different ages: $\chi^2(6) = 1598.85$, $p = 0$, with statistically significant differences between all ages (Table 26)

In litter 2, the mean GluN1 mRNA/cell peaked at P16 (Figure 8). There was a statistically significant difference in median GluN1 mRNA/cell in the MNTB at different ages $\chi^2(7) = 1440.907$, $p = 5.43e^{-307}$, with significant differences between most ages (Table 27)

GluN2A mRNA

In litter 1, the mean GluN2A mRNA/cell peaked at P12 (Figure 7). There was a statistically significant difference in median GluN2A mRNA/cell in the MNTB at different ages: $\chi^2(6) = 786.64$, $p = 1.18e^{-166}$, with statistically significant differences between most ages (Table 26).

In litter 2, the mean GluN2A mRNA levels were relatively low from P0 to P28 (Figure 8). There was a statistically significant difference in median GluN2A mRNA/cell in the MNTB at different ages $\chi^2(7) = 1035.60$, $p = 2.44e^{-219}$, with statistically significant differences between most ages (Table 27).

GluN2B mRNA

In litter 1, the mean GluN2B mRNA/cell appeared relatively constant from P0 to P28 (Figure 7). There was a statistically significant difference in median GluN2B mRNA/cell in the MNTB at different ages: $\chi^2(6) = 682.28$, $p = 4.09e^{-144}$, with statistically significant differences between most of the ages (Table 26).

In litter 2, the mean GluN2B mRNA/cell levels were relatively moderate from P0 to P28 (Figure 8). There was a statistically significant difference in median GluN2B mRNA/cell in the MNTB at different ages $\chi^2(7) = 99.03$, $p = 1.71e^{-18}$, with statistically significant differences between approximately half of the ages (Table 27).

GluN2C mRNA

In litter 1, the mean GluN2C mRNA/cell peaked at P0 (Figure 7). There was a statistically significant difference in median GluN2C mRNA/cell in the MNTB at different ages: $\chi^2(6) = 543.96$, $p = 2.83e^{-114}$, with statistically significant differences between most of the ages (Table 26).

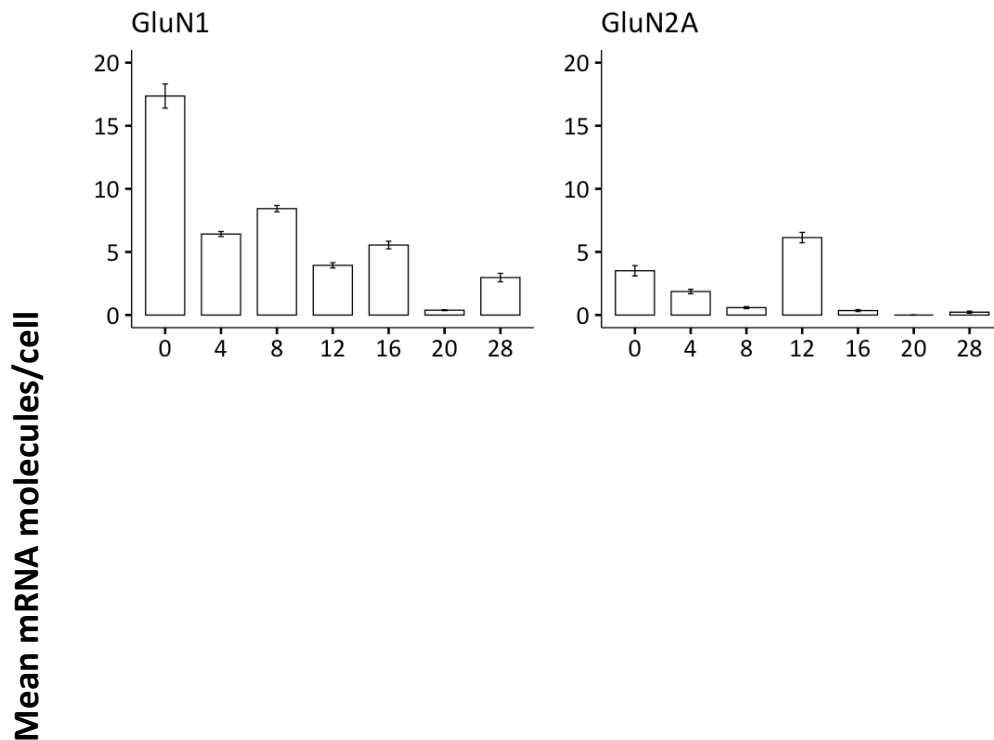
In litter 2, the mean GluN2C mRNA levels were relatively low from P0 to P28 (Figure 8). There was a statistically significant difference in median GluN2C mRNA/cell in

the MNTB at different ages $\chi^2(7) = 421.00$, $p = 7.44e^{-87}$, with statistically significant differences between most ages (Table 27).

GluN2D mRNA

In litter 1, the mean GluN2D mRNA/cell peaked at P8 (Figure 7). There was a statistically significant difference in median GluN2D mRNA/cell in the MNTB at different ages: $\chi^2(6) = 549.08$, $p = 2.23e^{-115}$, with statistically significant differences between most of the ages (Table 26).

In litter 2, the mean GluN2D mRNA/cell peaked at P16 (Figure 8). There was a statistically significant difference in median GluN2D mRNA/cell in the MNTB at different ages $\chi^2(7) = 1547.243$, $p = 0$, with statistically significant differences between most ages (Table 27).



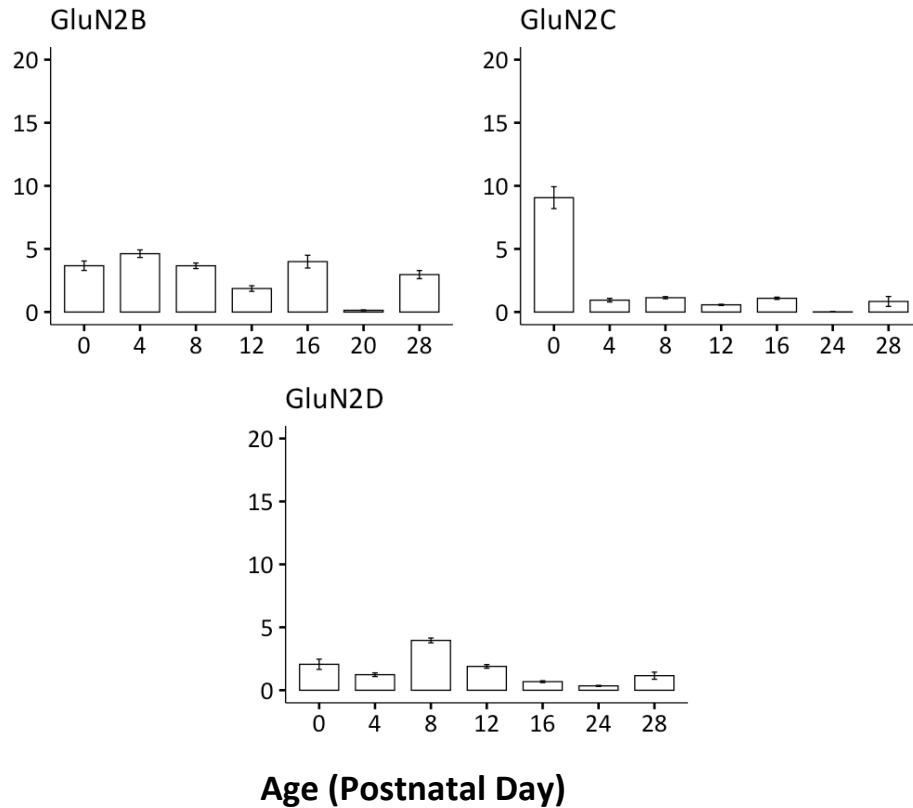


Figure 7: Mean NMDAR subunit mRNA molecules/cell in the MNTB of Litter 1 rats. Error bars are mean +/- SEM. Mean GluN1 mRNA/cell was highest at P0 and decreased towards P28. Mean GluN2A mRNA/cell peaked at P12. Mean GluN2B mRNA/cell appeared relatively constant from P0 to P28. Mean GluN2C mRNA/cell peaked at P0. Mean GluN2D mRNA/cell peaked at P8. Number of MNTB cells in SOC sections with GluN1/GluN2A/GluN2B probe solution: P0 = 85 in section 1 and 205 in section 2, P4 = 451 in section 1 and 344 in section 2, P8 = 521 in section 1 and 296 in section 2, P12 = 529 in section 1 and 884 in section 2, P16 = 107 in section 1 and 125 in section 2, P20 = 150 in section 1 and 153 in section 2, P24 = 378, P28 = 159 in section 1 and 106 in section 2. Number of MNTB cells in SOC sections with GluN1/GluN2C/GluN2D probe solution: P0 = 78 in section 1 and 131 in section 2, P4 = 386 in section 1 and 284 in section 2, P8 = 628 in section 1 and 533 in section 2, P12 = 309, P16 = 172 in section 1 and 224 in section 2, P24 = 189 in section 1 and 218 in section 2, P28 = 136.

Table 26. Age-related changes in median NMDAR subunit mRNA expression in the MNTB of Litter 1 rats. The following symbols, 1 (GluN1), A (GluN2A), B (GluN2B), C (GluN2C), and D (GluN2D) indicate a significant relationship between the two ages ($p < 0.05$ on Paired Wilcoxon Rank Sum Test) for the corresponding subunit mRNA. Note: No data for GluN1, GluN2A and GluN2B mRNA for P24, and no data for GluN2C and GluN2D mRNA for P20.

Age	P0	P4	P8	P12	P16	P20	P24
P4	1ABCD						
P8	1ABCD	1ABCD					
P12	1ABCD	1ABD	1ABCD				
P16	1ACD	1ABCD	1ABD	1ABCD			
P20	1AB	1AB	1AB	1AB	1AB		
P24	CD	CD	CD	CD	CD		
P28	1ACD	1ABC	1ABCD	1ABCD	1C	1AB	CD

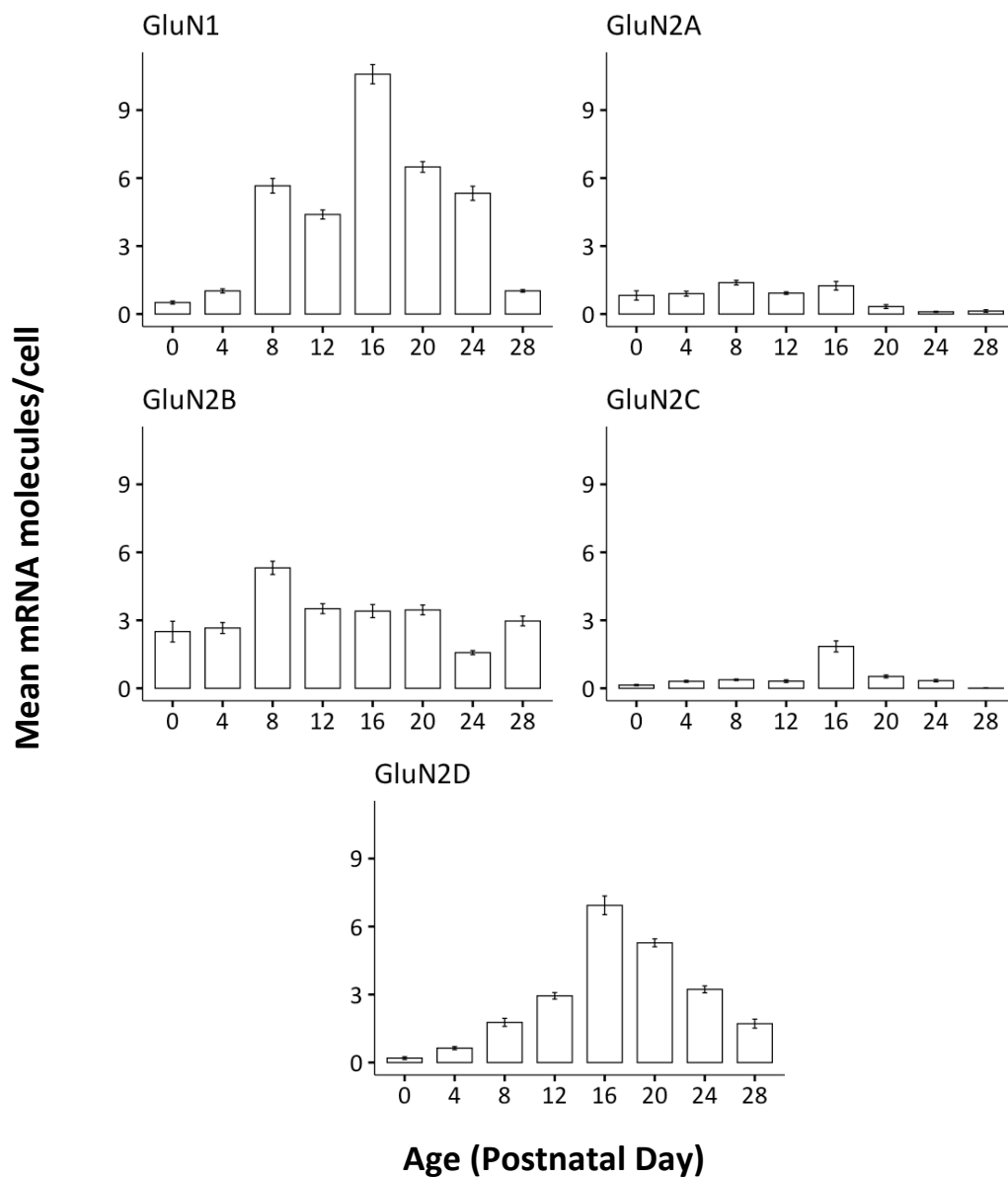


Figure 8: Mean NMDAR subunit mRNA expression/cell in the MNTB of Litter 2 rats. Error bars are mean +/- SEM. Mean GluN1 mRNA/cell peaked at P16. Mean GluN2A mRNA levels were relatively low from P0 to P28. Mean GluN2B mRNA/cell levels were relatively moderate from P0 to P28. Mean GluN2C mRNA levels were relatively low from P0 to P28. Mean GluN2D mRNA/cell peaked at P16. Number of MNTB cells in SOC sections with GluN1/GluN2A/GluN2B probe solution: P0 = 142 in section 1 and 70 in section 2, P4 = 225 in section 1 and 284 in section 2, P8 = 411 in section 1 and 310 in section 2, P12 = 522 in section 1 and 535 in section 2, P16 = 490 in section 1 and 344 in section 2, P20 = 713 in section 1 and 469 in section 2, P24 = 501 in section 1 and 569 in section 2, P28 = 415 in section 1 and 601 in section 2. Number of MNTB cells in SOC sections with GluN1/GluN2C/GluN2D probe solution: P0 = 257 in section 1 and 98 in section 2, P4 = 140 in section 1 and 256 in section 2, P8 = 425 in section 1 and 338 in section 2, P12 = 408 in section 1 and 482 in section 2, P16 = 502 in section 1 and 370 in section 2, P24 = 469 in section 1 and 827 in section 2, P28 = 394 in section 1 and 484 in section 2.

Table 27. Age-related changes in median NMDAR subunit mRNA expression in the MNTB of Litter 2 rats. The following symbols, 1 (GluN1), A (GluN2A), B (GluN2B), C (GluN2C), and D (GluN2D) indicate a significant relationship between the two ages ($p < 0.05$ on Paired Wilcox Rank Sum Test) for the corresponding subunit mRNA.

Age	P0	P4	P8	P12	P16	P20	P24
P4	CD						
P8	1BCD	1ABD					
P12	1D	1D	ABCD				
P16	1ACD	1ACD	1ABCD	1ACD			
P20	1ACD	1AD	1ABD	1ABCD	1ABC		
P24	1ACD	1ABD	ABD	AC	1ACD	1BD	
P28	1ACD	1AC	1ABCD	1ACD	1ACD	1ABCD	1ACD

LSO

GluN1 mRNA

In litter 1, the mean GluN1 mRNA/cell peaked at P0 (Figure 9). There was a statistically significant difference in median GluN1 mRNA/cell in the LSO at different ages $\chi^2(6) = 4780.342$, $p = 0$, with statistically significant differences between most ages (Table 28).

In litter 2, the mean GluN1 mRNA/cell at P0 was low, increased from P4 to P24, and fell back to low levels at P28 (Figure 10). There was a statistically significant difference in median GluN1 mRNA/cell in the LSO at different ages $\chi^2(7) = 1695.95$, $p = 0$, with statistically significant differences between most ages (Table 29).

GluN2A mRNA

In litter 1, the mean GluN2A mRNA/cell peaked at P0 (Figure 9). There was a statistically significant difference in median GluN2A mRNA/cell in the LSO at different ages $\chi^2(6) = 2485.25$, $p = 0$, with statistically significant differences between most ages (Table 28).

In litter 2, the mean GluN2A mRNA levels peaked at P8 (Figure 10). There was a statistically significant difference in median GluN2A mRNA/cell in the LSO at different ages $\chi^2(7) = 1040.77$, $p = 1.86e^{-220}$, with statistically significant differences between most ages (Table 29).

GluN2B mRNA

In litter 1, the mean GluN2B mRNA/cell was relatively constant from P0 to P28 (Figure 9). There was a statistically significant difference in median GluN2B mRNA/cell in the LSO at different ages $\chi^2(6) = 1230.38$, $p = 1.27e^{-262}$, with statistically significant differences between most ages (Table 28).

In litter 2, the mean GluN2B mRNA levels peaked at P8 (Figure 10). There was a statistically significant difference in median GluN2B mRNA/cell in the LSO at different ages $\chi^2(7) = 616.53$, $p = 6.70e^{-129}$, with statistically significant differences between most ages (Table 29).

GluN2C mRNA

In litter 1, the mean GluN2C mRNA/cell was relatively constant from P0 to P28 (Figure 9). There was a statistically significant difference in median GluN2C mRNA/cell in the LSO at different ages $\chi^2(6) = 1395.193$, $p = 2.66e^{-298}$. Median GluN2C mRNA/cell was significantly different between all ages except for P4 and P8 ($p = 1.00$), P4 and P16 ($p = 1.00$), and P8 and P16 ($p = .48$) (Table 28)

In litter 2, the mean GluN2C levels peaked from P8 and P16 (Figure 10). There was a statistically significant difference in median GluN2C mRNA/cell in the LSO at different ages $\chi^2(7) = 357.54$, $p = 3.00e^{-73}$, with statistically significant differences between most ages (Table 29).

GluN2D mRNA

In litter 1, the mean GluN2D mRNA/cell was relatively constant from P0 to P28 (Figure 9). There was a statistically significant difference in median GluN2D mRNA/cell in the LSO at different ages $\chi^2(6) = 1235.12$, $p = 1.20e^{-263}$, with statistically significant differences between most ages (Table 28).

In litter 2, the mean GluN2D levels peaked at P16 (Figure 10). There was a statistically significant difference in median GluN2D mRNA/cell in the LSO at different ages $\chi^2(7) = 1294.22$, $p = 2.96e^{-275}$, with statistically significant differences between most ages (Table 29).

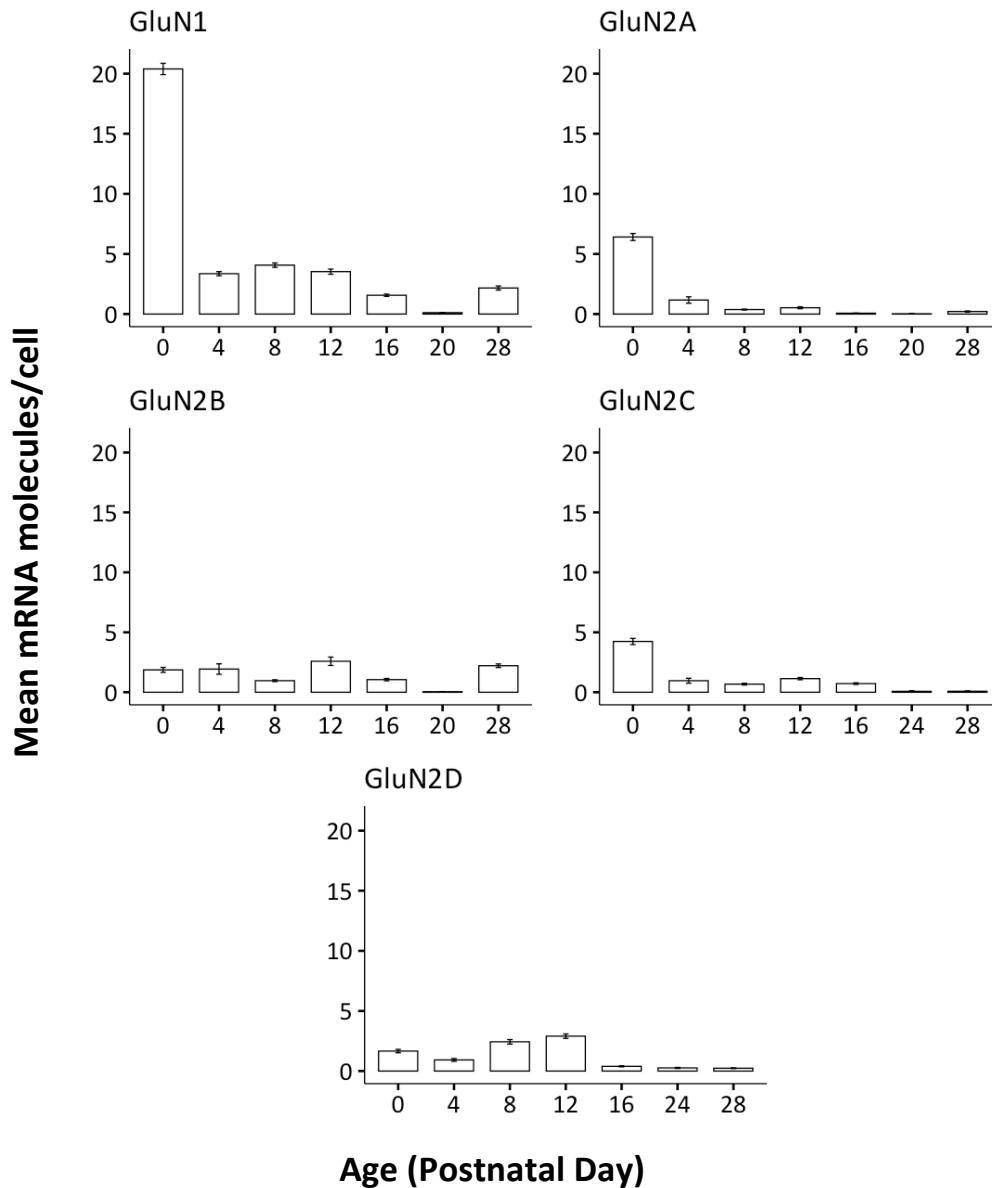


Figure 9: Mean NMDAR subunit mRNA expression/cell in the LSO of Litter 1 rats. Error bars are mean \pm SEM. Mean GluN1 mRNA/cell peaked at P0. Mean GluN2A mRNA/cell peaked at P0. Mean GluN2B mRNA/cell was relatively constant from P0 to P28. Mean GluN2C mRNA/cell was relatively constant from P0 to P28. Mean GluN2D mRNA/cell was relatively constant from P0 to P28. Number of LSO cells in SOC sections with GluN1/GluN2A/GluN2B probe solution: P0 = 344, P4 = 419, P8 = 482 in section 1 and 434 in section 2, P12 = 813, P16 = 434 in section 1 and 721 in section 2, P20 = 825 in section 1 and 917 in section 2, P24 = 273, P28 = 446 in section 1 and 442 in section 2. Number of LSO cells in SOC sections with GluN1/GluN2C/GluN2D probe solution: P0 = 375 in section 1 and 607 in section 2, P4 = 411 in section 1 and 307 in section 2, P8 = 555, P12 = 442,

P16 = 172 in section 1 and 224 in section 2, P24 = 466 in section 1 and 550 in section 2, P28 = 366.

Table 28. Age-related changes in median NMDAR subunit mRNA expression in the LSO of Litter 1 rats. The following symbols, 1 (GluN1), A (GluN2A), B (GluN2B), C (GluN2C), and D (GluN2D) indicate a significant relationship between the two ages ($p < 0.05$ on Paired Wilcoxon Rank Sum Test) for the corresponding subunit mRNA. Note: No data for GluN1, GluN2A, and GluN2B for P24, and no data for GluN2C and GluN2D for P20.

Age	P0	P4	P8	P12	P16	P20	P24
P4	1ABCD						
P8	1ABC	AD					
P12	1ABCD	1AD	1CD				
P16	1ABCD	1ABD	1ABD	1ABCD			
P20	1AB	1AB	1AB	1AB	1AB		
P24	CD	CD	CD	CD	C		
P28	1ACD	1ABCD	1ABCD	1ABCD	1ABC	1AB	C

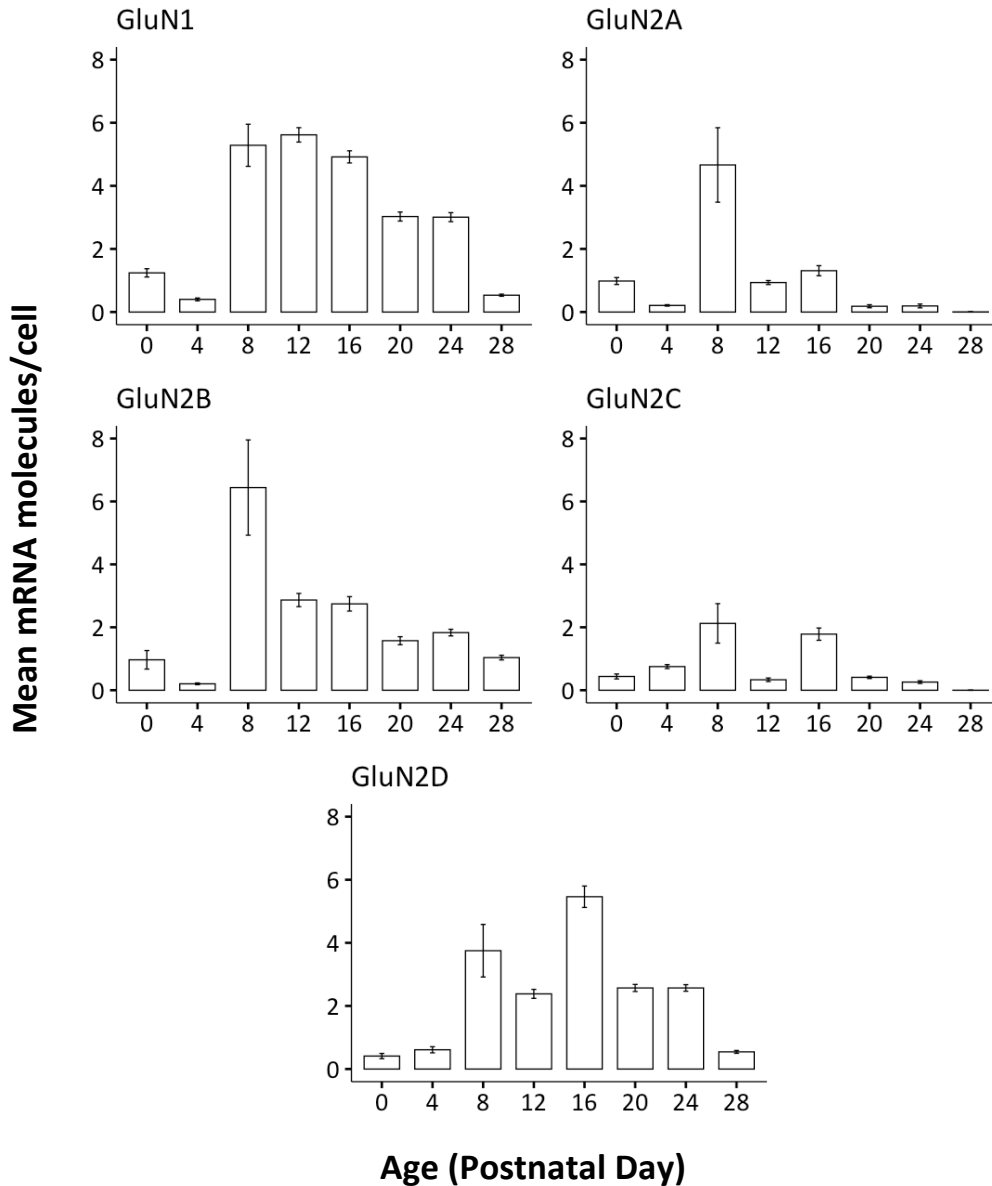


Figure 10: Mean NMDAR subunit mRNA expression/cell in the LSO of Litter 2 rats. Error bars are mean +/- SEM. Mean GluN1 mRNA/cell at P0 was low, increased from P4 to P24, and fell back to low levels at P28. Mean GluN2A mRNA levels peaked at P8. Mean GluN2B mRNA levels peaked at P8. Mean GluN2C levels peaked from P8 and P16. Mean GluN2D levels peaked at P16. Number of LSO cells in SOC sections with GluN1/GluN2A/GluN2B probe solution: P0 = 169 in section 1 and 130 in section 2, P4 = 448 in section 1 and 213 in section 2, P8 = 594 in section 1 and 436 in section 2, P12 = 478 in section 1 and 347 in section 2, P16 = 980 in section 1 and 607 in section 2, P20 = 834 in section 1 and 809 in section 2, P24 = 849 in section 1 and 769 in section 2, P28 = 666 in section 1 and 413 in section 2. Number of LSO cells in SOC sections with

GluN1/GluN2C/GluN2D probe solution: P0 = 274 in section 1 and 185 in section 2, P4 = 322 in section 1 and 354 in section 2, P8 = 665 in section 1 and 413 in section 2, P12 = 468 in section 1 and 358 in section 2, P16 = 980 in section 1 and 607 in section 2, P24 = 809 in section 1 and 587 in section 2, P28 = 383 in section 1 and 490 in section 2.

Table 29. Age-related changes in median GluN1 mRNA expression in the LSO of Litter 2 rats (+ indicates a significant relationship between two ages). The following symbols, 1 (GluN1), A (GluN2A), B (GluN2B), C (GluN2C), and D (GluN2D) indicate a significant relationship between the two ages ($p < 0.05$ on Paired Wilcoxon Rank Sum Test) for the corresponding subunit mRNA.

Age	P0	P4	P8	P12	P16	P20	P24
P4	1ABC						
P8	AD	1ABCD					
P12	1BD	1ABCD	1ABCD				
P16	1ABD	1BCD	1ABD	ABCD			
P20	1ABD	1ABCD	1ABD	1ABCD	1AD		
P24	1ABD	1ABCD	1ABD	1AB	1ABCD	BC	
P28	1ABC	1ABC	1ABCD	1ABCD	1ACD	1ACD	1ABCD

MSO

GluN1 mRNA

In litter 1, the mean GluN1 mRNA/cell peaked at P4 (Figure 11). There was a statistically significant difference in median GluN1 mRNA/cell at different ages $\chi^2(4) = 56.81$, $p = 1.36e^{-11}$ (Table 30)

In litter 2, the mean GluN1 mRNA/cell in the MSO stayed constant from birth to P24, with a slight increase from P8 to P20, before decreasing at P28 (Figure 12). There was a statistically significant difference in median GluN1 mRNA/cell in the MSO at different ages $\chi^2(7) = 93.20$, $p = 2.72e^{-17}$, with statistically significant differences between approximately half of the ages (Table 31).

GluN2A mRNA

In litter 1, the mean GluN2A mRNA/cell peaked from P4-P12 (Figure 11). There was a statistically significant difference in median GluN2A mRNA/cell at different ages $\chi^2(4) = 129.80$, $p = 4.29e^{-27}$, with statistically significant differences between most ages (Table 30).

In litter 2, the mean GluN2A mRNA levels were relatively low from P0 to P28 (Figure 12). There was a statistically significant difference in median GluN2A mRNA/cell at different ages $\chi^2(7) = 180.03$, $p = 1.92e^{-35}$, with statistically significant differences between most ages (Table 31).

GluN2B mRNA

In litter 1, the mean GluN2B mRNA/cell peaked at P4 (Figure 11). There was a statistically significant difference in median GluN2B mRNA/cell in the MSO at different ages $\chi^2(4) = 69.04$, $p = 3.62e^{-14}$, with statistically significant differences between most ages (Table 30).

In litter 2, the mean GluN2B mRNA levels peaked at P24 (Figure 12). There was a statistically significant difference in median GluN2B mRNA/cell in the MSO at different ages $\chi^2(7) = 30.62$, $p = 7.30e^{-5}$, with statistically significant differences between a small proportion of ages (Table 31).

GluN2C mRNA

In litter 1, the mean GluN2C mRNA/cell was relatively constant from P0 to P28 (Figure 11). There was a statistically significant difference in median GluN2C mRNA/cell in the MSO at different ages $\chi^2(3) = 52.52$, $p = 2.32e^{-11}$, with statistically significant differences between only a few ages (Table 30).

In litter 2, the mean GluN2C mRNA levels were low from P0 to P28 (Figure 12). There was a statistically significant difference in median GluN2C mRNA/cell in the MSO at different ages $\chi^2(7) = 68.35$, $p = 3.17e^{-12}$, with statistically significant differences between approximately half of the ages (Table 31).

GluN2D mRNA

In litter 1, the mean GluN2D mRNA/cell was relatively constant from P0 to P28 (Figure 11). There was not a statistically significant difference in median GluN2D mRNA/cell in the MSO at different ages $\chi^2(3) = 3.76$, $p = .29$ (Table 30).

In litter 2, the mean GluN2D mRNA levels peaked at P16 (Figure 12). There was a statistically significant difference in median GluN2D mRNA/cell in the MSO at different ages $\chi^2(7) = 161.19$, $p = 1.80e^{-31}$, with statistically significant differences between most ages (Table 31).

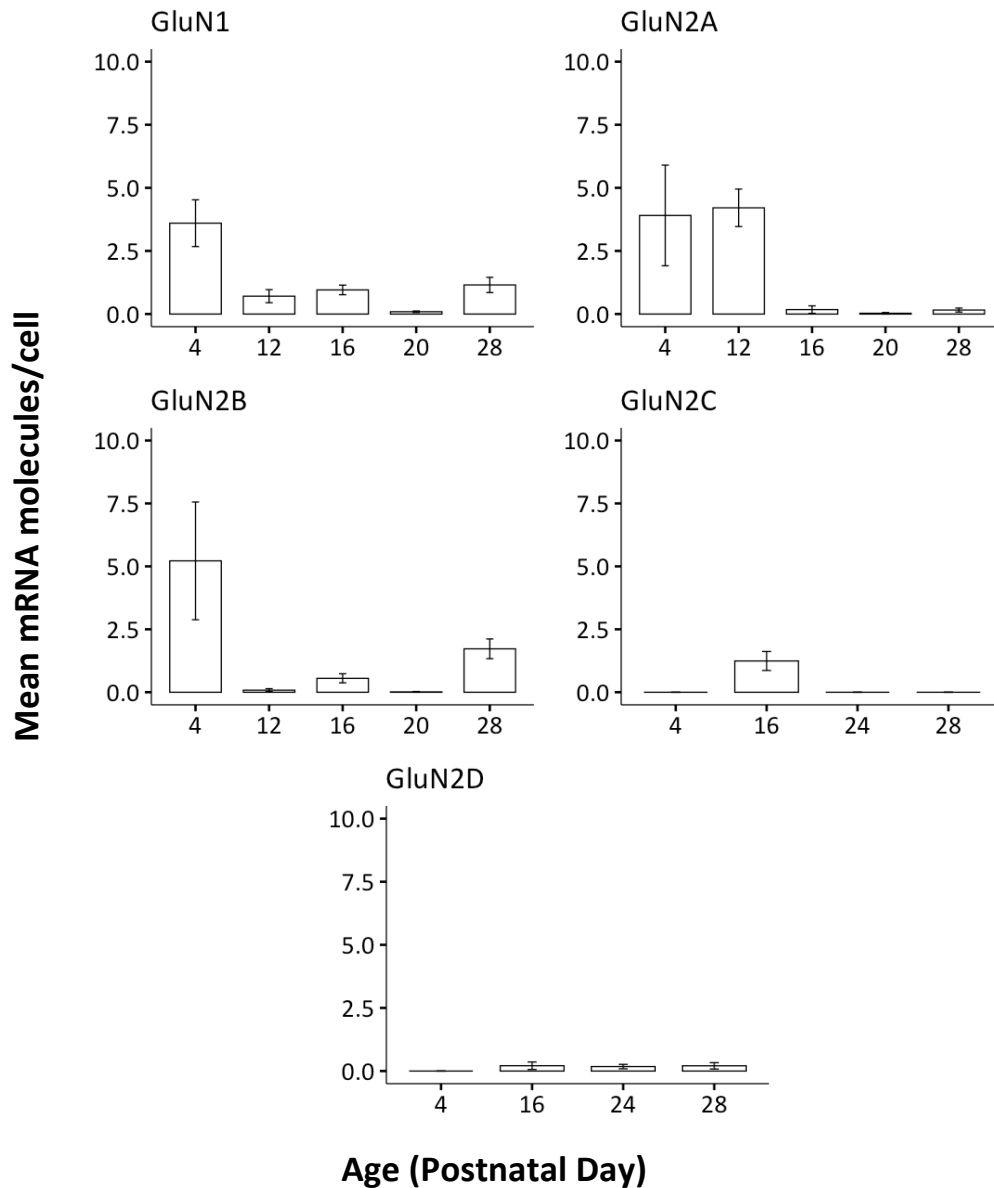


Figure 11: Mean NMDAR subunit mRNA expression/cell in the MSO of Litter 1 rats. Error bars are mean \pm SEM. In litter 1, the mean GluN1 mRNA/cell peaked at P4. Mean GluN2A mRNA/cell peaked from P4-P12. Mean GluN2B mRNA/cell peaked at P4. Mean GluN2C mRNA/cell was relatively constant from P0 to P28. Mean GluN2D mRNA/cell was relatively constant from P0 to P28. Number of MSO cells in SOC sections with GluN1/GluN2A/GluN2B probe solution: P4 = 32, P12 = 24, P16 = 43 in section 1 and 31 in section 2, P20 = 29 in section 1 and 39 in section 2, P28 = 31 in section 1 and 38 in section 2. Number of MSO cells in SOC sections with GluN1/GluN2C/GluN2D probe solution: P4 = 18, P16 = 46 in section 1 and 16 in section 2, P24 = 25 in section 1 and 37 in section 2, P28 = 29.

Table 30. Age-related changes in median NMDAR subunit mRNA expression in the MSO of Litter 1 rats. The following symbols, 1 (GluN1), A (GluN2A), B (GluN2B), C (GluN2C), and D (GluN2D) indicate a significant relationship between the two ages ($p < 0.05$ on Paired Wilcoxon Rank Sum Test) for the corresponding subunit mRNA. Note: No data for GluN1, GluN2A, and GluN2B for P24, and no data for GluN2C and GluN2D for P12 and P20.

Age	P4	P12	P16	P20
P12	AB			
P16	1ABC	A		
P20	1AB	1A	1B	
P24			C	
P28	1A	AB	BC	1B

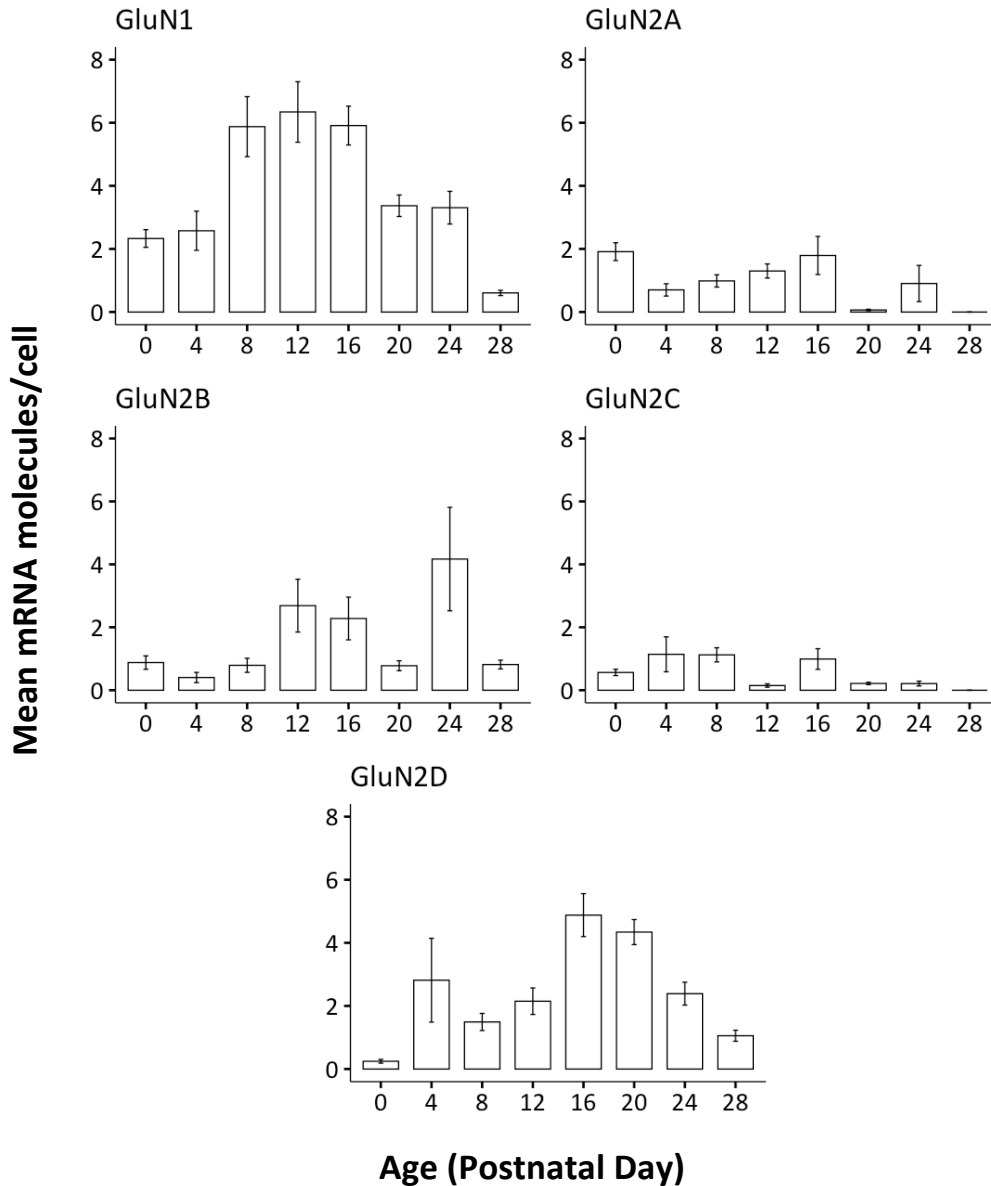


Figure 12: Mean NMDAR subunit mRNA expression/cell in the MSO of Litter 2 rats. Error bars are mean \pm SEM. Mean GluN1 mRNA/cell in the MSO stayed constant from birth to P24, with a slight increase from P8 to P20, before decreasing at P28. Mean GluN2A mRNA levels were relatively low from P0 to P28. Mean GluN2B mRNA levels peaked at P24. Mean GluN2C mRNA levels were low from P0 to P28. Mean GluN2D mRNA levels peaked at P16. Number of MSO cells in SOC sections with GluN1/GluN2A/GluN2B probe solution: P0 = 31 in section 1 and 27 in section 2, P4 = 24 in section 1 and 23 in section 2, P8 = 54 in section 1 and 46 in section 2, P12 = 48 in section 1 and 45 in section 2, P16 = 62 in section 1 and 49 in section 2, P20 = 57 in section 1 and 65 in section 2, P24 = 94 in section 1 and 73 in section 2, P28 = 45 in section 1 and 53 in section 2. Number of MSO

cells in SOC sections with GluN1/GluN2C/GluN2D probe solution: P0 = 52 in section 1 and 17 in section 2, P4 = 46 in section 1 and 46 in section 2, P8 = 71 in section 1 and 49 in section 2, P12 = 44 in section 1 and 36 in section 2, P16 = 60 in section 1 and 71 in section 2, P20 = 57 in section 1 and 65 in section 2, P24 = 44 in section 1 and 46 in section 2, P28 = 61 in section 1 and 29 in section 2.

Table 31. Age-related changes in median GluN1 mRNA expression in the MSO of Litter 2 rats (+ indicates a significant relationship between two ages). The following symbols, 1 (GluN1), A (GluN2A), B (GluN2B), C (GluN2C), and D (GluN2D) indicate a significant relationship between the two ages ($p < 0.05$ on Paired Wilcoxon Rank Sum Test) for the corresponding subunit mRNA.

Age	P0	P4	P8	P12	P16	P20	P24
P4	1A						
P8	D						
P12	CD	1BC	C				
P16	AD	1D	D	D			
P20	ACD	1ACD	ACD	AD	A		
P24	ACD	ABCD	ABCD	A	1A	BD	
P28	1ACD	AC	1AC	1AC	1ACD	1CD	1ACD

VNTB

GluN1 mRNA

In litter 1, the mean GluN1 mRNA/cell stayed relatively low from P0 to P28 (Figure 13). There was a statistically significant difference in median GluN1 mRNA/cell in the LNTB at different ages $\chi^2(2) = 10.89$, $p = .004$, with statistically significant differences between a few ages (Table 32).

In litter 2, the mean GluN1 mRNA/cell peaked at P20 (Figure 14). There was a statistically significant difference in median GluN1mRNA/cell in the LNTB at different ages $\chi^2(7) = 289.69$, $p = 9.62e^{-59}$, with significant differences between most ages (Table 33).

GluN2A mRNA

In litter 1, the mean GluN2A mRNA/cell was relatively low (Figure 13). There was a statistically significant difference in median GluN2A mRNA/cell in the VNTB at different ages $\chi^2(2) = 19.33$, $p = 6.35e^{-5}$, with statistically significant differences between approximately half of the ages (Table 32).

In litter 2, the mean GluN2A mRNA/cell was relatively low from P0 to P28 (Figure 14). There was a statistically significant difference in median GluN2A mRNA/cell in the

VNTB at different ages $\chi^2(7) = 194.55$, $p = 1.64e^{-38}$, with statistically significant differences between approximately half of the ages (Table 33).

GluN2B mRNA

In litter 1, the mean GluN2B mRNA/cell was relatively low (Figure 13). There was a statistically significant difference in median GluN2B mRNA/cell in the VNTB at different ages $\chi^2(2) = 24.19$, $p = 5.60e^{-6}$, with statistically significant differences between most ages (Table 32).

In litter 2, the mean GluN2B mRNA levels peaked at P20 (Figure 14). There was a statistically significant difference in median GluN2B mRNA/cell in the VNTB at different ages $\chi^2(7) = 108.40$, $p = 1.97e^{-20}$, with statistically significant differences between approximately half of the ages (Table 33).

GluN2C mRNA

In litter 1, the mean GluN2C mRNA/cell was relatively low (Figure 13). There was a statistically significant difference in median GluN2C mRNA/cell in the VNTB at different ages: $\chi^2(2) = 41.77$, $p = 8.49e^{-10}$, with statistically significant differences between most ages (Table 32).

In litter 2, the mean GluN2C mRNA levels were relatively low from P0 to P28 (Figure 14). There was a statistically significant difference in median GluN2C mRNA/cell in the VNTB at different ages $\chi^2(7) = 74.47$, $p = 1.84e^{-13}$, with statistically significant differences between only a few ages (Table 33).

GluN2D mRNA

In litter 1, the mean GluN2D mRNA/cell was relatively low (Figure 13). There was a statistically significant difference in median GluN2D mRNA/cell in the VNTB at different ages $\chi^2(2) = 6.09$, $p = .048$, with the only statistically significant difference being between P16 and P24 ($p = 0.040$) (Table 32).

In litter 2, the mean GluN2D mRNA/cell peaked from P16 to P20 (Figure 14). There was a statistically significant difference in median GluN2D mRNA/cell in the VNTB at different ages $\chi^2(7) = 328.853$, $p = 4.13e^{-67}$, with statistically significant differences between most ages (Table 33).

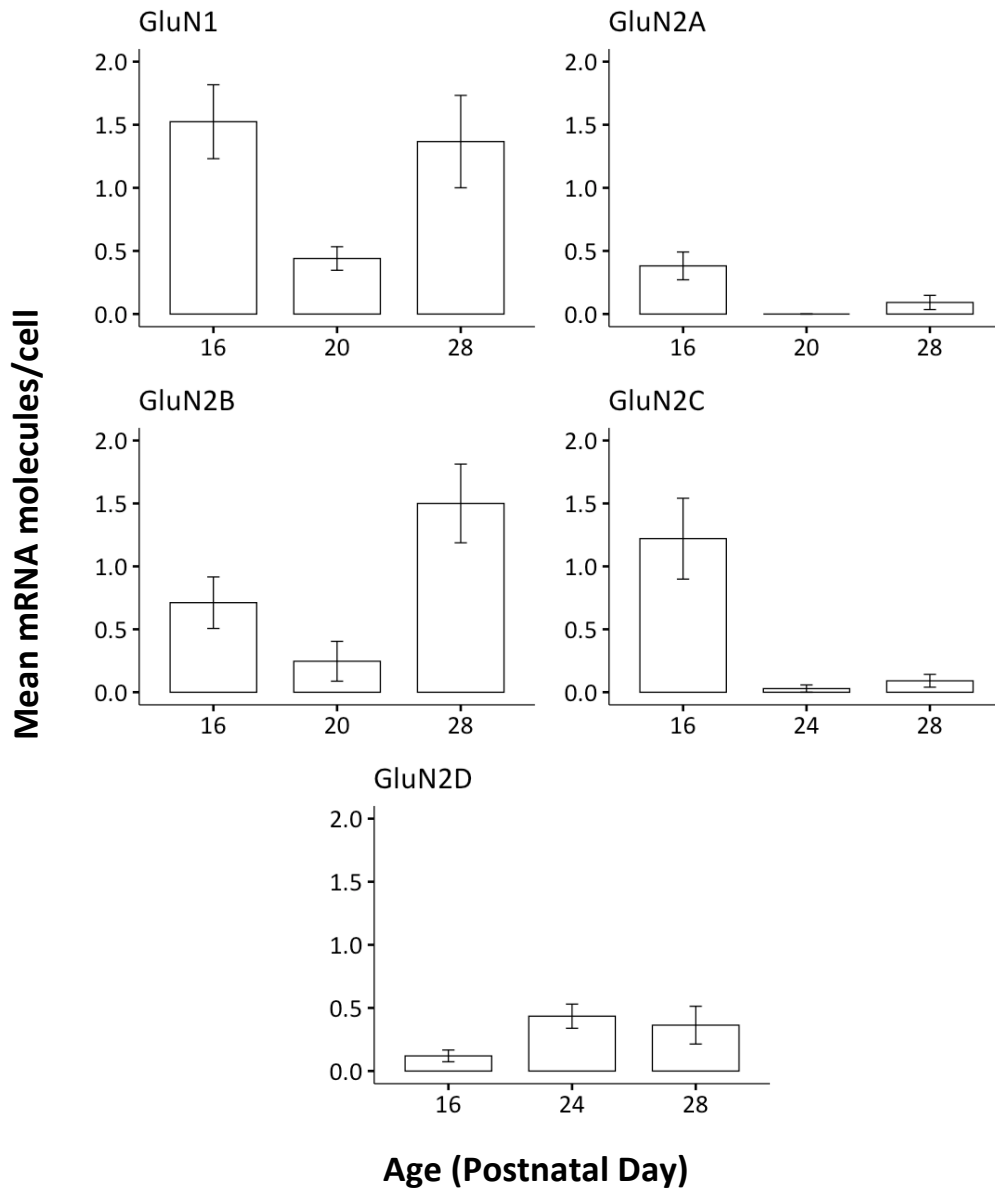
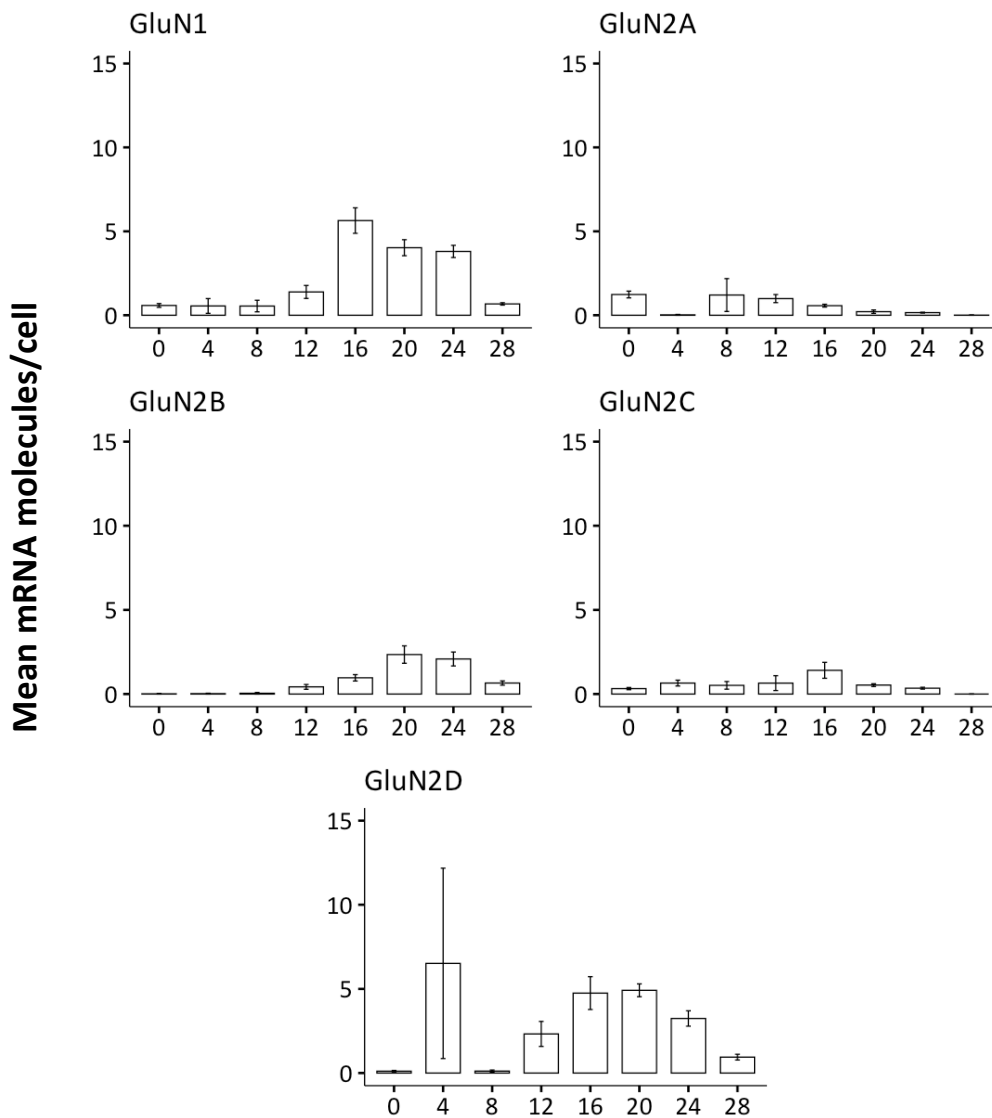


Figure 13: Mean NMDAR subunit mRNA expression/cell in the VNTB of Litter 1 rats. Error bars are mean \pm SEM. All mean NMDAR subunit mRNA/cell in the VNTB was relatively low. Number of VNTB cells in SOC sections with GluN1/GluN2A/GluN2B probe solution: P16 = 69 in section 1 and 28 in section 2, P20 = 37 in section 1 and 28 in section 2, and P28 = 50 in section 1 and 48 in section 2. Number of VNTB cells in SOC sections with GluN1/GluN2C/GluN2D probe solution: P16 = 50, P24 = 43 in section 1 and 26 in section 2, P28 = 33.

Table 32. Age-related changes in median NMDAR subunit mRNA expression in the VNTB of Litter 1 rats. The following symbols, 1 (GluN1), A (GluN2A), B (GluN2B), C (GluN2C), and D (GluN2D) indicate a significant relationship between the two ages ($p < 0.05$ on Paired Wilcoxon Rank Sum Test) for the corresponding subunit mRNA. Note: No data for GluN1, GluN2A, and GluN2B for P24, and no data for GluN2C and GluN2D for P20.

Age	P16	P20
P20	1A	
P24	CD	
P28	ABC	1B



Age (Postnatal Day)

Figure 14: Mean NMDAR subunit mRNA expression/cell in the VNTB of Litter 2 rats. Error bars are mean +/- SEM. Mean GluN1 mRNA/cell peaked at P20. Mean GluN2A mRNA/cell was relatively low from P0 to P28. Mean GluN2B mRNA levels peaked at P20. Mean GluN2C mRNA levels were relatively low from P0 to P28. Mean GluN2D mRNA/cell peaked from P16 to P20. Number of VNTB cells in SOC sections with GluN1/GluN2A/GluN2B probe solution: P0 = 25 in section 1 and 43 in section 2, P4 = 20 in section 1 and 21 in section 2, P8 = 38 in section 1 and 20 in section 2, P12 = 56 in section 1 and 66 in section 2, P16 = 97 in section 1 and 75 in section 2, P20 = 94 in section 1 and 108 in section 2, P24 = 155 in section 1 and 108 in section 2, P28 = 117 in section 1 and 149 in section 2. Number of VNTB cells in SOC sections with GluN1/GluN2C/GluN2D probe solution: P0 = 19 in section 1 and 71 in section 2, P4 = 50 in section 1 and 40 in section 2, P8 = 25 in section 1 and 35 in section 2, P12 = 84 in section 1 and 64 in section 2, P16 = 85 in section 1 and 1 in section 2, P20 = 108 in section 1 and 185 in section 2, P24 = 76 in section 1 and 85 in section 2, P28 = 88 in section 1 and 80 in section 2.

Table 33. Age-related changes in median NMDAR subunit mRNA expression in the VNTB of Litter 2 rats. The following symbols, 1 (GluN1), A (GluN2A), B (GluN2B), C (GluN2C), and D (GluN2D) indicate a significant relationship between the two ages ($p < 0.05$ on Paired Wilcoxon Rank Sum Test) for the corresponding subunit mRNA.

Age	P0	P4	P8	P12	P16	P20	P24
P4	1ACD						
P8	1ACD	D					
P12	D	1AD	1CD				
P16	1ABCD	1ABCD	1BCD	1BCD			
P20	1ABCD	1BD	1BD	1ABCD	AC		
P24	1ABCD	1BD	1BD	1ABC	ACD	D	
P28	ABCD	1C	1ACD	ACD	1ABCD	1ABCD	1ABCD

LNTB

GluN1 mRNA

In litter 1, the mean GluN1 mRNA/cell stayed relatively low from P0 to P28 (Figure 15). There was a statistically significant difference in median GluN1 mRNA/cell in the LNTB at different ages $\chi^2(2) = 35.07$, $p = 2.43e^{-8}$, with statistically significant differences between most ages (Table 34).

In litter 2, the mean GluN1 mRNA/cell peaked at P20 (Figure 16). There was a statistically significant difference in median GluN1mRNA/cell in the LNTB at different

ages $\chi^2(7) = 205.27$, $p = 8.80e^{-41}$, with significant differences between most ages (Table 35).

GluN2A mRNA

In litter 1, the mean GluN1 mRNA/cell stayed relatively low from P0 to P28 (Figure 15). There was not a statistically significant difference in median GluN2A mRNA/cell in the LNTB at different ages $\chi^2(2) = 4.35$, $p = .114$ (Table 34).

In litter 2, the mean GluN2A mRNA/cell stayed relatively low from P0 to P28 (Figure 16). There was a statistically significant difference in median GluN2A mRNA/cell in the LNTB at different ages $\chi^2(7) = 132.87$, $p = 1.58e^{-25}$, with statistically significant differences between half of the ages (Table 35).

GluN2B mRNA

In litter 1, the mean GluN2B mRNA/cell stayed relatively low (Figure 15). There was a statistically significant difference in median GluN2B mRNA/cell in the LNTB at different ages $\chi^2(2) = 99.31$, $p = 2.73e^{-22}$, with statistically significant differences between all ages (Table 34).

In litter 2, the mean GluN2B mRNA levels peaked at P12 (Figure 16). There was a statistically significant difference in median GluN2B mRNA/cell in the LNTB at different ages $\chi^2(7) = 76.70$, $p = 6.47e^{-14}$, with statistically significant differences between only a small proportion of ages (Table 35).

GluN2C mRNA

In litter 1, the mean GluN2C mRNA/cell stayed relatively low (Figure 15). There was a statistically significant difference in median GluN2C mRNA/cell in the LNTB at different ages $\chi^2(2) = 37.65$, $p = 6.69e^{-9}$, with statistically significant differences between all ages (Table 34).

In litter 2, the mean GluN2C mRNA levels were relatively low from P0 to P28 (Figure 16). There was a statistically significant difference in median GluN2C mRNA/cell in the LNTB at different ages $\chi^2(7) = 24.28$, $p = .001$, with statistically significant differences between only a small proportion of ages (Table 35).

GluN2D mRNA

In litter 1, the mean GluN2C mRNA/cell stayed relatively low (Figure 15). There was a statistically significant difference in median GluN2D mRNA/cell in the LNTB at different ages $\chi^2(2) = 18.51$, $p = 9.54e^{-5}$. Median GluN2D mRNA/cell was only significantly different between P16 and P28 ($p = .0002$) (Table 34).

In litter 2, the mean GluN2D mRNA levels peaked from P16 to P24 (Figure 16). There was a statistically significant difference in median GluN2D mRNA/cell in the LNTB at different ages $\chi^2(7) = 255.95$, $p = 1.50e^{-51}$, with statistically significant differences between most ages (Table 35).

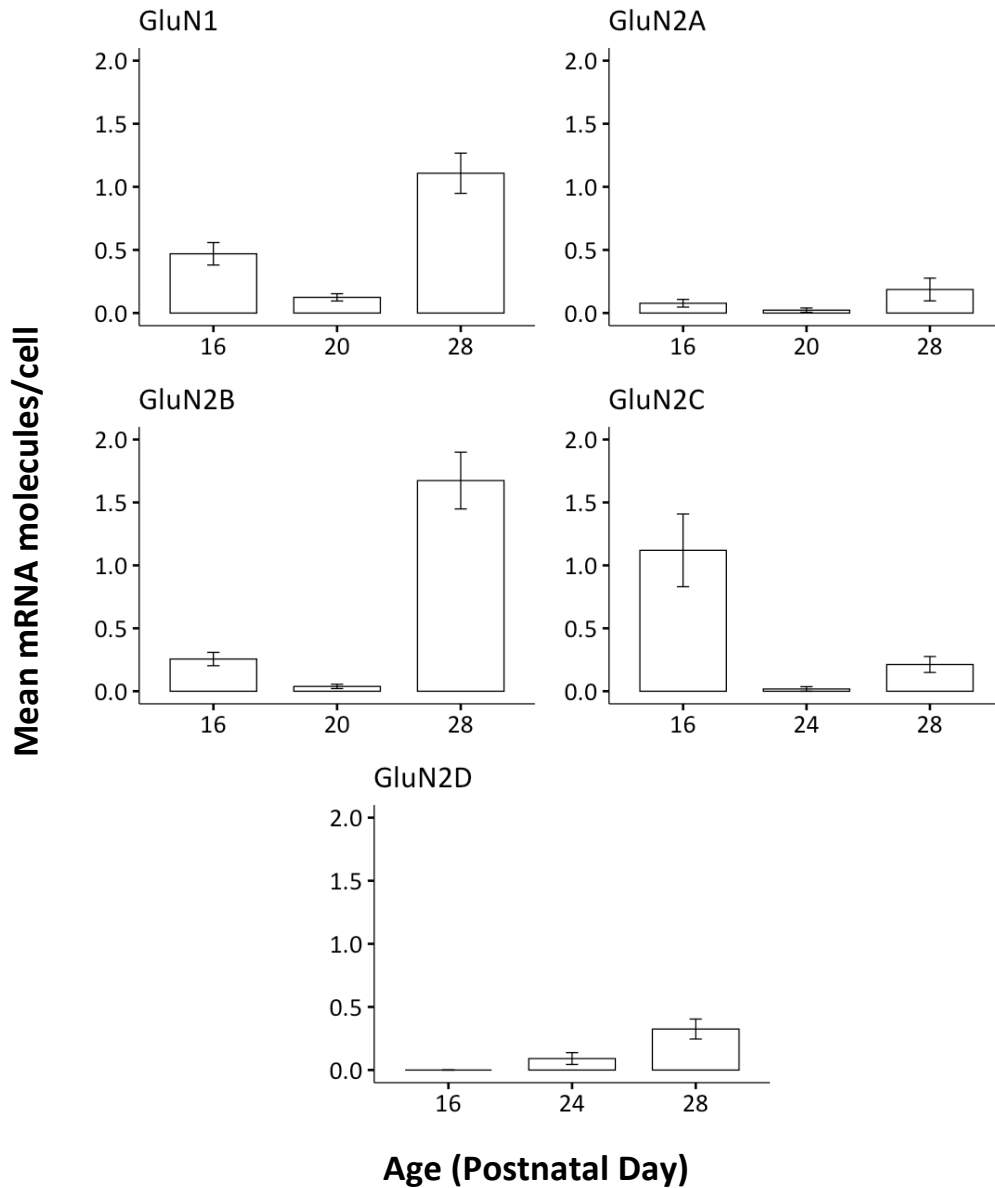


Figure 15: Mean NMDAR subunit mRNA expression/cell in the LNTB of Litter 1 rats. Error bars are mean \pm SEM. Mean GluN1 mRNA/cell stayed relatively low from P0 to P28. Mean GluN1 mRNA/cell stayed relatively low from P0 to P28. Mean GluN2B mRNA/cell stayed relatively low. Mean GluN2C mRNA/cell stayed relatively low. Mean GluN2D mRNA/cell stayed relatively low. Number of LNTB cells in SOC sections with GluN1/GluN2A/GluN2B probe solution: P16 = 87 in section 1 and 42 in section 2, P20 = 59 in section 1 and 71 in section 2, and P28 = 122 in section 1 and 114 in section 2. Number of LNTB cells in SOC sections with GluN1/GluN2C/GluN2D probe solution: P16 = 67, P24 = 55, and P28 = 80.

Table 34. Age-related changes in median NMDAR subunit mRNA expression in the LNTB of Litter 1 rats. The following symbols, 1 (GluN1), A (GluN2A), B (GluN2B), C (GluN2C), and D (GluN2D) indicate a significant relationship between the two ages ($p < 0.05$ on Paired Wilcoxon Rank Sum Test) for the corresponding subunit mRNA. Note: No data for GluN1, GluN2A, and GluN2B for P24, and no data for GluN2C and GluN2D for P20.

Age	P16	P20
P20	B	
P24	C	
P28	1BCD	1BC

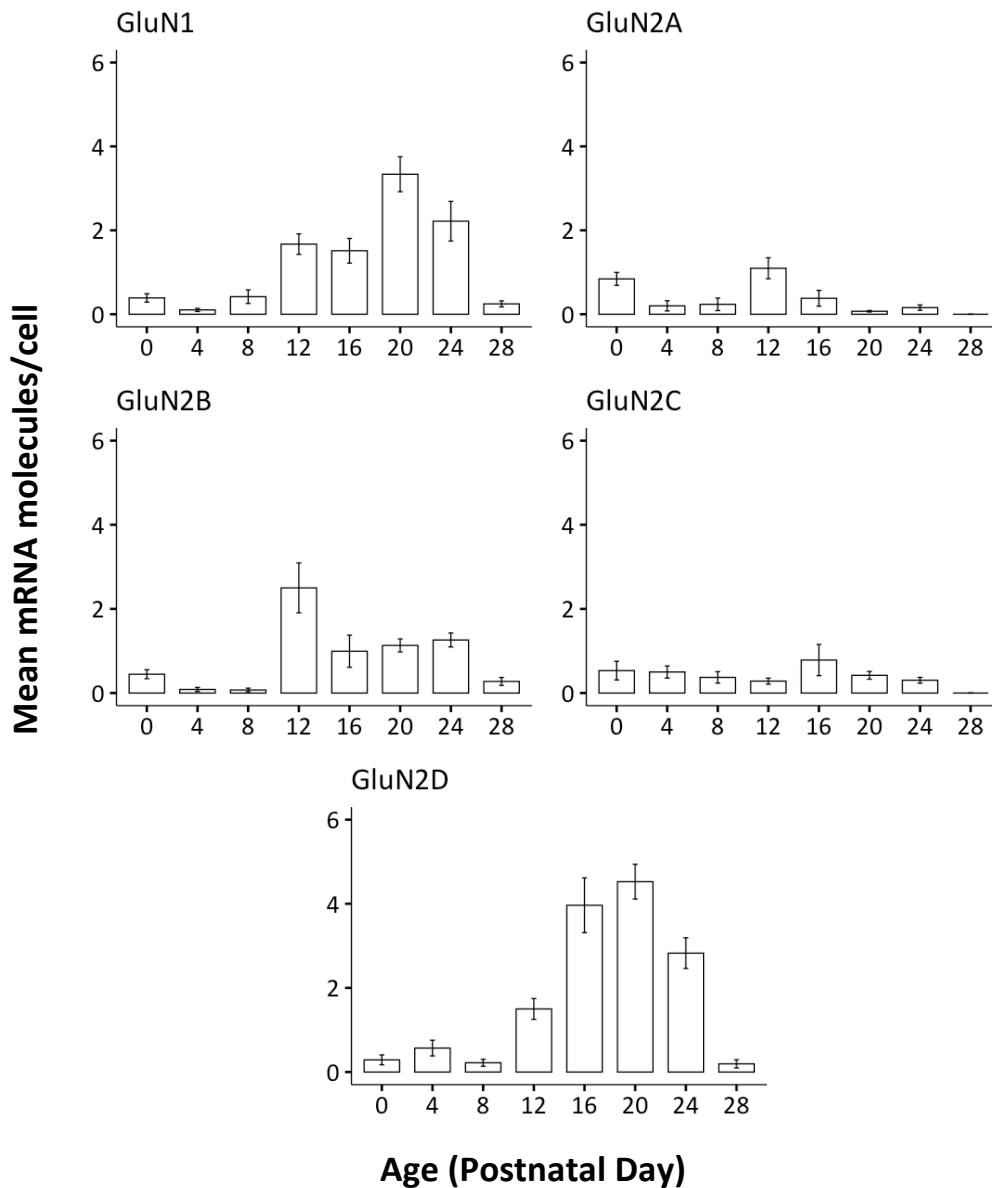


Figure 16: Mean NMDAR subunit mRNA expression/cell in the LNTB of Litter 2 rats. Error bars are mean +/- SEM. Mean GluN1 mRNA/cell peaked at P20. Mean GluN2A mRNA/cell stayed relatively low from P0 to P28. Mean GluN2B mRNA levels peaked at P12. Mean GluN2C mRNA levels were relatively low from P0 to P28. Mean GluN2D mRNA levels peaked from P16 to P24. Number of LNTB cells in SOC sections with GluN1/GluN2A/GluN2B probe solution: P0 = 36 in section 1 and 40 in section 2, P4 = 29 in section 1 and 6 in section 2, P8 = 28 in section 1 and 114 in section 2, P12 = 50 in section 1 and 96 in section 2, P16 = 82 in section 1 and 81 in section 2, P20 = 99 in section 1 and 98 in section 2, P24 = 95 in section 1 and 89 in section 2, P28 = 65 in section 1 and 40 in section 2. Number of LNTB cells in SOC sections with GluN1/GluN2C/GluN2D probe solution: P0 = 33 in section 1 and 12 in section 2, P4 = 29 in section 1 and 44 in section 2, P8 = 50 in section 1 and 36 in section 2, P12 = 60 in section 1 and 74 in section 2, P16 = 72 in section 1 and 67 in section 2, P20 = 153 in section 1 and 99 in section 2, P24 = 83 in section 1 and 78 in section 2, P28 = 23 in section 1 and 54 in section 2.

Table 35. Age-related changes in median NMDAR subunit mRNA expression in the LNTB of Litter 2 rats. The following symbols, 1 (GluN1), A (GluN2A), B (GluN2B), C (GluN2C), and D (GluN2D) indicate a significant relationship between the two ages ($p < 0.05$ on Paired Wilcoxon Rank Sum Test) for the corresponding subunit mRNA.

Age	P0	P4	P8	P12	P16	P20	P24
P4	A						
P8	A						
P12	1D	1D	1BD				
P16	AD	1D	1D	1AD			
P20	1AD	1BD	1BD	1AD	1B		
P24	1ABD	1BD	1BD	A	CB	1D	
P28	AC	C	A	1ACD	1CD	1BCD	1ABCD

SPN

GluN1 mRNA

In litter 1, the mean GluN1 mRNA/cell peaked at P4 (Figure 17). There was a statistically significant difference in median GluN1 mRNA/cell in the SPN at different ages $\chi^2(2) = 365.612$, $p = 4.06e^{-80}$ (Table 36).

In litter 2, the mean GluN1 mRNA expression in the SPN peaked at around P16 (Figure 18). There was a statistically significant difference in median GluN1 mRNA/cell in the SPN at different ages $\chi^2(7) = 825.42$, $p = 6.05e^{-174}$, with statistically significant differences between most ages (Table 37).

GluN2A mRNA

In litter 1, the mean GluN1 mRNA/cell peaked at P4 (Figure 17). There was a statistically significant difference in median GluN2A mRNA/cell in the SPN at different ages $\chi^2(2) = 64.77$, $p = 8.60e^{-15}$, with statistically significant differences between most of the ages (Table 36).

In litter 2, the mean GluN2A mRNA levels slightly peaked from P12 to P20 (Figure 18). There was a statistically significant difference in median GluN2A mRNA/cell in the SPN at different ages $\chi^2(7) = 246.27$ $p = 1.72e^{-49}$, with statistically significant differences between most of the ages (Table 37).

GluN2B mRNA

In litter 1, the mean GluN2B mRNA/cell peaked at P4 (Figure 17). There was a statistically significant difference in median GluN2B mRNA/cell in the SPN at different ages $\chi^2(2) = 336.68$, $p = 7.79e^{-74}$. Median GluN2B mRNA/cell was significantly different between all ages (Table 36).

In litter 2, the mean GluN2B mRNA peaked at P16 to P20 (Figure 18). There was a statistically significant difference in median GluN2B mRNA/cell in the SPN at different ages $\chi^2(7) = 206.70$, $p = 4.37e^{-41}$, with statistically significant differences in median GluN2B mRNA/cell in approximately half of the ages (Table 37).

GluN2C mRNA

In litter 1, the mean GluN2C mRNA/cell was relatively low (Figure 17). There was a statistically significant difference in median GluN2C mRNA/cell in the SPN at different ages $\chi^2(2) = 167.52$, $p = 4.20e^{-37}$. Median GluN2C mRNA/cell was significantly different between all ages (Table 36).

In litter 2, the mean GluN2C mRNA expression was relatively constant, with a slight increase from P4 to P16 (Figure 18). There was a statistically significant difference in median GluN2C mRNA/cell in the SPN at different ages $\chi^2(7) = 231.59$, $p = 2.28e^{-46}$, with statistically significant differences between approximately half of the ages (Table 37).

GluN2D mRNA

In litter 1, the mean GluN2D mRNA/cell was relatively low (Figure 17). There was not a statistically significant difference in median GluN2D mRNA/cell in the SPN at different ages $\chi^2(2) = 1.83$, $p = .40$ (Table 36).

In litter 2, the mean GluN2D mRNA expression in the SPN peaked at around P16 (Figure 18). There was a statistically significant difference in median GluN2D mRNA/cell in the SPN at different ages $\chi^2(7) = 550.67$, $p = 1.01e^{-114}$, with statistically significant differences between most ages (Table 37).

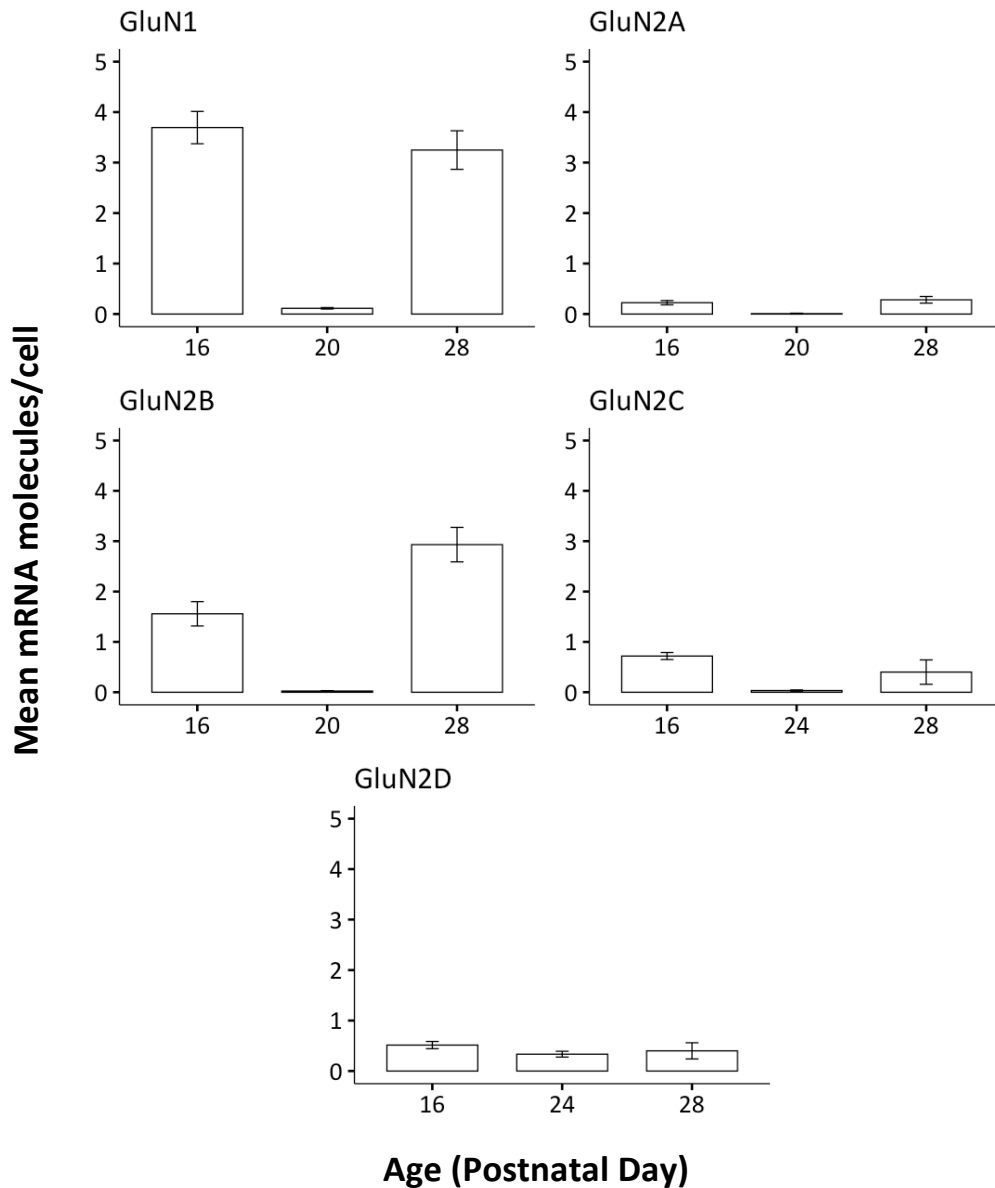


Figure 17: Mean NMDAR subunit mRNA expression/cell in the SPN of Litter 1 rats. Error bars are mean \pm SEM. Mean GluN1 mRNA/cell peaked at P4. Mean GluN1 mRNA/cell peaked at P4. Mean GluN2B mRNA/cell peaked at P4. Mean GluN2C mRNA/cell was relatively low. Mean GluN2D mRNA/cell was relatively low. Number of SPN cells in SOC sections with GluN1/GluN2A/GluN2B probe solution: P16 = 143 in section 1 and 137 in section 2, P20 = 216 in section 1 and 275 in section 2, and P28 = 172 in section 1 and 179 in section 2. Number of SPN cells in SOC sections with GluN1/GluN2C/GluN2D probe solution: P16 = 330 in section 1 and 193 in section 2, P24 = 171 in section 1 and 122 in section 2, and P28 = 186.

Table 36. Age-related changes in median NMDAR subunit mRNA expression in the SPN of Litter 1 rats. The following symbols, 1 (GluN1), A (GluN2A), B (GluN2B), C (GluN2C), and D (GluN2D) indicate a significant relationship between the two ages ($p < 0.05$ on Paired Wilcoxon Rank Sum Test) for the corresponding subunit mRNA. Note: No data for GluN1, GluN2A, and GluN2B for P24, and no data for GluN2C and GluN2D for P20.

Age	P16	P20	P24
P20	1AB		
P24	C		
P28	BC	1AB	C

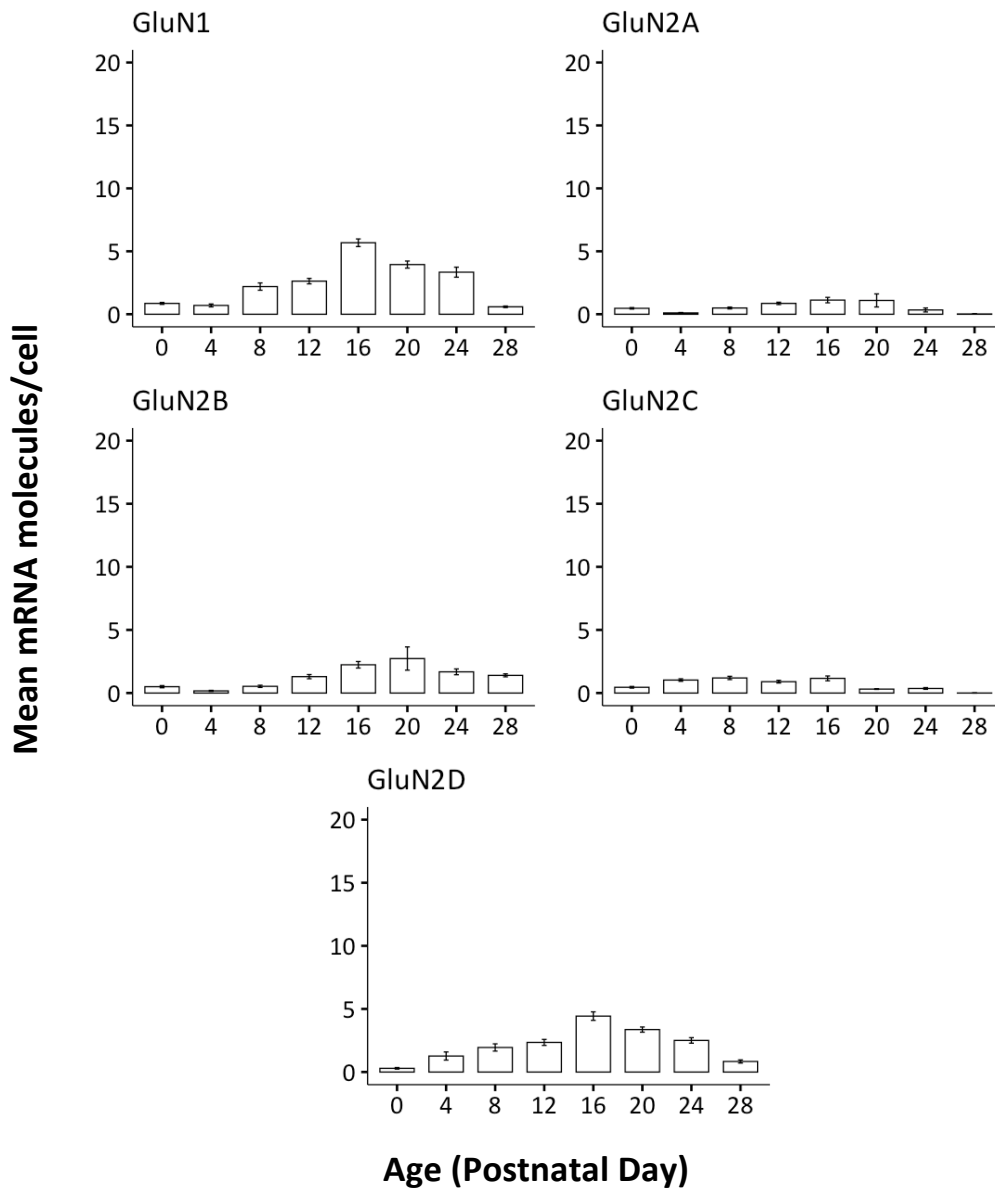


Figure 18: Mean NMDAR subunit mRNA expression/cell in the SPN of Litter 2 rats. Error bars are mean +/- SEM. Mean GluN1 mRNA expression in the SPN peaked at around P16. Mean GluN2A mRNA levels slightly peaked from P12 to P20. Mean GluN2B mRNA peaked at P16 to P20. Mean GluN2C mRNA expression was relatively constant, with a slight increase from P4 to P16. Mean GluN2D mRNA expression in the SPN peaked at around P16. Number of SPN cells in SOC sections with GluN1/GluN2A/GluN2B probe solution: P0 = 145 in section 1 and 165 in section 2, P4 = 85 in section 1 and 85 in section 2, P8 = 157 in section 1 and 182 in section 2, P12 = 195 in section 1 and 157 in section 2, P16 = 249 in section 1 and 377 in section 2, P20 = 269, P24 = 308 in section 1 and 241 in section 2, P28 = 252 in section 1 and 229 in section 2. Number of SPN cells in SOC sections with GluN1/GluN2C/GluN2D probe solution: P0 = 117 in section 1 and 130 in section 2, P4 = 123 in section 1 and 183 in section 2, P8 = 211 in section 1 and 126 in section 2, P12 = 187 in section 1 and 123 in section 2, P16 = 213 in section 1 and 352 in section 2, P20 = 408 in section 1 and 269 in section 2, P24 = 239 in section 1 and 191 in section 2, P28 = 213 in section 1 and 151 in section 2.

Table 37. Age-related changes in median NMDAR subunit mRNA expression in the SPN of Litter 2 rats. The following symbols, 1 (GluN1), A (GluN2A), B (GluN2B), C (GluN2C), and D (GluN2D) indicate a significant relationship between the two ages ($p < 0.05$ on Paired Wilcoxon Rank Sum Test) for the corresponding subunit mRNA.

Age	P0	P4	P8	P12	P16	P20	P24
P4	1ACD						
P8	CD	1A					
P12	1ABD	1ABD	1ABD				
P16	1ABD	1ABD	1ABD	1AD			
P20	1ABD	1ABCD	1ABCD	1ACD	1AC		
P24	1ABD	1ABCD	1ABC	C	1ACD	1AD	
P28	BCD	BCD	1ABCD	1ABCD	1ACD	1ABCD	1ACD

GluN1 Protein in the MNTB, LSO, and MSO

Mean and median GluN1 immunoreactivity appeared to decrease in the MNTB, LSO, and MSO from P0 to P28 (Figures 19 and 20). Median GluN1 immunoreactivity was only statistically significantly different across ages in the MNTB (MNTB: $\chi^2(7) = 16.47$, $p = .02$; LSO: $\chi^2(7) = 12.31$, $p = .09$; MSO: $\chi^2(6) = 10.68$, $p = .10$).

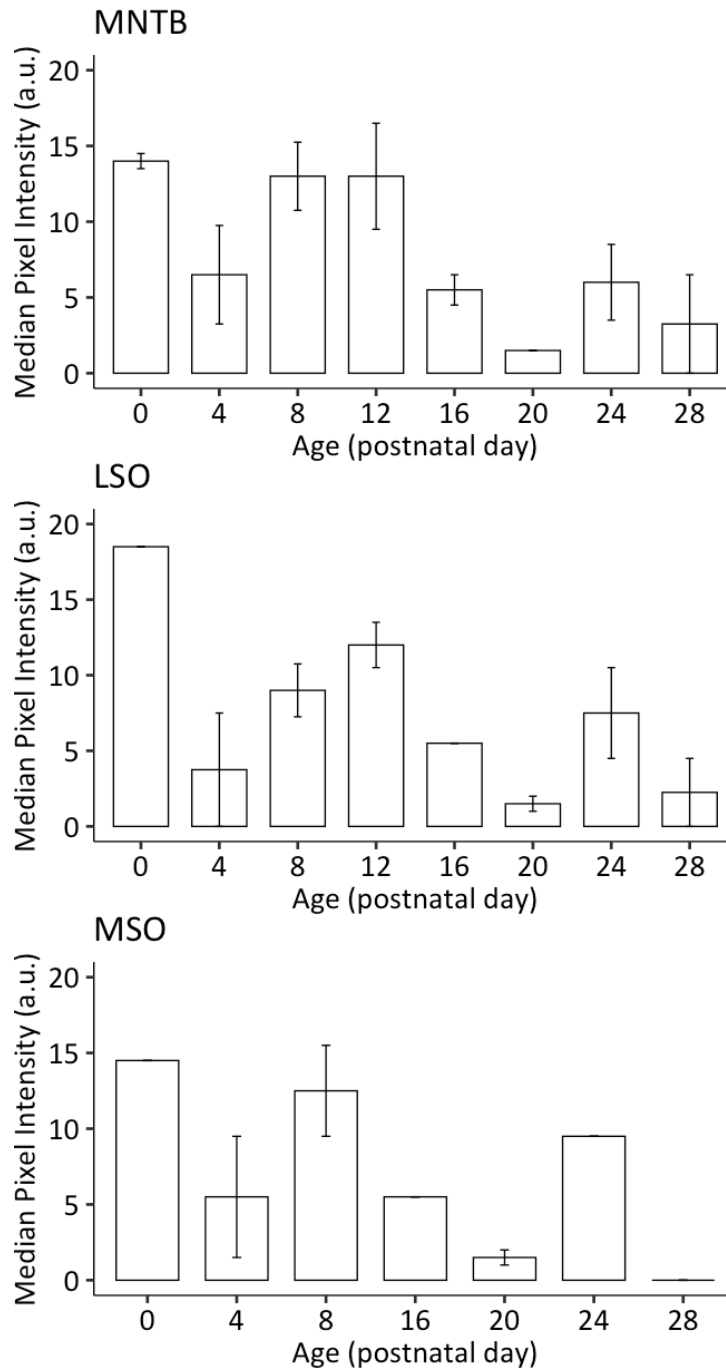
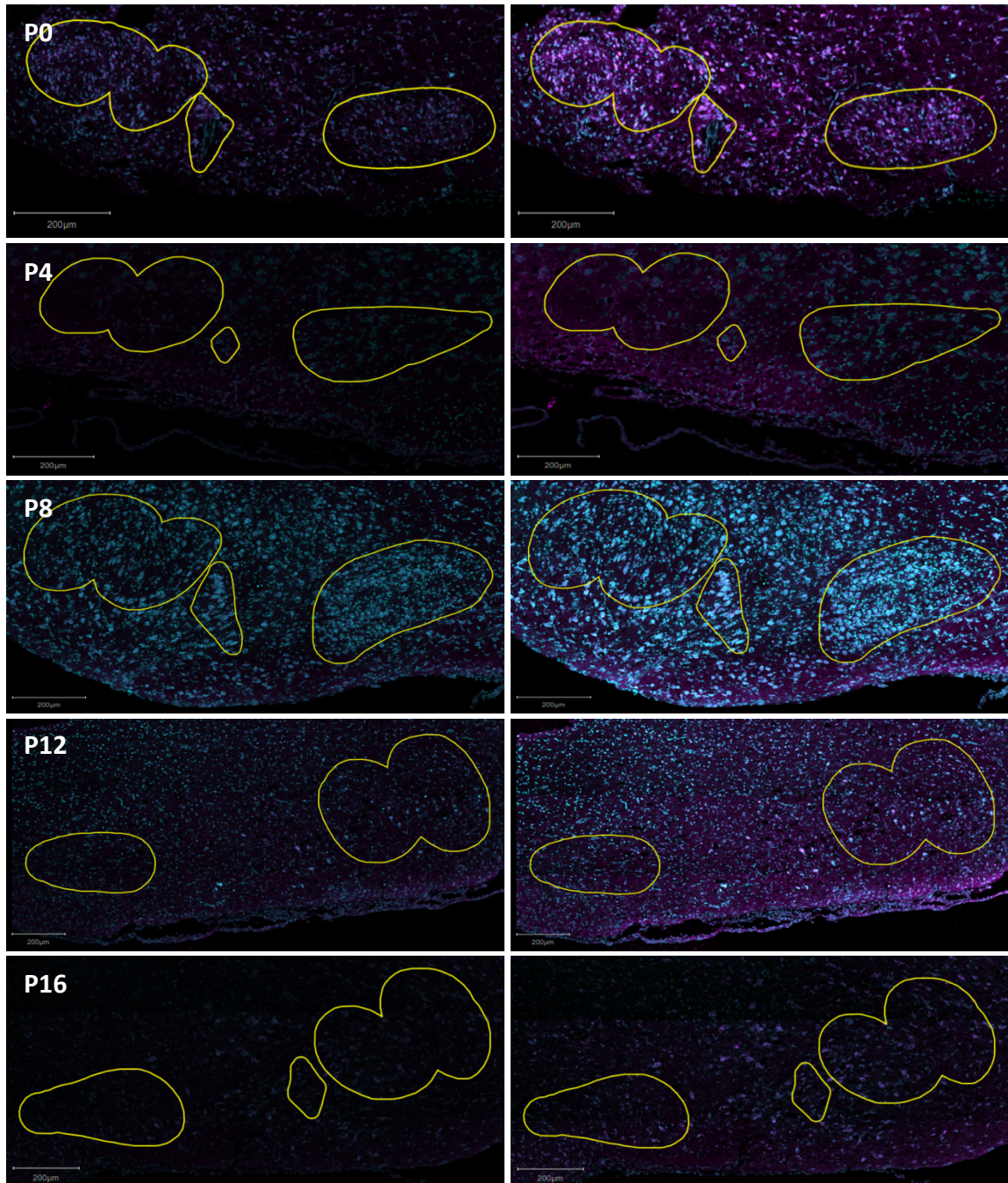


Figure 19: Median GluN1 protein expression in the MNTB, LSO, and MSO of 1 litter of rats. Error bars are interquartile range. Mean and median GluN1 immunoreactivity appeared to decrease in the MNTB, LSO, and MSO from P0 to P28. Median GluN1 immunoreactivity was only statistically significantly different across ages in the MNTB (MNTB: $\chi^2(7) = 16.47$, $p = .02$; LSO: $\chi^2(7) = 12.31$, $p = .09$; MSO: $\chi^2(6) = 10.68$, $p = .10$). a.u. = Arbitrary Units.



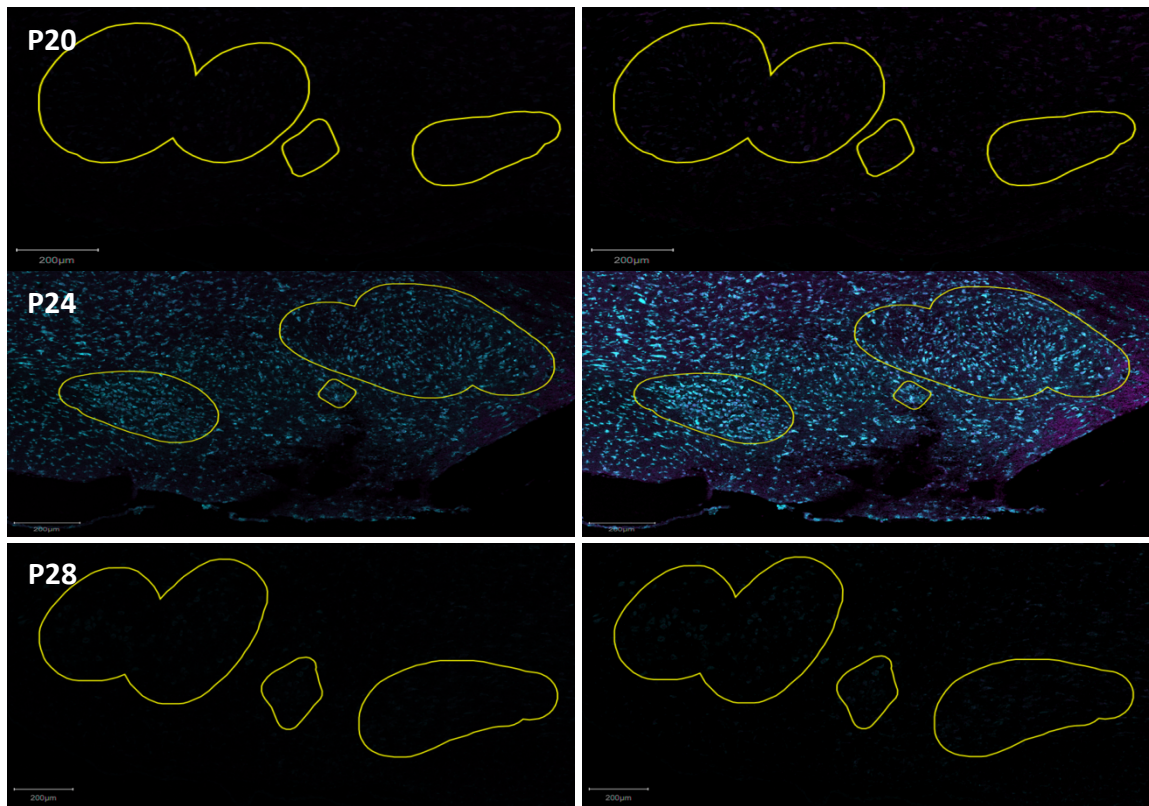


Figure 20: Representative images of GluN1 protein expression in primary nuclei, MNTB, LSO, and MSO, of the rat SOC from P0 to P28. Right column: raw, unaltered representative image. Left column: minimum and maximum look-up table display-adjusted version (reversible) of representative images for visualization purposes; all images were altered using the same parameters. Magenta: GluN1 staining; Cyan: NeuroTrace 435/455 staining. Scale bars = 200 μm for all ages. Median and mean GluN1 expression appears to decline from P0 to P28 in all three nuclei.

Discussion

NMDARs in the immature MNTB to LSO pathway might be involved in its refinement. The heterogeneity in NMDAR subunit composition equips the receptor with an array of possible kinetic, pharmacological, and signalling properties. To gain insight into which of these properties could potentially be involved in the refinement of the MNTB to LSO pathway, I measured the expression of NMDAR subunit mRNA for subunits in the GluN1 and GluN2 family from P0 to P28. I found that the expression levels of subunit mRNA from P0 to P28 in the GluN2 family varied in most nuclei, suggesting a subunit substitution occurring during circuit refinement. However, the peak in GluN1 expression in each nucleus also suggests that the overall number of NMDARs rises and falls in the SOC throughout the refinement of its many circuits.

Changes in NMDAR mRNA expression in primary and periolivary SOC nuclei

In Litter 1, GluN1 mRNA expression peaked between P0 to P4 in all primary nuclei (Figure 7, 8 and 9). GluN2A mRNA expression was highest at birth in the LSO (Figure 8) and was highest from P4-P12 in the MSO (Figure 9). In the MSO, GluN2B levels peaked at similar times as GluN2A expression, around P4. I did not observe a clear GluN2B to GluN2A switch in the two litters. GluN2B expression in all other nuclei was relatively constant and low. In all primary nuclei, GluN2D levels were low from P0 to P28. VNTB, LNTB, and SPN data for litter 1 do not contain the full set of ages due to the tissue sectioning angle of the sections that were used for the assay.

In Litter 2, GluN1 mRNA peaked from a timepoint between P8 to P20 in all nuclei. The three primary nuclei of the SOC and the VNTB showed the same rise and fall time course of GluN1 expression. In the LSO, both GluN2A and GluN2B mRNA levels peaked at the same age (P8), suggesting that the commonly suggested GluN2B-to-GluN2A substitution is unlikely in the MNTB-to-LSO-pathway during refinement. The LSO was the only nucleus to show an increase in GluN2A expression from P0 to P28, suggesting a smaller role of GluN2A in the refinement of the SOC altogether. The MNTB in litter 2 was the only nucleus in both litters that showed a peak, at P0, in GluN2C expression. All other nuclei showed the same expression pattern for GluN2C, where levels were low from P0 to P28, suggesting that most NMDARs in the SOC do not contain the GluN2C subunit during a period of major circuit refinement. All nuclei showed a peak in GluN2D expression from P16 to P20, suggesting that if a subunit substitution were to underlie the decrease in ifenprodil sensitivity in the LSO, it could be due to an increase in GluN2D-containing NMDARs. The mechanism of how levels of all NMDAR subunits decrease in the SOC throughout this period is unknown.

Changes in control probe expression

Most nuclei in both litters exhibited fluctuations in control probe expression across ages. As a result of this observation and several factors including potential

biological variability, noise, and a small sample size prevent me from making meaningful conclusions about the age-related changes in gene expression. A potential solution for future experiments using this technique would be to use control probes that are more relevant to my main purpose of using the control probes: I need to ensure that any age-related changes I observe in my target probes are a result of true biological change, and not noise. Notably, researchers who conducted a genome-wide microarray analysis of approximately 41 000 genes in the rat showed that differences in gene expression in the SOC varied the most between P4 to P25 (Ehmann et al. 2013). They also found that several transcription factors were upregulated prior to hearing onset. Therefore, genes that are expressed at known levels during early postnatal development in the SOC should be used as controls, in lieu of those provided in the RNAscope assay. This approach would allow for correction of general developmental expression trends in probes. Potential control probes could be for genes that have differential expression before and after hearing onset (P10-P12) in rats. For example, the genes for myelin-associated oligodendrocyte basic protein, *Mobp*, and myelin-oligodendrocyte glycoprotein, *Mog*, increase in expression after hearing onset in rats (Ehmann et al. 2013). The genes for potassium voltage-gated channel subfamily B member 1, *Kcnb1*, and H member 1, *Kcnh1*, decrease in expression after hearing onset in rats (Ehmann et al. 2013). Validation of control probes in specific circuits should be considered for future RNAscope assays.

GluN1 protein expression

To calibrate the changes in mRNA expression to protein expression, I ran a pilot immunostaining run for the GluN1 subunit using one litter. Synaptic receptors are notoriously challenging to raise specific antibodies against, and there are few validated NMDAR subunit antibodies available for immunohistochemistry (see Limitations). The GluN1 antibody I used in this study was one of few available NMDAR subunit antibodies validated in rats for immunohistochemistry (Zhang et al. 2018). I found that median and mean GluN1 staining appeared to decrease from P0 to P28 in the primary nuclei of the SOC. However, only the MNTB appeared to have a statistically significant difference in staining intensity across ages. Previous electrophysiological studies of NMDAR activity in the MNTB to LSO pathway show that NMDAR-mediated charge transfer and peak current amplitude decrease after P9 (Case and Gillespie 2011). The expression of GluN1 protein in the LSO is likely to be decreasing and should be reassessed in additional litters.

Differentiating subunit substitution from a decrease in NMDAR expression

If subunits in the GluN1 and GluN2 families are decreasing towards P28, how might we determine if there is a subunit substitution occurring as well, rather than just an overall reduction in NMDARs? Despite the reductions in NMDAR subunit levels across all the subunits measured, the differing peaks in expression suggest that the levels of

each subunit at any given stage in refinement vary. For this to occur, the subunit composition of the NMDARs at a given stage of refinement must change. In all subunits that were measured, expression levels did not change drastically from P0 to P28, which suggests that changes in subunit composition are likely to be subtle. For example, a diheterotetrameric receptor with only GluN1 and GluN2B subunits may become a triheterotetrameric receptor containing GluN2B and GluN2A/C/D subunits during development. With the current method used to quantify each subunit, it would be challenging to distinguish between di- and tri-heteromeric receptors.

Temporal order of subunit changes between nuclei

A subunit substitution from GluN2B to GluN2A-containing NMDARs is often used as a proxy for circuit maturation. It may be the case that the temporal order of subunit substitutions between different nuclei could indicate a guidance process for refinement, where nuclei with GluN2A-containing NMDARs guide the refinement of nuclei that contain GluN2B-containing NMDARs. This guidance could potentially occur through different signalling properties or biasing a synapse towards different forms of synaptic plasticity. This was not the case in the findings of this study, as there was no GluN2B to GluN2A switch in any nucleus in either litter.

Limitations

Cell type-specific expression

Differential expression of NMDAR subtypes extends into neuronal types. Within a given neuron, differential expression further extends to synapse type. With *in-situ* hybridization, it is not possible to know the receptor subtype that a given synapse contains. Within a given nucleus, it may be possible to identify the NMDAR subtypes present in specific neuron types. However, this would require a cell detection technique that can identify the subtle characteristics that define different neuron types in each nucleus. A potential technique could be to counterstain neurons using a neuronal marker, like NeuN, and then to train a cell segmentation algorithm, like CellPose, to classify the stained neurons based on their morphology (Stringer et al. 2021). This counterstaining technique also removes the issue that occurs with NeuroTrace counterstaining, as NeuroTrace also stains glia, in addition to neurons. To further modify this potential counterstaining technique, additional markers that are specific to astrocytes, oligodendrocytes, and microglia should be used as well. However, age-dependent expression of these markers may be a caveat. This is the case with several astrocyte markers like GFAP and S100b, which tend to work for mature, but not immature astrocytes (Preston et al. 2019).

Maximizing mRNA signal captured in each section

To image mRNA probe signals for all six nuclei, I had to take a tile-scan of each unilateral SOC at 40x magnification, using a single optical section. This resulted in an extensive time requirement to image each SOC. Due to this approach, it is likely that mRNA probe signal was missed because the signal was outside of the imaged optical section. A proposed solution to this issue is to restrict the tile-scanning area to a more manageable portion of a given nucleus and take images of several adjacent optical sections to assess the changes in probe signal over a greater depth.

Developmental changes in transcription and translation at each age

Levels of detected mRNA in each age could be altered by the age-dependent changes in transcriptional and translational machinery and regulation. Several factors can modify ribosomes and translation factors, including environmental factors (Sauert et al. 2015). The development of transcriptional and translational machinery throughout circuit refinement should be assessed to allow a more in-depth interpretation of the changes in mRNA levels seen in this study. Furthermore, comparing transcript expression to protein expression necessitates considering how transcript levels correlate with protein levels in the cell. An analysis of correlations in mRNA vs. protein expression for several genes suggests that there is a time-delay between mRNA and protein expression (Wang et al. 2010), which should be taken into account when comparing expression levels.

Sources of error in immunohistochemistry staining

The images presented of the GluN1 protein staining run reveal inconsistent staining patterns in the NeuroTrace counterstain (see Figure 20). The tissue preparation protocol and/or imaging techniques that I used did not produce images that were of sufficient quality to draw meaningful conclusions about GluN1 protein levels in the SOC. There are several potential sources of error, including: 1) a discrepancy in the actual laser output vs. the set laser output of the confocal microscope that was used, 2) the sensitivity and specificity of the antibody, and 3) the tissue processing method.

The ability to quantify protein expression from immunofluorescence is challenging due to the confounding factors that can influence the output of immunoassays (see Jensen et al., 2017 for review). To obtain a more reliable dataset, this staining run should be replicated in at least two more litters to increase confidence that the observed differences in immunofluorescence across ages reflect age-related changes in the number of GluN1 subunit protein present in each nucleus.

Variability in expression levels

The mean and median NMDAR subunit mRNA expression levels vary across ages, subunits, and nuclei. How does this influence my ability to make conclusions about expression levels of each subunit? Because of the small sample sizes in these

experiments, it is not possible to make meaningful conclusions about changes in expression levels because I cannot be confident that the variability in the values reflects biological variability. The distribution of the data (i.e., spread) can indicate how closely the values fall with respect to the mean/median. For example, a large distribution of expression values taken from a small sample size of rats, not cells, is likely representative of experimental noise, rather than biological variability.

Troubleshooting

Inter-litter differences, Sex differences, and Sample Size

There are several differences in the expression levels obtained for the two *in-situ* hybridization litters. Aside from actual differences in expression between the two litters, the expression levels could have been different due to several confounding factors: 1) the sections collected for the second litter differed in that all ages were processed the same way, whereas ages P0 to P12 in litter one were counterstained according to the DAPI protocol provided in the RNAscope instructions, 2) my ability to obtain sections with all six nuclei at all ages improved by the time I began sectioning the second litter, and 3) a few of the P16-P28 sections in the first litter exhibited hazy NeuroTrace staining, which made it challenging to detect neurons and probes in those sections. Therefore, the results of the second litter are likely closer to the actual NMDAR subunit levels throughout circuit refinement. Although the RNAscope assay used in this study has relatively specific probe binding, the expression patterns observed in the second litter should be replicated in at least two more litters. With the current sample of two litters, comparing sex differences in NMDAR subunit expression is challenging because each animal for each age was selected randomly from its litter, it is not possible to ensure that there are both male and female rat data for each time point. A solution to this would be to collect more than two litters to increase the chance of having both sexes for a given age's data. We could also collect a male and female rat for each age in each litter, but this solution assumes that the litter is large enough to have two rats per time point and that there is a balance between male and female rats in the litter. To increase confidence in identifying the sex of younger ages (P0-P8), where both sexes possess similar dimorphic features, at the time of perfusion, a section of the tail tip of the rat could be taken for polymerase chain reaction test to assess for the *Kdm5c* gene on the X chromosome for female rats and for the *Kdm5d* gene on the Y chromosome for male rats (Dhakal and Soares 2017). It is important to note, however, that researchers who conducted a whole-genome microarray analysis of the P16 rat SOC found that very few genes had sex differences in their expression, in comparison to the rest of the brain (Ehmann et al. 2008). Similar whole-genome analyses should be conducted on a larger age-group to assess the presence of sex differences before or after P16.

RNAscope: Annotating SOC nuclei

Advanced Cell Diagnostic's guidelines for the RNAscope Fluorescent Multiplex suggest using DAPI as a counterstain in the assay. DAPI does not facilitate the identification of SOC nuclei as it does not exclusively stain neurons and glia, as NeuroTrace does. Therefore, to identify SOC nuclei in the sections, I stained sections that flanked the RNAscope sections with NeuroTrace 640/660. After imaging the NeuroTrace-stained sections, I could then annotate the SOC nuclei and transfer those annotations onto my RNAscope images. However, staining the flanking sections with NeuroTrace 640/660 did not facilitate identifying the SOC nuclei because it was not possible to precisely align the annotations from the NeuroTrace images onto the DAPI stain from the RNAscope images as there were no landmarks to use. To troubleshoot this issue, I used NeuroTrace 435/455 instead of DAPI in the RNAscope assay; Counterstaining with NeuroTrace 435/455 appropriately stained neurons and glia and made it possible to annotate each nucleus without having to use annotations from a flanking section. Therefore, I decided to use NeuroTrace 435/455 instead of DAPI for the remaining assay in litter 1 and all the assays in litter 2.

Conclusion

NMDARs are involved in the refinement of classical glutamatergic circuits and are hypothesized to be involved in the refinement of glutamate-releasing immature inhibitory circuits. In the immature inhibitory MNTB to LSO pathway, in the SOC, the functional heterogeneity among NMDAR subtypes may be available to the circuit during refinement. In this study, I show that in the SOC, NMDAR subunits in the GluN1 and GluN2 family follow different expression patterns from P0 to P28 between ages and nuclei. In addition, all subunits show a decline in expression towards P28. These findings are consistent with changes in the levels of different NMDAR subunits and a decline in NMDARs. A future direction would be to replicate these findings using a larger sample size, with markers for specific cell types.

References

- Alamilla J, Gillespie DC. 2011. Glutamatergic inputs and glutamate-releasing immature inhibitory inputs activate a shared postsynaptic receptor population in lateral superior olive. *Neuroscience*. 196:285–296. doi:10.1016/j.neuroscience.2011.08.060.
- Albrecht O, Dondzillo A, Mayer F, Thompson JA, Klug A. 2014. Inhibitory projections from the ventral nucleus of the trapezoid body to the medial nucleus of the trapezoid body in the mouse. *Front Neural Circuits*. 8:83. doi:10.3389/fncir.2014.00083.
- Angulo MC, Rossier J, Audinat E. 1999. Postsynaptic Glutamate Receptors and Integrative Properties of Fast-Spiking Interneurons in the Rat Neocortex. *J Neurophysiol*. 82(3):1295–1302. doi:10.1152/jn.1999.82.3.1295.
- Banerjee A, Larsen RS, Philpot BD, Paulsen O. 2016. Roles of Presynaptic NMDA Receptors in Neurotransmission and Plasticity. *Trends Neurosci*. 39(1):26–39. doi:10.1016/j.tins.2015.11.001.
- Bankhead P, Loughrey MB, Fernández JA, Dombrowski Y, McArt DG, Dunne PD, McQuaid S, Gray RT, Murray LJ, Coleman HG, et al. 2017. QuPath: Open source software for digital pathology image analysis. *Sci Rep*. 7(1):16878. doi:10.1038/s41598-017-17204-5.
- Banks MI, Smith PH. 1992. Intracellular recordings from neurobiotin-labeled cells in brain slices of the rat medial nucleus of the trapezoid body. *J Neurosci*. 12(7):2819–2837. doi:10.1523/JNEUROSCI.12-07-02819.1992.
- Bliss TVP, Collingridge GL. 1993. A synaptic model of memory: long-term potentiation in the hippocampus. *Nature*. 361(6407):31–39. doi:10.1038/361031a0.
- Bredt DS, Snyder SH. 1989. Nitric oxide mediates glutamate-linked enhancement of cGMP levels in the cerebellum. *Proc Natl Acad Sci*. 86(22):9030–9033. doi:10.1073/pnas.86.22.9030.
- Cant NB, Casseday JH. 1986. Projections from the anteroventral cochlear nucleus to the lateral and medial superior olivary nuclei. *J Comp Neurol*. 247(4):457–476. doi:10.1002/cne.902470406.
- Cant NB, Hyson RL. 1992. Projections from the lateral nucleus of the trapezoid body to the medial superior olivary nucleus in the gerbil. *Hear Res*. 58(1):26–34. doi:10.1016/0378-5955(92)90005-8.

Case DT, Alamilla J, Gillespie DC. 2014. VGLUT3 does not synergize GABA/glycine release during functional refinement of an inhibitory auditory circuit. *Front Neural Circuits*. 8:140. doi:10.3389/fncir.2014.00140.

Case DT, Gillespie DC. 2011. Pre- and postsynaptic properties of glutamatergic transmission in the immature inhibitory MNTB-LSO pathway. *J Neurophysiol*. 106(5):2570–2579. doi:10.1152/jn.00644.2010.

Case DT, Zhao X, Gillespie DC. 2011. Functional Refinement in the Projection from Ventral Cochlear Nucleus to Lateral Superior Olive Precedes Hearing Onset in Rat. *PLoS ONE*. 6(6). doi:10.1371/journal.pone.0020756.
<https://www.ncbi.nlm.nih.gov/pmc/articles/PMC3111428/>.

Caspary DM, Faingold CL. 1989. Non-N-methyl-d-aspartate receptors may mediate ipsilateral excitation at lateral superior olivary synapses. *Brain Res*. 503(1):83–90. doi:10.1016/0006-8993(89)91707-1.

Castillo PE, Chiu CQ, Carroll RC. 2011. Long-term synaptic plasticity at inhibitory synapses. *Curr Opin Neurobiol*. 21(2):328–338. doi:10.1016/j.conb.2011.01.006.

Cathala L, Misra C, Cull-Candy S. 2000. Developmental profile of the changing properties of NMDA receptors at cerebellar mossy fiber-granule cell synapses. *J Neurosci Off J Soc Neurosci*. 20(16):5899–5905.

Chatterton JE, Awobuluyi M, Premkumar LS, Takahashi H, Talantova M, Shin Y, Cui J, Tu S, Sevarino KA, Nakanishi N, et al. 2002. Excitatory glycine receptors containing the NR3 family of NMDA receptor subunits. *Nature*. 415(6873):793–798. doi:10.1038/nature715.

Christopherson KS, Hillier BJ, Lim WA, Brecht DS. 1999. PSD-95 Assembles a Ternary Complex with the N-Methyl-d-aspartic Acid Receptor and a Bivalent Neuronal NO Synthase PDZ Domain. *J Biol Chem*. 274(39):27467–27473. doi:10.1074/jbc.274.39.27467.

Clause A, Kim G, Sonntag M, Weisz CJC, Vetter DE, Rűbsamen R, Kandler K. 2014. The Precise Temporal Pattern of Prehearing Spontaneous Activity Is Necessary for Tonotopic Map Refinement. *Neuron*. 82(4):822–835. doi:10.1016/j.neuron.2014.04.001.

Cramer KS, Sur M. 1995. Activity-dependent remodeling of connections in the mammalian visual system. *Curr Opin Neurobiol*. 5(1):106–111. doi:10.1016/0959-4388(95)80094-8.

Cull-Candy SG, Leszkiewicz DN. 2004. Role of Distinct NMDA Receptor Subtypes at Central Synapses. *Sci STKE*. 2004(255):re16–re16. doi:10.1126/stke.2552004re16.

Dhakal P, Soares MJ. 2017. Single Step PCR-Based Genetic Sex Determination for Rat Tissues and Cells. *BioTechniques*. 62(5):232–233. doi:10.2144/000114548.

Ehmann H, Hartwich H, Salzig C, Hartmann N, Clément-Ziza M, Ushakov K, Avraham KB, Bininda-Emonds ORP, Hartmann AK, Lang P, et al. 2013. Time-dependent gene expression analysis of the developing superior olivary complex. *J Biol Chem*. 288(36):25865–25879. doi:10.1074/jbc.M113.490508.

Ehmann H, Salzig C, Lang P, Friauf E, Nothwang HG. 2008. Minimal sex differences in gene expression in the rat superior olivary complex. *Hear Res*. 245(1–2):65–72. doi:10.1016/j.heares.2008.08.008.

Ehrlich I, Löhrike S, Friauf E. 1999. Shift from depolarizing to hyperpolarizing glycine action in rat auditory neurones is due to age-dependent Cl⁻ regulation. *J Physiol*. 520(1):121–137. doi:https://doi.org/10.1111/j.1469-7793.1999.00121.x.

Ernst AF, Wu HH, El-Fakahany EE, McLoon SC. 1999. NMDA Receptor-Mediated Refinement of a Transient Retinotectal Projection during Development Requires Nitric Oxide. *J Neurosci*. 19(1):229–235. doi:10.1523/JNEUROSCI.19-01-00229.1999.

Forsythe ID, Westbrook GL. 1988. Slow excitatory postsynaptic currents mediated by N-methyl-D-aspartate receptors on cultured mouse central neurones. *J Physiol*. 396:515–533. doi:10.1113/jphysiol.1988.sp016975.

Gamlin CR, Yu W-Q, Wong ROL, Hoon M. 2018. Assembly and maintenance of GABAergic and Glycinergic circuits in the mammalian nervous system. *Neural Develop*. 13(1):12. doi:10.1186/s13064-018-0109-6.

Garthwaite J, Charles SL, Chess-Williams R. 1988. Endothelium-derived relaxing factor release on activation of NMDA receptors suggests role as intercellular messenger in the brain. *Nature*. 336(6197):385–388. doi:10.1038/336385a0.

Gillespie DC, Kim G, Kandler K. 2005. Inhibitory synapses in the developing auditory system are glutamatergic. *Nat Neurosci*. 8(3):332–338. doi:10.1038/nn1397.

Glendenning KK, Baker BN, Hutson KA, Masterton RB. 1992. Acoustic chiasm V: Inhibition and excitation in the ipsilateral and contralateral projections of LSO. *J Comp Neurol*. 319(1):100–122. doi:10.1002/cne.903190110.

Goodman CS, Shatz CJ. 1993. Developmental mechanisms that generate precise patterns of neuronal connectivity. *Cell*. 72:77–98. doi:10.1016/S0092-8674(05)80030-3.

Gould J, Morgan C. 1941. Hearing in the rat at high frequencies. *Science*. 94:168–168. doi:10.1126/science.94.2433.168.

Gu X, Zhou L, Lu W. 2016. An NMDA receptor-dependent mechanism underlies inhibitory synapse development. *Cell Rep*. 14(3):471–478. doi:10.1016/j.celrep.2015.12.061.

Guinan JJ, Norris BE, Guinan SS. 1972. Single Auditory Units in the Superior Olivary Complex: II: Locations of Unit Categories and Tonotopic Organization. *Int J Neurosci*. 4(4):147–166. doi:10.3109/00207457209164756.

Hollmann M. 1999. Structure of Ionotropic Glutamate Receptors. In: Jonas P, Monyer H, editors. *Ionotropic Glutamate Receptors in the CNS*. Berlin, Heidelberg: Springer. (Handbook of Experimental Pharmacology). p. 3–98. https://doi.org/10.1007/978-3-662-08022-1_1.

Illing R-B, Kraus KS, Michler SA. 2000. Plasticity of the superior olivary complex. *Microsc Res Tech*. 51(4):364–381. doi:10.1002/1097-0029(20001115)51:4<364::AID-JEMT6>3.0.CO;2-E.

Irving R, Harrison JM. 1967. The superior olivary complex and audition: A comparative study. *J Comp Neurol*. 130(1):77–86. doi:10.1002/cne.901300105.

Jensen K, Krusenstjerna-Hafstrøm R, Lohse J, Petersen KH, Derand H. 2017. A novel quantitative immunohistochemistry method for precise protein measurements directly in formalin-fixed, paraffin-embedded specimens: analytical performance measuring HER2. *Mod Pathol*. 30(2):180–193. doi:10.1038/modpathol.2016.176.

Joshi I, Wang L-Y. 2002. Developmental profiles of glutamate receptors and synaptic transmission at a single synapse in the mouse auditory brainstem. *J Physiol*. 540(Pt 3):861–873. doi:10.1113/jphysiol.2001.013506.

Kandler K, Friauf E. 1995. Development of glycinergic and glutamatergic synaptic transmission in the auditory brainstem of perinatal rats. *J Neurosci*. 15(10):6890–6904. doi:10.1523/JNEUROSCI.15-10-06890.1995.

Kapfer C, Seidl AH, Schweizer H, Grothe B. 2002. Experience-dependent refinement of inhibitory inputs to auditory coincidence-detector neurons. *Nat Neurosci*. 5(3):247–254. doi:10.1038/nn810.

Katz LC, Shatz CJ. 1996. Synaptic Activity and the Construction of Cortical Circuits. *Science*. 274(5290):1133–1138.

Kim G, Kandler K. 2003. Elimination and strengthening of glycinergic/GABAergic connections during tonotopic map formation. *Nat Neurosci.* 6(3):282–290. doi:10.1038/nn1015.

Kiss A, Majorossy K. 1983. Neuron morphology and synaptic architecture in the medial superior olivary nucleus. *Exp Brain Res.* 52(3):315–327. doi:10.1007/BF00238026.

Kullmann DM, Asztely F. 1998. Extrasynaptic glutamate spillover in the hippocampus: evidence and implications. *Trends Neurosci.* 21(1):8–14. doi:10.1016/s0166-2236(97)01150-8.

Kuwabara N, Zook JM. 1992. Projections to the medial superior olive from the medial and lateral nuclei of the trapezoid body in rodents and bats. *J Comp Neurol.* 324(4):522–538. doi:10.1002/cne.903240406.

Liu L, Wong TP, Pozza MF, Lingenhoehl K, Wang Y, Sheng M, Auberson YP, Wang YT. 2004. Role of NMDA receptor subtypes in governing the direction of hippocampal synaptic plasticity. *Science.* 304(5673):1021–1024. doi:10.1126/science.1096615.

Liu Q, Wong-Riley MTT. 2002. Postnatal expression of neurotransmitters, receptors, and cytochrome oxidase in the rat pre-Bötzinger complex. *J Appl Physiol Bethesda Md* 1985. 92(3):923–934. doi:10.1152/japplphysiol.00977.2001.

Malenka RC, Nicoll RA. 1993. NMDA-receptor-dependent synaptic plasticity: multiple forms and mechanisms. *Trends Neurosci.* 16(12):521–527. doi:10.1016/0166-2236(93)90197-T.

Mayer ML. 2006. Glutamate receptors at atomic resolution. *Nature.* 440(7083):456–462. doi:10.1038/nature04709.

Momiyama A, Feldmeyer D, Cull-Candy SG. 1996. Identification of a native low-conductance NMDA channel with reduced sensitivity to Mg²⁺ in rat central neurones. *J Physiol.* 494 (Pt 2):479–492. doi:10.1113/jphysiol.1996.sp021507.

Monyer H, Burnashev N, Laurie DJ, Sakmann B, Seeburg PH. 1994. Developmental and regional expression in the rat brain and functional properties of four NMDA receptors. *Neuron.* 12(3):529–540. doi:10.1016/0896-6273(94)90210-0.

Monyer H, Sprengel R, Schoepfer R, Herb A, Higuchi M, Lomeli H, Burnashev N, Sakmann B, Seeburg PH. 1992. Heteromeric NMDA receptors: molecular and functional distinction of subtypes. *Science.* 256(5060):1217–1221. doi:10.1126/science.256.5060.1217.

Morest DK. 1968. The growth of synaptic endings in the mammalian brain: A study of the calyces of the trapezoid body. *Z Für Anat Entwicklungsgeschichte*. 127(3):201–220. doi:10.1007/BF00526129.

Müller M. 1990. Quantitative comparison of frequency representation in the auditory brainstem nuclei of the gerbil, *Pachyuromys duprasi*. *Exp Brain Res*. 81(1):140–149. doi:10.1007/BF00230110.

Noh J, Seal RP, Garver JA, Edwards RH, Kandler K. 2010. Glutamate co-release at GABA/glycinergic synapses is crucial for the refinement of an inhibitory map. *Nat Neurosci*. 13(2):232–238. doi:10.1038/nn.2478.

Nordeen KW, Killackey HP, Kitzes LM. 1983. Ascending projections to the inferior colliculus following unilateral cochlear ablation in the neonatal gerbil, *Meriones unguiculatus*. *J Comp Neurol*. 214(2):144–153. doi:10.1002/cne.902140204.

Nuovo GJ, Elton TS, Nana-Sinkam P, Volinia S, Croce CM, Schmittgen TD. 2009. A methodology for the combined in situ analyses of the precursor and mature forms of microRNAs and correlation with their putative targets. *Nat Protoc*. 4(1):107–115. doi:10.1038/nprot.2008.215.

Paoletti P, Ascher P, Neyton J. 1997. High-Affinity Zinc Inhibition of NMDA NR1–NR2A Receptors. *J Neurosci*. 17(15):5711–5725. doi:10.1523/JNEUROSCI.17-15-05711.1997.

Paoletti P, Bellone C, Zhou Q. 2013. NMDA receptor subunit diversity: impact on receptor properties, synaptic plasticity and disease. *Nat Rev Neurosci*. 14(6):383–400. doi:10.1038/nrn3504.

Paoletti P, Neyton J. 2007. NMDA receptor subunits: function and pharmacology. *Curr Opin Pharmacol*. 7(1):39–47. doi:10.1016/j.coph.2006.08.011.

Perez-Otano I, Schulteis CT, Contractor A, Lipton SA, Trimmer JS, Sucher NJ, Heinemann SF. 2001. Assembly with the NR1 subunit is required for surface expression of NR3A-containing NMDA receptors. *J Neurosci Off J Soc Neurosci*. 21(4):1228–1237.

Philpot BD, Sekhar AK, Shouval HZ, Bear MF. 2001. Visual Experience and Deprivation Bidirectionally Modify the Composition and Function of NMDA Receptors in Visual Cortex. *Neuron*. 29(1):157–169. doi:10.1016/S0896-6273(01)00187-8.

Preston AN, Cervasio DA, Laughlin ST. 2019. Visualizing the brain's astrocytes. *Methods Enzymol*. 622:129–151. doi:10.1016/bs.mie.2019.02.006.

PubChem. Polr2a - polymerase (RNA) II (DNA directed) polypeptide A (house mouse).
<http://pubchem.ncbi.nlm.nih.gov/gene/Polr2a/mouse>.

PubChem. Ppib - peptidylprolyl isomerase B (house mouse).
<http://pubchem.ncbi.nlm.nih.gov/gene/Ppib/mouse>.

PubChem. Ubc - ubiquitin C (house mouse).
<http://pubchem.ncbi.nlm.nih.gov/gene/Ubc/mouse>.

PubChem. dapB - 4-hydroxy-tetrahydrodipicolinate reductase (Escherichia coli str. K-12 substr. MG1655). http://pubchem.ncbi.nlm.nih.gov/gene/dapB/Escherichia_coli_str._K-12_substr._MG1655.

Rietzel H-J, Friauf E. 1998. Neuron types in the rat lateral superior olive and developmental changes in the complexity of their dendritic arbors. *J Comp Neurol.* 390(1):20–40. doi:10.1002/(SICI)1096-9861(19980105)390:1<20::AID-CNE3>3.0.CO;2-S.

Saldaña E, Merchañ MA. 1992. Intrinsic and commissural connections of the rat inferior colliculus. *J Comp Neurol.* 319(3):417–437. doi:10.1002/cne.903190308.

Sanes DH, Friauf E. 2000. Development and influence of inhibition in the lateral superior olivary nucleus. *Hear Res.* 147(1):46–58. doi:10.1016/S0378-5955(00)00119-2.

Sanes DH, Goldstein NA, Ostad M, Hillman DE. 1990. Dendritic morphology of central auditory neurons correlates with their tonotopic position. *J Comp Neurol.* 294(3):443–454. doi:10.1002/cne.902940312.

Sanes DH, Siverls V. 1991. Development and specificity of inhibitory terminal arborizations in the central nervous system. *J Neurobiol.* 22(8):837–854. doi:10.1002/neu.480220805.

Sauert M, Temmel H, Moll I. 2015. Heterogeneity of the translational machinery: Variations on a common theme. *Biochimie.* 114:39–47. doi:10.1016/j.biochi.2014.12.011.

Schwartz IR. 1992. The Superior Olivary Complex and Lateral Lemniscal Nuclei. In: Webster DB, Popper AN, Fay RR, editors. *The Mammalian Auditory Pathway: Neuroanatomy*. New York, NY: Springer. (Springer Handbook of Auditory Research). p. 117–167. https://doi.org/10.1007/978-1-4612-4416-5_4.

Shigeki. 2020. Randomize.m Code.

Smith PH, Joris PX, Yin TCT. 1993. Projections of physiologically characterized spherical bushy cell axons from the cochlear nucleus of the cat: Evidence for delay lines to the medial superior olive. *J Comp Neurol.* 331(2):245–260. doi:10.1002/cne.903310208.

Sommer I, Lingenhöhl K, Friauf E. 1993. Principal cells of the rat medial nucleus of the trapezoid body: an intracellular in vivo study of their physiology and morphology. *Exp Brain Res.* 95(2). doi:10.1007/BF00229781.
<http://link.springer.com/10.1007/BF00229781>.

Spangler KM, Cant NB, Henkel CK, Farley GR, Warr WB. 1987. Descending projections from the superior olivary complex to the cochlear nucleus of the cat. *J Comp Neurol.* 259(3):452–465. doi:10.1002/cne.902590311.

Stotler WA. 1953. An experimental study of the cells and connections of the superior olivary complex of the cat. *J Comp Neurol.* 98(3):401–431. doi:10.1002/cne.900980303.

Stringer C, Wang T, Michaelos M, Pachitariu M. 2021. Cellpose: a generalist algorithm for cellular segmentation. *Nat Methods.* 18(1):100–106. doi:10.1038/s41592-020-01018-x.

Tollin DJ. 2003. The Lateral Superior Olive: A Functional Role in Sound Source Localization. *The Neuroscientist.* 9(2):127–143. doi:10.1177/1073858403252228.

Tritsch NX, Rodríguez-Contreras A, Crins TTH, Wang HC, Borst JGG, Bergles DE. 2010. Calcium action potentials in hair cells pattern auditory neuron activity before hearing onset. *Nat Neurosci.* 13(9):1050–1052. doi:10.1038/nn.2604.

Tsuchitani C. 1977. Functional organization of lateral cell groups of cat superior olivary complex. *J Neurophysiol.* 40(2):296–318. doi:10.1152/jn.1977.40.2.296.

Vetter DE, Saldaña E, Mugnaini E. 1993. Input from the inferior colliculus to medial olivocochlear neurons in the rat: A double label study with PHA-L and cholera toxin. *Hear Res.* 70(2):173–186. doi:10.1016/0378-5955(93)90156-U.

Wang F, Flanagan J, Su N, Wang L-C, Bui S, Nielson A, Wu X, Vo H-T, Ma X-J, Luo Y. 2012. RNAscope: A Novel in Situ RNA Analysis Platform for Formalin-Fixed, Paraffin-Embedded Tissues. *J Mol Diagn.* 14(1):22–29. doi:10.1016/j.jmoldx.2011.08.002.

Wang H, Wang Q, Pape UJ, Shen B, Huang J, Wu B, Li X. 2010. Systematic investigation of global coordination among mRNA and protein in cellular society. *BMC Genomics.* 11(1):1–9. doi:10.1186/1471-2164-11-364.

Warr WB, Beck JE. 1996. Multiple projections from the ventral nucleus of the trapezoid body in the rat. *Hear Res.* 93(1):83–101. doi:10.1016/0378-5955(95)00198-0.

Wehr M, Zador AM. 2003. Balanced inhibition underlies tuning and sharpens spike timing in auditory cortex. *Nature*. 426(6965):442–446. doi:10.1038/nature02116.

Weinrich L, Sonntag M, Arendt T, Morawski M. 2018. Neuroanatomical characterization of perineuronal net components in the human cochlear nucleus and superior olivary complex. *Hear Res*. 367:32–47. doi:10.1016/j.heares.2018.07.005.

Wilent WB, Contreras D. 2005. Dynamics of excitation and inhibition underlying stimulus selectivity in rat somatosensory cortex. *Nat Neurosci*. 8(10):1364–1370. doi:10.1038/nn1545.

Willard FH, Ryugo DK. Anatomy of the central auditory system. In: *The Auditory Psychobiology of the Mouse*. Springfield, IL: Charles C. Thomas. p. 201–304.

Williams K. 1993. Ifenprodil discriminates subtypes of the N-methyl-D-aspartate receptor: selectivity and mechanisms at recombinant heteromeric receptors. *Mol Pharmacol*. 44(4):851–859.

Yao L, Rong Y, Ma X, Li H, Deng D, Chen Y, Yang S, Peng T, Ye T, Liang F, et al. 2022. Extrasynaptic NMDA Receptors Bidirectionally Modulate Intrinsic Excitability of Inhibitory Neurons. *J Neurosci*. 42(15):3066–3079. doi:10.1523/JNEUROSCI.2065-21.2022.

Yin TC, Chan JC. 1990. Interaural time sensitivity in medial superior olive of cat. *J Neurophysiol*. 64(2):465–488. doi:10.1152/jn.1990.64.2.465.

Zhang H, Mu L, Wang D, Xia D, Salmon A, Liu Q, Wong-Riley MTT. 2018. Uncovering a critical period of synaptic imbalance during postnatal development of the rat visual cortex: role of brain-derived neurotrophic factor. *J Physiol*. 596(18):4511–4536. doi:10.1113/JP275814.

Zhang Z, Peterson M, Liu H. 2013. Essential role of postsynaptic NMDA receptors in developmental refinement of excitatory synapses. *Proc Natl Acad Sci*. 110(3):1095–1100. doi:10.1073/pnas.1212971110.